Towfish Design, Simulation and Control

Eric M. Schuch

Thesis submitted to the faculty of the Virginia Polytechnic Institute and State University
in partial fulfillment of the requirements for the degree of

Masters of Science
In
Aerospace Engineering

Dr. Craig A Woolsey, Chair
Dr. Eugene Cliff
Dr. Wayne Neu

June 28th, 2004
Blacksburg, Virginia

Keywords: Towfish, Simulation, PID, Tethered Vehicles, Underwater Vehicles, Towed Vehicles

Towfish Design, Simulation and Control

Eric M. Schuch

Abstract

Sampling small scale ocean turbulence is one of the most important problems in oceanography. The turbulence can be near the noise level of current microscale profiling techniques and these techniques do not provide spatially and temporally dense measurements and can be labor intensive. A 5 beam acoustic Doppler current profiler (VADCP) can more accurately measure three components of fluid velocity in a column. By towing such a device in a sensor platform, called a towfish, one may measure turbulent mixing in a vertical swath of the ocean. If the towfish attitude is not precisely regulated, however, the turbulence measurements can be irreversibly corrupted. A two-part tow that includes a depressor weight between the towing vessel and the towfish can provide some degree of disturbance rejection. Passive devices alone, however, can not meet the performance requirements for measuring ocean turbulence.

This thesis presents a design for a two-stage towing system which will be used to measure ocean turbulence. The focus is on the towfish, which includes independently actuated stern planes for pitch and roll disturbance rejection.

The thesis also describes design and analysis of an active control system to precisely regulate the pitch and roll attitude of a streamlined towfish. A three dimensional numerical model is presented and a PID controller is developed to provide active attitude stabilization. The effect of random depressor motions on the towfish dynamics is assessed for both the uncontrolled and the feedback-controlled case. The numerical investigation also considers variations in parameters such as tether length and CG location.

Acknowledgements

Deep appreciation is given to Dr. Craig Woolsey for all of his guidance that and aid during the course of this thesis. I give great thanks to Dr. Jan Crane for all of his invaluable assistance that was given to help understand the dynamics of towed vehicles and various critical design considerations. I thank Dr. Ann Gargett for the opportunity to work on towfish and Chris Powell for all his help with the development of the towfish. I also acknowledge the help of the Aerospace and Ocean Engineering faculty, James Lambert, Bruce Stanger and Stephen Edwards and the help of the Human Powered Sub Team as well as Nate Lambeth, Amy Linklater, Andy Parker and Brian McCarter, who contributed much of their time to the electronic and physical construction of the towfish. This project is supported by the National Science Foundation under Grant OCE-0220745.

Table of Contents

Nomenclature

Roman	
A	Jacobian of the nonlinear towfish equations with respect to the states
A_{lat}	Jacobian of the nonlinear towfish equations with respect to lateral/directional states
A_{long}	Jacobian of the nonlinear towfish equations with respect to the longitudinal states
A_{pitch}	Pitch mode approximation A matrix
A_{roll}	Roll mode approximation A matrix
AR	Aspect ratio
b	Tip to tip span
B	Jacobian of the nonlinear towfish equations with respect to the inputs
B_{lat}	Jacobian on the nonlinear towfish equations with respect to the inputs for the lateral/directional states
B_{long}	Jacobian on the nonlinear towfish equations with respect to the inputs for the longitudinal states
B_{pitch}	Pitch mode approximation B matrix
B_{roll}	Roll mode approximation B matrix
$\overline{b}$	Effective damping constant
c	Mean chord of a fin
C_{bi}	Force coefficient vector of the i^{th} fin in body axes
C_{ci}	Force coefficient vector of the i^{th} fin in water current axes
C_D	Drag coefficient of the tether
$C_{D\alpha b}$	Slope of the body drag coefficient an a function of the angle μ
C_{Db0}	Additional zero degree angle of attack body drag
C_{D0}	Zero degree angle of attack body drag
C_f	Coefficient of friction of the hull
c_i	i^{th} column of the inverse modal matrix
C_i	Diagonalizied i^{th} column of the inverse modal matrix
c_{ij}	ij^{th} entry of the inverse modal matrix
C_{lp}	Roll rate damping coefficient
$C_{L\alpha}$	Approximated lift curve slope of tail fin
$C_{L\alpha 2D}$	Lift curve slope for a theoretical two-dimensional hydrofoil
$C_{L\alpha b}$	Slope of the body lift coefficient as a function of the angle μ
C_{mq}	Pitch rate damping coefficient
C_{nr}	Yaw rate damping coefficient
$C_{m\alpha b}$	Slope of the pitching moment coefficient of the hull as a function of the angle μ
c_r	Root chord of a fin
c_t	Tip chord of a fin
D	Inertial coupling matrix and added mass matrix
D_b	Diameter of the towfish hull
d_i	Actual fin deflection of the i^{th} fin

e	Eccentricity
EA	Young's modulus multiplied by cross-sectional area of the tether
F_{axial}	Force acting along the x_b axis
F_{body}	Force developed by the body, represented in the body axis
$F_{buoyancy}$	Towfish buoyancy represented in the body axis
F_{ext}	External forces on the towfish represented in the body axis
f_i	Representation of the i^{th} non-linear equation of motion
$F_{lateral}$	Forces acting along the y_b axis
F_{normal}	Forces acting along the z_b axis
F_{tail}	Forces developed by the tail represented in the body axes
F_{td}	Tow force represented in the tether (cable) axes
F_{tow}	Towing force represented in the body axes
F_{weight}	Towfish dry weight represented in the body axis
g	Acceleration due to gravity
H	Significant wave height
I_j	Inertia of the towfish where $j = x, y, z, xy, xz, yx$
I_{yplate}	Moment of inertia of a rectangular flat plate
J	Inertia and added inertia matrix
k_1, k_2, k_3	Body added mass/inertia parameters
k_{cr}	Critical gain
k_d	Derivative gain
k_i	Integral gain
k_p	Proportional gain
$K_{\dot{p}f}$	Fin added inertia in roll
$K_{\dot{p}f}^{2D}$	Two-dimensional fin added inertia in roll
$k_{\theta cr}$	Pitch channel critical gain
$K_{\phi cr}$	Roll channel critical gain
$k_{\theta p}$	Pitch channel proportional gain
$k_{\phi p}$	Roll channel proportional gain
$\bar{k}$	Effective spring constant
L	Length of the pigtail section of the tether
l_b	Hull length
l_f	Length from the body axes origin to the fin geometric center
L_p	Roll rate damping
l_t	Length from the body axes origin to the hydrodynamic center of the fins
m	Mass of the towfish including fluid inside the hull
M	Mass and added mass matrix
M_{body}	Moment developed by the body
$M_{damping}$	Moment due to hydrodynamic damping
M_{ext}	External torques on the towfish
m_{fin}	Mass of a fin
M_{pitch}	Moment on the towfish about the y_b axis
M_q	Pitch rate damping
$M_{\dot{q}f}$	Fin added inertia in pitch due to pitch acceleration

$M_{\dot{q}plate}$	Added inertia of a flat rectangular plate in pitch due to acceleration in pitch
$M_{\dot{q}plate}^{2D}$	Two-dimensional added inertia of a flat rectangular plate in pitch
M_{roll}	Moment on the towfish about the x_b axis
M_{tail}	Moment on the towfish developed from the tail about the CB
M_{tow}	Moment on the towfish due to the towing force about the CB
M_{weight}	Moment on the towfish due to the CG offset from the CB about the CB
M_{yaw}	Moment on the towfish about the y_b axis
$M_{\dot{w}f}$	Fin added inertia in pitch due to acceleration along the z_b axis
$\mathcal{M}$	Modal matrix
N_r	Yaw rate damping
$N_{\dot{r}f}$	Fin added inertia in yaw due to yaw acceleration
$N_{\dot{v}f}$	Fin added inertia in yaw due to acceleration along the y_b axis
P	Linear component of the impulse with respect to the body axes
p	Towfish roll rate represented in the body axes
P_{cr}	Critical period
$P_{\theta cr}$	Critical period of oscillations of the pitch angle
$P_{\phi cr}$	Critical period of oscillations of the roll angle
q	Towfish pitch rate represented in the body axes
$\dot{q}_{fin}$	Pitch rate of a fin
$\bar{q}$	Dynamic pressure
r	Towfish yaw rate represented in the body axis
r_i	i^{th} row of the modal matrix
R_{IB}	Rotation matrix from body coordinates to inertial coordinates
R_{IT}	Rotation matrix from water current coordinates to body coordinates
S	Sensitivity matrix
S_b	Frontal area of the hull
$S_{n,i}$	n^{th}, i^{th} entry of the sensitivity matrix
S_t	Planform area of the rudder or stern plane, tip to tip
T	Total energy of the fluid body system of the towfish
T_{fin}	Required torque to turn a fin
T_d	Derivative time
T_i	Integral time
$T_{\theta d}$	Pitch channel derivative time
$T_{\theta i}$	Pitch channel integral time
$T_{\phi d}$	Roll channel derivative time
$T_{\phi i}$	Roll channel integral time
u	Axial velocity of the towfish
U_0	Reference velocity
$U_{depressor}$	Depressor inertial velocity
v	Lateral velocity of the towfish
V	Towfish velocity vector represented in a body fixed coordinate system
v_i	i^{th} eigenvector
V_{PH}	Pressure housing internal volume

V_{req}	Required volume
V_t	Tail volume ratio
Vol	Volume of the towfish hull
w	Normal velocity of the towfish
W_b	Towfish dry weight
x	Inertial x position of the towfish
X	Towfish states
X_{aci}	Hydrodynamic center of the ith fin with respect to the body axes
x_b	Body frame x axis
x_c	Water current frame x axis
x_{cg}	Axial location of the CG with respect to the body axes
X_{CG}	Location of the center of gravity with respect to the body axes
x_{depth}	Depressor depth
$X_{depressor}$	Inertial position of the depressor
X_I	Inertial position of the towfish
X_{lat}	Towfish lateral/directional states
X_{long}	Towfish longitudinal states
$X_{nominal}$	Nominal motion of the towfish
y	Inertial y position of the towfish
y_{ac}	Lateral location of the hydrodynamic center for stern plane 2 or 4 with respect to the body axes
y_b	Body y axis
y_c	Water current y axis
y_{cg}	Lateral location of the CG with respect to the body axes
y_{random}	Random depressor position in the inertial y axis
$Y_{\dot{r}f}$	Added mass in the y_b direction due to yaw acceleration
$Y_{\dot{v}f}$	Added mass in the y_b direction due to acceleration along the y_b axis
z	Inertial z position of the towfish
z_b	Body z axis
z_c	Water current z axis
z_{cg}	Vertical location of the CG with respect to the body axes
$Z_{\dot{q}f}$	Added mass in the z_b direction due to pitch acceleration
z_{random}	Random depressor position in the inertial z axis
$Z_{\dot{w}f}$	Added mass in the z_b direction due to acceleration along the z_b axis

Greek	
α	Angle of attack
α_0	Added mass parameter
α_{TE}	Coefficient of thermal expansion
β	Angle of sideslip
β_0	Added mass parameter
δ	Vector of requested fin deflections
δ_i	Requested fin deflection of the ith fin

δ_a	Combination of stern plane deflections as an effective aileron deflection
δ_e	Combination of stern plane deflections as an effective elevator deflection
$\delta_{nominal}$	Nominal vector of control inputs
ΔT	Temperature change inside pressure housing
ε	Span efficiency factor
ϕ	Towfish roll angle
Φ_I	Towfish angular position vector with respect to inertial space
γ	Tow force "angle of attack" with respect to the inertial x axis
μ	Direction cosine equivalent of the angle of attack and side slip combination
η	Efficiency factor of a fin in the flow from the body
Π	Angular component of the impulse with respect to the body axes
ρ	Water density
σ	Tow force "angle of sideslip" with respect to inertial x-z plane
τ	Actuator time constant
τ_a	Response time constant
θ	Towfish pitch angle
Ω	Towfish angular velocity represented in a body fixed coordinate system
ω_{dep}	Depressor pendulum frequency
ω_n	Natural frequency
ψ	Towfish yaw angle
ζ	Damping ratio

List of Figures and Tables

1. Introduction

1.1. Problem Statement

Advances in sensor technology have enabled new measurement techniques for ocean scientists. In the past, velocity profiles of the water column (or "current profiles") were measured by dropping a tethered instrument at a point, letting it fall freely to a desired depth, and then recovering the instrument and moving on. Naturally, this tedious process can not provide high spatial or temporal sample rates. Recently, acoustic Doppler current profilers (ADCP's) have allowed scientists to instantaneously measure the horizontal components of fluid velocity throughout a column of water. By translating an ADCP along a horizontal path, one may obtain a velocity profile in a vertical plane. Because ADCPs dramatically improve measurement efficiency, they make it feasible for scientists to scan the ocean for sparsely distributed oceanographic features.

One such application involves searching for and characterizing small-scale ocean turbulence.[15] Ocean turbulence is a mixing process which transports thermal energy and nutrients between layers of water. For these reasons, it is quite important for physical oceanographers and marine biologists to have accurate models of the process. Three dimensional turbulence is not resolved at the spatial scales of current numerical models; physical measurements are required in order to accurately characterize this phenomenon. Regions of strong turbulent mixing are sparsely distributed and time-varying, making them difficult to discover and sample using conventional methods. Using a special five-beam ADCP (or "VADCP"), however, pockets of turbulence can be quickly identified and then carefully measured.

Figure 1 RD Instruments VADCP

Figure 1 shows a VADCP which is owned and operated by the Center for Coastal Physical Oceanography (CCPO) at Old Dominion University (ODU). This is a custom-designed sensor which was built by RD Instruments, a well-known manufacturer of conventional (four-beam) ADCPs. The VADCP contains 5 transducers which operate at 1200 kHz. The transducers are arranged such that four of the beams form a tetrahedron about the fifth beam. Each of these four beams is inclined 30 degrees from the fifth beam and spaced 90 degrees from its neighbors. See Figure 2. These four beams measure the

two components of fluid velocity which are orthogonal to the fifth beam. The fifth beam measures the remaining velocity component. Conventional ADCPs do not provide this third component of fluid velocity.

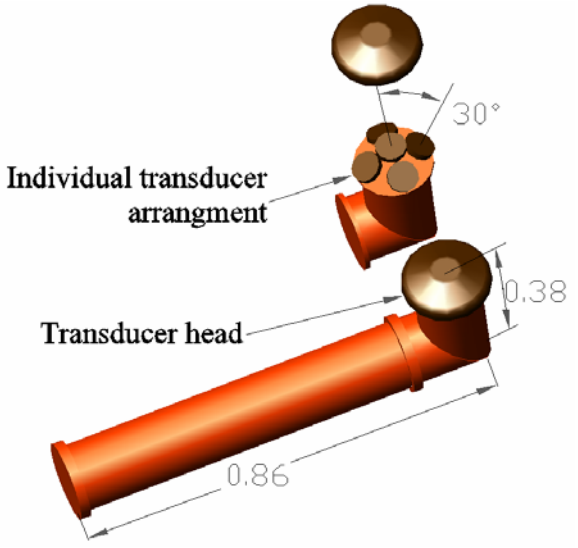

Figure 2 VADCP Schematic Units in meters

When using a conventional ADCP to measure velocity profiles, an ocean scientist translates the sensor through the water, either by towing it behind a vessel or mounting it directly in the vessel's hull. The result is a map of the fluid velocity throughout a swath of fluid. To measure turbulence (specifically, the turbulent kinetic energy dissipation rate), one must obtain all three components of velocity. This can be done using a VADCP. The sensor is oriented such that the fifth beam is aligned vertically, i.e., with the direction of gravity, and is translated through the water. One may compute the turbulent kinetic energy dissipation rate from the resulting measurements.[15]

Because the vertical component of fluid velocity is orders of magnitude smaller than the lateral components, it is essential that the sensor be precisely aligned (less than one degree of tilt). Any misalignment would contaminate the measurement of the vertical component of velocity. This attitude regulation requirement presents a considerable challenge, even in light to moderate sea states. The effect of waves on the vessel's motion, and the resulting effect on the VADCP, can easily corrupt measurements beyond use. Using a clever towing arrangement, however one may significantly reduce the effect of wave disturbances.

The two stage tow is a useful and simple way to attenuate disturbances due to a towing vessel's motion.[15] [19] [27] [28] The assembly consists of an umbilical towing cable which is attached to a "towfish" that houses a suite of sensors. A depressor weight is also attached to the umbilical tether, somewhere along its length. The portion of tether between the towing vessel and the depressor is called the "main catenary" while the portion between the depressor and the towfish is called the "pigtail." While the depressor experiences disturbance forces transmitted from the towing vessel, the length of the

pigtail can be adjusted to attenuate the effect of these disturbances on the towfish. In some applications, the cable properties (weight, buoyancy, drag) along the main catenary are adjusted to shape the catenary in order to obtain even better disturbance attenuation. See Figure 3.

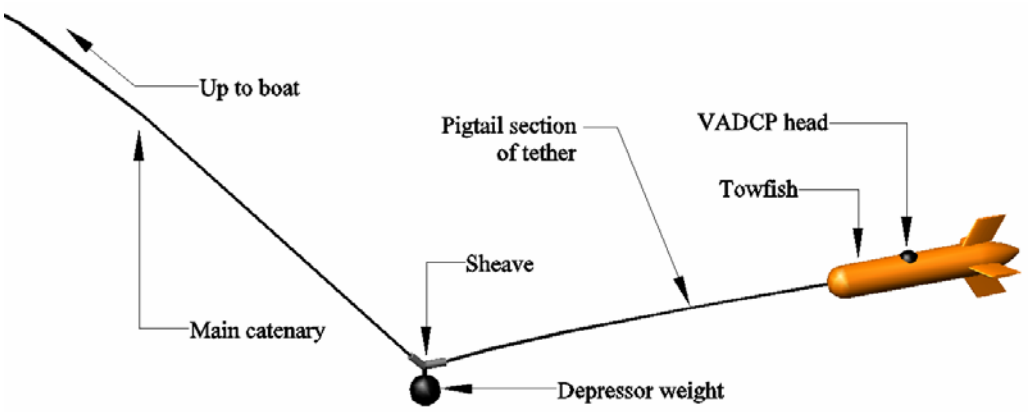

Figure 3 Representation of towfish in tow

While a two stage towing arrangement provides good passive disturbance rejection, it can not compensate for pitch and roll biases due to center of gravity (CG) offsets or asymmetric flow about the towfish. As demonstrated by Dr. Ann Gargett of CCPO, these effects can easily violate the performance requirement of less than one degree tilt.[15] Using just a metal frame as the towfish, she demonstrated a two stage towing arrangement which maintained a tilt angle less than two degrees. Because the towfish had no actuators, it was necessary to iteratively trim, launch, and recover the platform in order to minimize the biases. This can be a tedious process when the scope (total tether length) is several thousand meters. Alternatively, one may incorporate servo-actuated stern planes in the towfish to actively reject such biases and to enhance stability.[29] [29]

In a collaborative effort sponsored by the National Science Foundation's Ocean Technology Interdisciplinary Coordination program, Virginia Tech is constructing a towfish to house a VADCP for the purpose of measuring ocean turbulence. The towfish has a streamlined body, fixed rudders and two independently actuated stern planes to provide control in pitch and roll. See Figure 3. The towfish is expected to operate in the coastal oceans at depths up to 200 meters. The towfish must regulate its attitude (tilt angle) within 1 degree of nominal at speeds ranging from 1 to 3 m/s.

Because the VADCP is a custom instrument, it would be very difficult to replace, if lost. For this reason, the towfish will be trimmed to be somewhat buoyant. Should the tether break at the tow point, the towfish would float to the surface where an integrated VHF pinger would provide a recovery signal. Because the density of ocean water can vary up 3% due solely to salinity changes, the towfish should be approximately 5% buoyant.

Besides the VADCP, the system includes two servo-actuators, an on-board computer, power electronics, and a sensor suite containing

- an inertial measurement unit,
- a depth sensor,
- an altimeter, and
- a xenon strobe light and VHF pinger.

The sensor outputs and VADCP measurements will be transmitted to a supervisory computer aboard the towing vessel. AC power is supplied to the towfish from the ship and converted locally to DC. Details of the design process, including mechanical design and control design, are provided in the remaining chapters.

Because the control problem involves precise attitude regulation, it is reasonable to implement a conventional PID controller for this purpose. The controller is validated numerically for various operational parameters (such as towing speed and pigtail length). Simulations include wave and other disturbance models as well as a simplified model for the tether dynamics.

1.2. Technology Review

Different types of towfish have been used many times to carry a variety of oceanographic equipment. Both single tows, which consist of just the towfish, and two part tows, which include a depressor weight or a float, have been used with actively and passively stable towfish. There are several manufacturers of such devices. Specialty Devices, Inc. and Open Seas Instrumentation Inc. have developed towed vehicles but these are too small to carry the VADCP. There are also autonomous underwater vehicles (AUV's) and remotely operated vehicles (ROV's) that have been designed and developed by universities and commercial institutions. AUV's can not transmit large amounts of data in real time, so the scientist would be unable to view the turbulence data and adjust the survey plan accordingly while conventional ROV's are extremely slow.

The tow cable not only transmits but also generates disturbances. These disturbances depend on the cable used, mass and drag of the depressor and mass and drag of the towfish. For example, the cable may shed vortices causing it to strum. This strumming can be removed with the use of faring. Different modes of the cable introduce different types of disturbances.[5][2] The motion of a single body towed system can be characterized by two modes. The pendulum mode is similar to a mass swinging on a string. The bowing mode involves the cable bowing back and forth. Single part towing arrangements, with the tow point at or slightly forward from the center of gravity (CG), typically transmit surge and heave of the ship tow point to heave of the towfish. This can also cause a pitch disturbance due to the tail fins.[28] Because the tow point is slightly forward from the CG, surge and heave in the towing ship of a single tow arrangement can also translate into pitch disturbances of the towfish. Another effect is kiting which can be either ship-induced or towfish-induced.[5] Ship-induced kiting causes sway in the towfish whereas towfish-induced kiting causes sway and roll in the towfish. A well-shaped catenary like that in Figure 4 can help reduce some of these effects. A slightly buoyant tether allows for some curvature in the pigtail section of the tether. This can soften the

surge and heave effects of the depressor. Fewer disturbances are seen by the towfish for longer pigtail scopes. Although the shape of the main catenary and pigtail and the presence of the depressor help reduce pitch disturbances, yaw and roll disturbances are transmitted to the towfish with little or no attenuation.[27] The same can be said for sway or surge motion of the towfish.[19] Reference [19] shows that a relatively large ratio of depressor heave to towfish heave can cause greater disturbances in pitch. Heaving between the towed vehicle and depressor depends on the disturbance frequency of the towing vessel and the length of the pigtail. The greater the frequency or the longer the length of the pigtail, the smaller the heave of the towfish relative to the depressor and the smaller the resulting pitch motion is.[19]

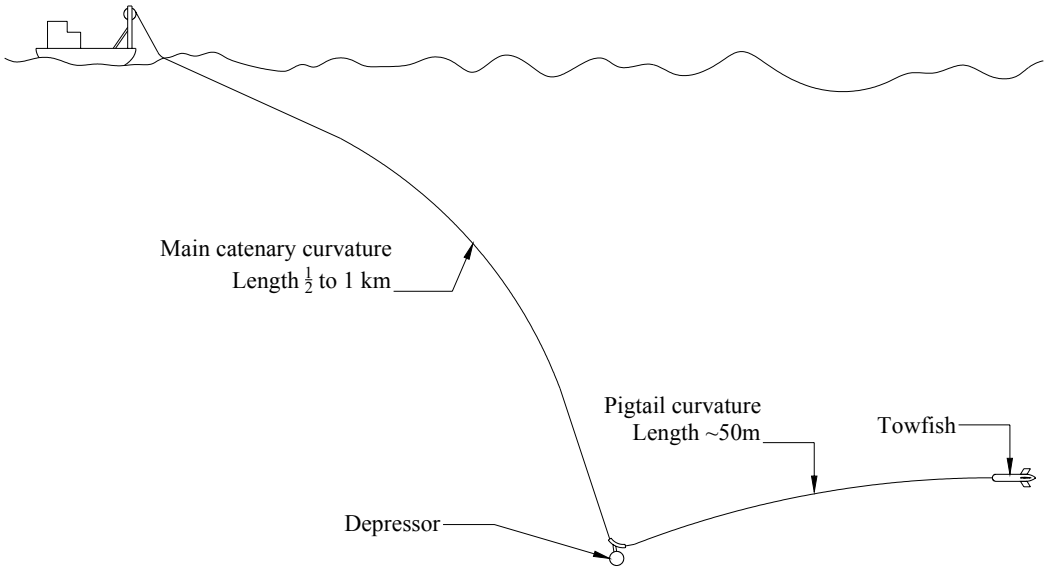

Figure 4 Possible tow configuration

Results for airborne towed vehicles can also be applied to underwater towed vehicles.[4] Though the medium through which the vehicle travels may be different, a parametric study of air vehicles can provide insight for the towfish. Because drag nominally acts along the centerline of the towed body, an increase in drag will have little effect on its pitch angle and will cause the bow in the main catenary to decrease, as described in reference [4]. This will make the towed vehicle more susceptible to surge disturbances of the towing vehicle. An increase in horizontal tail span will also increase drag but it will help to reduce the steady state equilibrium pitch angle. The vertical tail will also introduce more drag although increasing the span helps reduce the yaw and roll motions of the towed vehicle. Increasing the scope of the cable helps to reduce lateral and longitudinal response of the towed vehicle. The most benefit is gained from the pitch response to surge in the towing vehicle.

There are many tradeoffs in the design of a towfish. Typically the fin size can be increased and one can expect more stability. Increasing the span will allow this increase in stability whereas increasing the chord can ultimately reduce the stability due to the reduction in aspect ratio. Even still, increasing the span can cause yaw deflections from

an aileron input (deflection of the stern planes antisymmetrically). Although the yaw angle is not directly being controlled and not a design constraint this should be taken into consideration. Placement of the center of gravity can affect both static and dynamic stability. In the static case, it can cause a steady state pitch deflection and in the dynamic case, if the pitch deflection is great enough, the longitudinal and lateral states can couple causing lateral instabilities.[18] However, a low CG can be helpful in restoring both pitch and roll and is often preferred.

To develop a reasonable control law, the towfish should be modeled so that simulations can be performed. However, modeling a body traveling through a fluid can be complex. There are linear and nonlinear hydrodynamic terms as well as poorly modeled phenomena such as separation of the flow from the body. Typically, the hydrodynamic forces of the towfish are modeled with coefficients determined from the vehicle geometry. This allows the model to be either complex or simple; accounting for nonlinear hydrodynamic effects may not be crucial depending on the operating envelope. Modeling of the tow cable significantly increases the complexity. A simple model is ideal but it should capture the important characteristics of the towed vehicle, cable and depressor.

Before developing a model, it is important to review existing models. Both [16] and [19] have developed models for a cable-depressor-towfish arrangement which simulate the dynamics of the towing cable and depressor, as well as the towfish, however the vehicle in [19] is not controlled. The simulation in reference [16] cannot be used for high frequency dynamics where cable lengths exceed 1 km.[16] It is expected that the cable length required for the towfish to reach a depth of 200 meters will be close to 1 km as can be seen from Figure 5 and Table 1. The authors discuss three different control strategies one of which is a PID controller which was found to be limited by saturation and integral wind up problems although it showed slight improvements in pitch control.[16] This reference verifies the advantages of the use of a depressor weight to reduce ship induced motion of the towfish. It also shows that less cable scope can be used to reach a specific depth with the use of a depressor.

Longitudinal motion stabilization was discussed in [29] and [31]. A moving mass controller can significantly enhance the stability of underwater vehicles traveling at low speeds.[29] Due to the mass of the vehicle and size requirements, a moving mass actuator would require too much space to implement and the towfish travels fast enough for the fins to be effective. A towfish with an actuated stern plane and wing allows for both attitude and depth control which is often required for bottom following missions.[31],[26] In [32], it was shown that a PID controller is not able to meet both pitch and depth requirements. However, precise depth control is not necessary for this vehicle so a wing is not required and a PID controller should be sufficient.

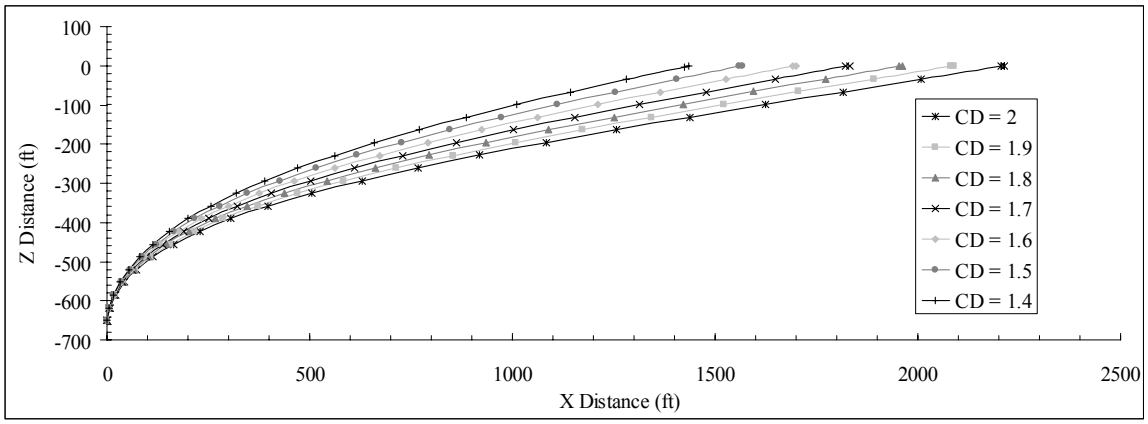

Figure 5 Cable profiles for a single body tow at 6 kts using a 0.325 inch diameter bare cable with a specific weight of 5 for various drag coefficients. Towed body is 800 lbs,1 ft diameter sphere. Created with a program called QCAT developed by the Naval Surface Warfare Center

Table 1 Cable scopes from Figure 5

C_D	Scope, ft	(meters)
2	2344.22	715
1.9	2226.79	679
1.8	2106.59	642
1.7	1986.12	605
1.6	1863.7	568
1.5	1741.58	531
1.4	1620.25	494

Full simulations are not only important for a controller design but are also important to understand the inherent stability of the towing configuration. They can allow the designer to capture the complex hydrodynamics that affects the towed vehicle and depressor. However, this is not necessary for the problem at hand as Dr. Ann Gargett has shown successful tows which can maintain stability in pitch and roll to within ±2 degrees.[15] This level of stability was obtained for a towed vehicle that was neither streamlined nor actively controlled. The same towing arrangement will be implemented, however an actively controlled streamlined towfish will be used.

This paper will show that a conventional PID controller can enhance the performance of a towfish in a two part towing arrangement. This type of controller will be shown to be robust. Mode approximations will provide insight into the linear dynamics of the towfish which will aid in determining critical parameters of the design. This thesis serves as a design document and, to some extent, a user's manual for the proposed towfish.

1.3. Outline of Thesis

Section 2 covers the kinematics and dynamics of a towed streamlined body with a rear cruciform tail configuration that has actuated stern planes and fixed rudders. The center of gravity (CG) will nominally rest directly below the center of buoyancy (CB). Both the nonlinear and linear equations will be developed.

A semi-empirical hydrodynamic force representation will be derived. A tow force model will be developed that will only focus on the motions of the depressor rather than the interaction of the towfish, ship and depressor. Approximations to modes of the towfish motion will be made and fin sizing will be discussed.

Section 3 will review design parameters and how they affect critical design choices. Section 4 will describe the PID control design. Various methods will be discussed and the Zeigler-Nichols frequency method used as a starting point for gain tuning. Gains will be discussed for various speeds and pigtail lengths. The controller will be validated using a Matlab™ simulation based on the hydrodynamic model in Section 2. Section 5 will show the results of simulations with a random input. Towfish parameters will be varied to investigate the robustness of the controller.

Section 6 will describe the mechanical design and all components. In Section 7, conclusions about towfish design limitations are drawn.

2. Equations of Motion

In the pursuit of efficient and cost effective solutions to today's vehicle engineering problems, it is important to evaluate the performance of any design before it is created. To do so, computer simulations are often employed to validate a design. For computer simulations, the equations of motion are needed. The following sections describe the model used to derive and validate the controller. The parameters of the towfish used for simulation are given in Appendix A – Towfish Parameters. All units are SI unless otherwise stated.

2.1. Kinematics and Dynamics

The kinematic relationships for a body with 6 degrees of freedom (DOF) are given first. Next, the dynamic equations are presented for a streamlined cylindrical body with fins being towed in a quiescent fluid. The equations are linearized and specific modes are studied to gain insight into design issues. This representation is used in a nonlinear Matlab™ simulation which includes actuator rate limits.

A body fixed coordinate system is placed at the center of buoyancy (CB) which is the center of mass of the fluid displaced by the body. This is assumed to be approximately at the geometric center of the body. The x_b and z_b axes lie in the plane of symmetry containing the rudder. The x_b axis points out of the nose and the y_b axis completes the right-handed reference frame. The variable $X_I = [x, y, z]^T$ is the towfish position relative to an inertial frame, $\Phi_I = [\phi, \theta, \psi]^T$ are the Euler angles representing the towfish attitude with respect to the inertial frame, $V = [u, v, w]^T$ is the inertial velocity represented in the body fixed frame and $\Omega = [p, q, r]^T$ is the towfish angular velocity with respect to the inertial axes represented in the body frame . See Figure 6.

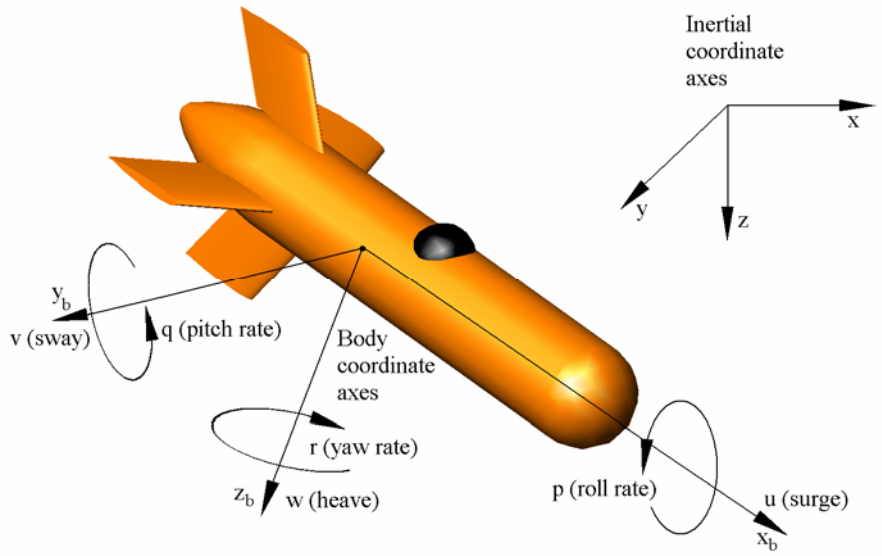

Figure 6 Body and inertial coordinate axes definition. Body axes located at the center of buoyancy

The state of the towfish can be written as follows

$$X = \begin{bmatrix} X_I \\ \Phi_I \\ V \\ \Omega \end{bmatrix} \tag{1}$$

The translational kinematic equation is[11]

$$\dot{X}_I = R_{IB} V \tag{2}$$

Where the matrix R_{IB} is a rotation matrix from the body coordinates to inertial coordinates. Using a conventional 3-2-1 rotation:

$$R_{IB} = \begin{bmatrix} \cos\psi\cos\theta & -\sin\psi\cos\phi + \cos\psi\sin\theta\sin\phi & \sin\psi\sin\phi + \cos\psi\cos\phi\sin\theta \\ \sin\psi\cos\theta & \cos\psi\cos\phi + \sin\phi\sin\theta\sin\psi & -\cos\psi\sin\phi + \sin\theta\sin\psi\cos\phi \\ -\sin\theta & \cos\theta\sin\phi & \cos\theta\cos\phi \end{bmatrix}$$

The rotational kinematic equation is[11]

$$\begin{bmatrix} \dot{\phi} \\ \dot{\theta} \\ \dot{\psi} \end{bmatrix} = \begin{bmatrix} 1 & \sin\phi\tan\theta & \cos\phi\tan\theta \\ 0 & \cos\phi & -\sin\phi \\ 0 & \dfrac{\sin\phi}{\cos\theta} & \dfrac{\cos\phi}{\cos\theta} \end{bmatrix} \begin{bmatrix} p \\ q \\ r \end{bmatrix} \tag{3}$$

The dynamic equations are presented for a cylindrical body with a 6 to 1 fineness ratio that is shown in Figure 7.

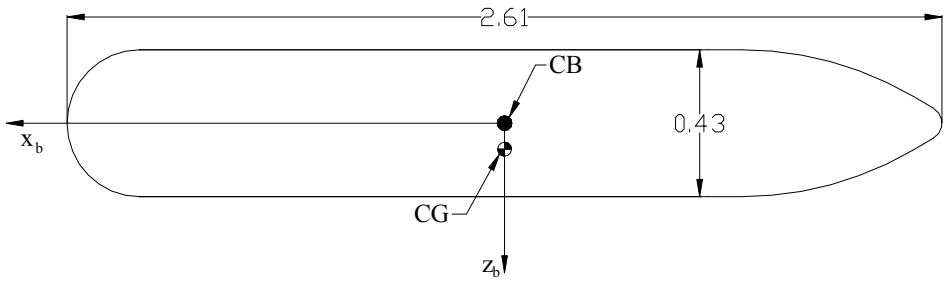

Figure 7 Location of CB and CG. Units in meters

Significant forces are required to accelerate the fluid around the body as it moves through the fluid. These forces are taken into account with added mass terms. Define the 3x3 matrix M as the rigid body mass and added mass matrix given by

$$M = \begin{bmatrix} m(1+k_1) & 0 & 0 \\ 0 & m(1+k_2)+Y_{\dot{v}f} & 0 \\ 0 & 0 & m(1+k_2)+Z_{\dot{w}f} \end{bmatrix}$$

The rigid body inertia and added inertia matrix is

$$J = \begin{bmatrix} I_x + K_{\dot{p}f} & -I_{xy} & -I_{xz} \\ -I_{xy} & I_y(1+k_3)+M_{\dot{q}f} & -I_{yz} \\ -I_{xz} & -I_{yz} & I_z(1+k_3)+N_{\dot{r}f} \end{bmatrix}$$

The added mass coefficients, $Y_{\dot{v}f}$, $Z_{\dot{w}f}$ and added inertia coefficients, $M_{\dot{q}f}$, $N_{\dot{r}f}$, $K_{\dot{p}f}$ are due to the fins where, because of symmetry:

$$M_{\dot{q}f} = N_{\dot{r}f} \text{ and } Y_{\dot{v}f} = Z_{\dot{w}f}$$

To estimate the added mass of the fins, the added mass of a two-dimensional plate is used. From Newman[24], the two-dimensional added mass for a plate is.

$$Y_{\dot{v}f}^{2D} = \pi\rho\left(c/2\right)^2$$

where *c* is the chord length of the fins and water density is ρ. $Y_{\dot{v}f}$ is then calculated from Fossen[10] as

$$Y_{\dot{v}f} = \int_{-b/2}^{b/2} Y_{\dot{v}f}^{2D}\,dx = Y_{\dot{v}f}^{2D} b$$

where *b* is the tip to tip span of the fins. From Lewis[21], the added inertia from the fins is

$$N_{\dot{r}f} = l_f^2 Y_{\dot{v}f}$$

Where l_f is the length from the body axis origin to the fin's geometric center.

$K_{\dot{p}f}$ is calculated from Fossen[10] as

$$K_{\dot{p}f} = \int_{-c/2}^{c/2} K_{\dot{p}f}^{2D}\,dx = K_{\dot{p}f}^{2D} c$$

where the two dimensional added inertia coefficient, $K_{\dot{p}f}^{2D}$, is determined from Newman[24] as

$$K_{jf}^{2D} = \frac{2}{\pi}\rho\left(\frac{b}{2}\right)^4$$

For the body the added mass and added inertia terms are approximated by equations for a prolate spheroid for. Fossen[10] gives the values

$$k_1 = \frac{\alpha_0}{2-\alpha_0},\ k_2 = \frac{\beta_0}{2-\beta_0},\ k_3 = \frac{e^4(\beta_0-\alpha_0)}{(2-e^2)(2e^2-(2-e^2)(\beta_0-\alpha_0))}$$

where

$$\alpha_0 = \frac{2(1-e^2)}{e^3}\frac{1}{2}\ln\left(\frac{1+e}{1-e}\right) - e,\ \beta_0 = \frac{1}{e^2} - \frac{1-e^2}{2e^3}\ln\left(\frac{1+e}{1-e}\right)$$

and where e is the eccentricity:

$$e = (1-(D_b/l_b)^2)^{1/2}$$

The spheroid has a minor axis of length D_b and a major axis of length l_b. Although not a prolate spheroid, the towfish can be reasonably approximated as one. See Figure 8. The towfish nose is made bluff to reduce destabilizing separation when the vehicle is side slipping or has a non-zero angle of attack.

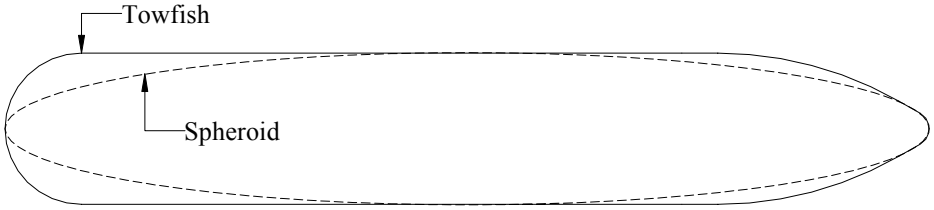

Figure 8 Comparison of towfish to prolate spheroid

The matrix D represents inertial coupling between translational and rotational motion which arises when the CG does not coincide with the body coordinate origin, in this case the CB:

$$D = \begin{bmatrix} 0 & -mz_{cg} & my_{cg} \\ mz_{cg} & 0 & -mx_{cg} + M_{\dot{w}f} \\ -my_{cg} & mx_{cg} + N_{\dot{v}f} & 0 \end{bmatrix}$$

where Lewis[21] gives for the added mass terms

$$N_{\dot{v}f} = l_f Y_{\dot{v}f}$$

and because of symmetry,

$$N_{\dot{v}f} = M_{\dot{w}f}$$

Note that

$$D^T = \begin{bmatrix} 0 & mz_{cg} & -my_{cg} \\ -mz_{cg} & 0 & mx_{cg} + Y_{\dot{r}f} \\ my_{cg} & -mx_{cg} + Z_{\dot{q}f} & 0 \end{bmatrix}$$

where Lewis[21] gives

$$Y_{\dot{r}f} = l_f Y_{\dot{v}f}$$

and because of symmetry

$$Z_{\dot{q}f} = Y_{\dot{r}f}$$

Kirchhoff's equations for motion of a rigid body in an ideal fluid, generalized to include exogenous forces and torques, are

$$\dot{P} = P \times \Omega + F_{ext} \tag{4}$$

$$\dot{\Pi} = \Pi \times \Omega + P \times V + M_{ext} \tag{5}$$

where P and Π are the linear and angular components of the impulse, respectively, which is required to generate the motion of the body and fluid.[20] Let T represent the total kinetic energy of the body-fluid system:

$$\mathrm{T} = \frac{1}{2}\left(\Omega^T J\Omega + 2\Omega^T DV + V^T MV\right)$$

Then

$$P = \frac{\partial \mathrm{T}}{\partial \mathrm{V}} = MV + D^T\Omega \tag{6}$$

$$\Pi = \frac{\partial \mathrm{T}}{\partial \Omega} = J\Omega + DV \tag{7}$$

With equations (6) and (7), we can rewrite (4) and (5) as

$$\begin{bmatrix} M & D^T \\ D & J \end{bmatrix} \begin{bmatrix} \dot{V} \\ \dot{\Omega} \end{bmatrix} = \begin{bmatrix} \left(MV + D^T\Omega\right)\times\Omega + F_{ext} \\ \left(J\Omega + DV\right)\times\Omega + \left(MV + D^T\Omega\right)\times V + M_{ext} \end{bmatrix} \tag{8}$$

F_{ext} and M_{ext} are the external force and moment vectors defined as

$$F_{ext} = \begin{bmatrix} F_{axial} \\ F_{lateral} \\ F_{normal} \end{bmatrix} = F_{body} + F_{tail} + F_{tow} + F_{weight} + F_{buoyancy}$$

$$M_{ext} = \begin{bmatrix} M_{roll} \\ M_{pitch} \\ M_{yaw} \end{bmatrix} = M_{body} + M_{tail} + M_{tow} + M_{damping} + M_{weight}$$

The force and moment terms are defined in Table 2.

Table 2 Definition of force and moment subscripts

Force/Moment	Description
F_{ext}	External force applied to the towfish represented in the body axes
F_{axial}	Component of F_{ext} along the x_b axis
$F_{lateral}$	Component of F_{ext} along the y_b axis
F_{normal}	Component of F_{ext} along the z_b axis
F_{body}	Hydrodynamic force acting on the external surface of the hull represented in the body axes
F_{tail}	Hydrodynamic force acting on the stern plane and rudder represented in the body axes
F_{tow}	Towing force from the pigtail acting at the nose of the towfish represented in the body axes
F_{weight}	Weight of the towfish represented in the body axes
$F_{buoyancy}$	Buoyancy of the towfish represented in the body axes
M_{ext}	External moment applied to the towfish represented in the body axes
M_{roll}	Component of M_{ext} about the x_b axis
M_{pitch}	Component of M_{ext} about the y_b axis
M_{yaw}	Component of M_{ext} about the z_b axis
M_{body}	Hydrodynamic moment acting on the external surface of the hull represented in the body axes
M_{tail}	Hydrodynamic moment due to the stern plane and rudder represented in the body axes
M_{tow}	Towing moment from the pigtail acting represented in the body axes
$M_{damping}$	Damping moment on the towfish represented in the body axes
M_{weight}	Moment due to CG offset represented in the body axes

2.2. Body Force and Moment

The forces and moments contributed by the body are determined from empirical data taken from the US Airship Akron and prediction methods found in Nelson.[23] NACA Report No. 432[13] describes the results of force measurements on a 1/40 scale model of the US Airship Akron. The airship has a fineness ratio of 5.9 which is comparable to the towfish fineness ratio of 6. Geometrically, the hull of the airship and the towfish are similar.[14] The airship was tested at various Reynolds numbers which are comparable to those that will be experienced by the towfish. One noticeable difference between the two vehicles is that the model airship was given a smooth sanded surface. The finish of the towfish is un-sanded fiberglass with multiple drain holes. To compensate for the added drag on the towfish an empirical formula from Hoerner[17] is used.

The data used are taken from Table I in NACA Report No. 432[13] for a Reynolds number of 3.3×10^6. The Reynolds number of the towfish will be around 1.5×10^6. The data presented are non-dimensionalized using dynamic pressure and the hull volume. Lift, drag and pitching moment are calculated for various pitch angles for the Akron. Data are used up to about a 12 degree pitch angle. A linear fit is used for the pitching moment and lift while a quadratic fit is used for drag. The plotted data and polynomial fit for drag can be seen in Figure 9. The model is symmetric about the x_b-y_b and x_b-z_b planes therefore the drag is expected to be nominally at a minimum when it has only velocity along the x_b axis. This requires the drag data from the U.S. Akron to be slightly modified.

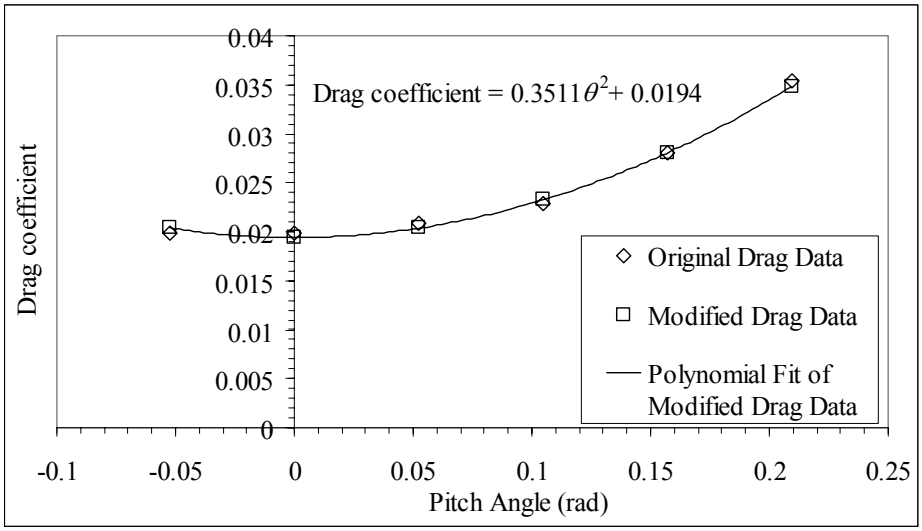

Figure 9 US Akron drag data. Data modified to force the zero pitch angle to be the minimum for the polynomial fit to determine $C_{D\alpha b}$ and C_{D0}

From Figure 9, assuming that the pitch angle of the Akron data is approximately equal to the angle of attack of the Akron, it is determined that

$$C_{D\alpha b} = 0.3511,\ C_{D0} = 0.0194$$

The additional zero degree angle of attack drag from Hoerner is[17]

$$C_{Db0} = 0.44(D_b / l_b) + 4C_f (l_b / D_b) + 4C_f \sqrt{D_b / l_b}$$

where l_b is the length of the body, C_f is the skin friction coefficient of the hull and D_b is the diameter of the hull

Figure 10 show the linear fit for the lift data

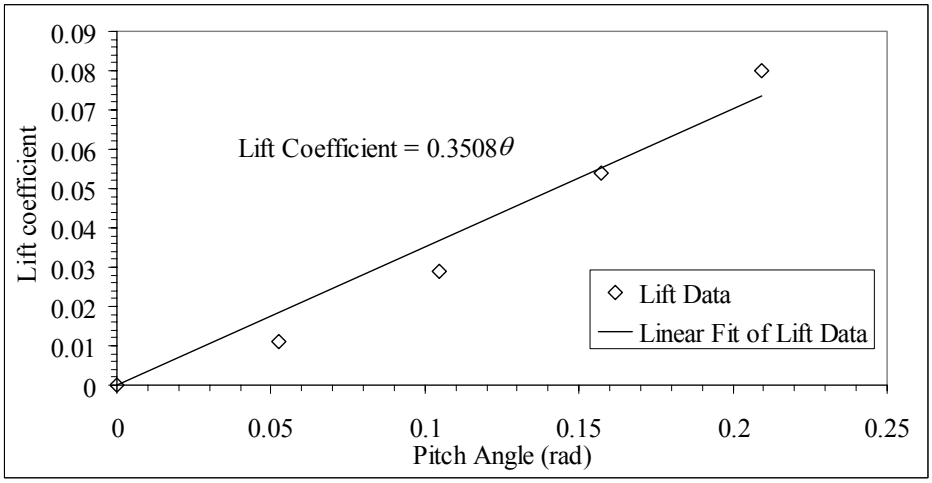

Figure 10 US Akron lift data used to determine $C_{L\alpha b}$

From Figure 10 it is determined that

$$C_{L\alpha b} = 0.3508$$

Next, define a "current" frame whose origin is at the vehicle CB. The current x axis is defined by the velocity vector of the towfish with respect to the local body of water. The z_c axis is perpendicular to the x_c axis and is in the plane of symmetry of the vehicle and rudder (opposed to the plane of symmetry of the vehicle and stern planes) and the y_c axis completes the right hand coordinate frame. The variables α and β are the hydrodynamic angles defined by the velocities in the body axes as

$$\alpha = \arctan\left(\frac{w}{u}\right)$$

$$\beta = \arcsin\left(\frac{v}{|V|}\right)$$

$$|V| = \sqrt{u^2 + v^2 + w^2}$$

The matrix R_{BC} is a rotation matrix from the local water current axes to body axes that is defined by

$$R_{BC} = \begin{bmatrix} \cos(\alpha)\cos(\beta) & -\cos(\alpha)\sin(\beta) & -\sin(\alpha) \\ \sin(\beta) & \cos(\beta) & 0 \\ \cos(\beta)\sin(\alpha) & -\sin(\alpha)\sin(\beta) & \cos(\alpha) \end{bmatrix}$$

The variable μ, shown in Figure 11, can also be considered a hydrodynamic angle.

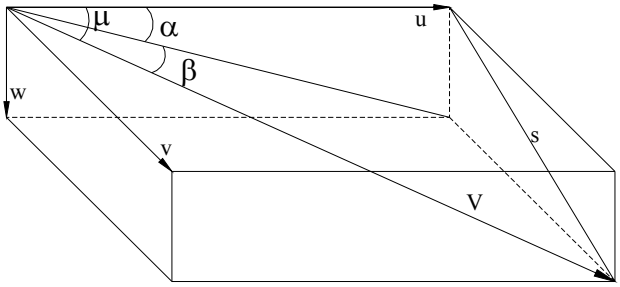

Figure 11 Hydrodynamic angles

From the figure the following can be seen

$$s = \sqrt{v^2 + w^2}$$

$$\sin(\mu) = \frac{s}{|V|}$$

Therefore

$$\mu = \arcsin\left(\sqrt{\frac{v^2 + w^2}{|V|^2}}\right)$$

For small angles

$$\mu \approx \sqrt{\beta^2 + \alpha^2}$$

Assuming that the pitch angle of the Akron data is approximately equal to the angle of attack of the Akron then the slope of the linear fit in Figure 10 is $C_{L\alpha b}$, the lift slope coefficient. Because of the symmetry of the towfish about the x_b axis the side force due to side slip is assumed to have the same relationship that lift does with angle of attack. In both cases a linear lift and side force relationship is assumed. For drag, a parabolic relationship is assumed. The drag coefficient, $C_{D\alpha b}$, and zero degree angle of attack/side

slip drag C_{D0} are determined from Figure 9. Because of symmetry of the towfish the angle of attack and side slip angle are combined into a single angle μ. Therefore the hydrodynamic forces developed by the body can be written as

$$F_{body} = R_{BC}\left(\begin{bmatrix} -C_{D\alpha b}\mu^2 + C_{D0} \\ -C_{L\alpha b}\beta \\ -C_{L\alpha b}\alpha \end{bmatrix}\bar{q}Vol^{2/3} + \begin{bmatrix} -C_{Db0} \\ 0 \\ 0 \end{bmatrix}\bar{q}S_b\right)$$

where dynamic pressure is defined by

$$\bar{q} = \frac{1}{2}\rho|V|^2$$

and the reference area of the body is defined by

$$S_b = \pi\frac{D_b^2}{4}$$

The pitching moment on the body was again taken from data on the U.S. Airship Akron; see Figure 12.

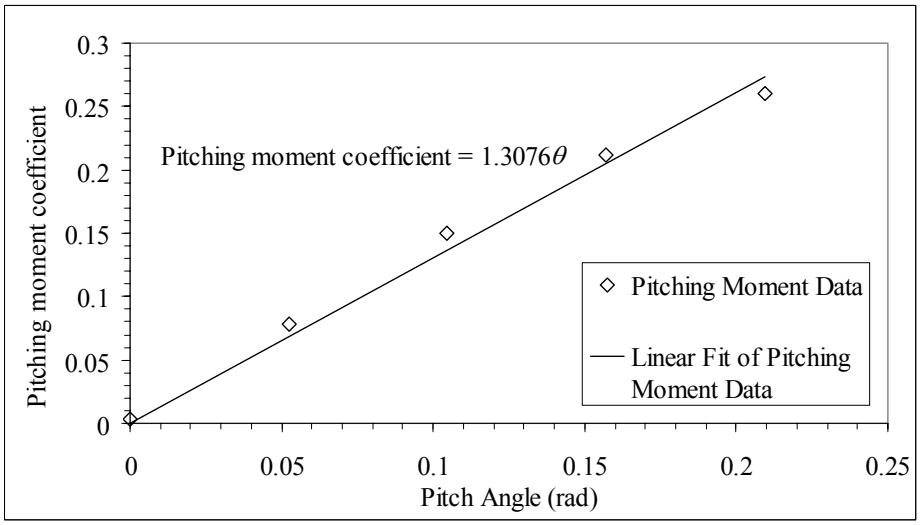

Figure 12 US Akron pitching moment data used to determine $C_{m\alpha b}$

From Figure 12 it is determined that

$$C_{m\alpha b} = 1.3076$$

Therefore the pitching and yawing moment due to a nonzero angle of attack or side slip is

$$M_{body} = \begin{bmatrix} 0 \\ -C_{m\alpha b}\beta \\ C_{m\alpha b}\alpha \end{bmatrix} \bar{q} Vol$$

2.3. Tail Force and Moment

The forces and moments from the fins are composed of the lift due to angle of attack for the stern planes, side force due to side slip for the rudder and induced drag for both. The fin lift curve slope is approximated as[1]

$$C_{L\alpha} = \frac{2\pi}{1 + \frac{2\pi}{\pi AR}}$$

where AR is the aspect ratio.

The force coefficients for each fin represented in the water current axes are defined as follows

$$C_{c1} = \begin{bmatrix} \frac{-C_{L\alpha}\beta^2}{\pi\varepsilon AR} \\ -C_{L\alpha}\beta \\ 0 \end{bmatrix}, C_{c2} = \begin{bmatrix} \frac{-C_{L\alpha}(\alpha + d_2)^2}{\pi\varepsilon AR} \\ 0 \\ -C_{L\alpha}(\alpha + d_2) \end{bmatrix}, C_{c3} = \begin{bmatrix} \frac{-C_{L\alpha}\beta^2}{\pi\varepsilon AR} \\ -C_{L\alpha}\beta \\ 0 \end{bmatrix}, C_{c4} = \begin{bmatrix} \frac{-C_{L\alpha}(\alpha + d_4)^2}{\pi\varepsilon AR} \\ 0 \\ -C_{L\alpha}(\alpha + d_4) \end{bmatrix}$$

The fin deflections d_2 and d_4 correspond to fin numbers 2 and 4, respectively, and are independently actuated. The parameter ε is the span efficiency factor.[1] Note that a positive fin deflection is leading edge up and trailing edge down. The force developed from the fins can be represented as

$$F_{tail} = R_{BC}(C_{c1} + C_{c2} + C_{c3} + C_{c4})\bar{q} S_t 1/2$$

Because the area, S_t, is the planform area of the entire span of either the vertical tail or the horizontal tail, the factor of ½ is necessary to calculate the planform area of a single fin. The 'c' subscript means the coefficient is represented in the water current axes and the numerical subscript refers to a specific tail fin. The numbering of the fins can be seen in Figure 13 where the towfish is shown upright.

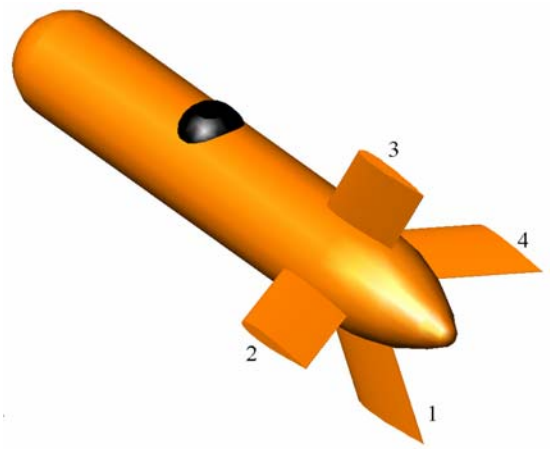

Figure 13 Fin numbering

Let the vector X_{aci} represent the distance from the body axis origin to the hydrodynamic center of the ith fin. The moment provided by the tail is

$$M_{tail} = \bar{q} S_t \frac{1}{2} \sum_{i=1}^{4} X_{aci} \times C_{bi}$$

where

$$C_{bi} = R_{BC} C_{ci}, \; i = 1,2,3,4$$

First order actuator dynamics are included using the equations

$$\dot{d}_2 = \frac{1}{\tau}(\delta_2 - d_2), \; \dot{d}_4 = \frac{1}{\tau}(\delta_4 - d_4)$$

The actuator specifications include a rate limit of 90 deg/second. This rate limit can be crudely accounted for by choosing the actuator time constant, τ, appropriately. First, consider that the fin stall angle is about 20 degrees; the fins will be hard limited to this range. Given the rate limit of 90 deg/second, it would take 0.22 seconds for the actuators to reach 20^o. For a first order, exponential response, 99.3% of the commanded angle is reached in 5τ seconds. Therefore, the constant τ is taken to be 0.044 seconds. This ensures that, in simulations, the fins will travel at their maximum rate of 90 deg/second when the commanded angle is 20 degrees.

2.4. Towing Force and Moment

The towing force (F_{tow}) can be complicated. It is affected by the length of cable, weight of the depressor, size and shape of the tow vessel, roughness of seas and lift and drag on the cable among other things. As an infinite dimensional system, the tether has its own dynamic modes with boundary conditions given by the towing vessel, depressor and

towfish motions. Constructing a model of the towing tether, which would include the main catenary and pigtail, is beyond the scope of this paper. Such simulations can be found in references [2], [16], [19], [31], [18] and [26]. A simulation program called DYNTOCABS developed by J.W. Kamman and the Naval Surface Warfare Center-Panama City (NSWC-PC) is a very powerful tool to simulate multiple bodies in tow. The user manual is available from NSWC-PC.

Preliminary towing results, obtained by Dr. Ann Gargett, show good stability (+/- 2^o pitch and roll) in a two part towing arrangement with a non-streamlined body without active control. Although the interaction of the tether, depressor and towfish are complicated, the towing arrangement used has shown inherent stability. Therefore, the tow ship and main catenary are ignored in the present model; the focus is on random motions of the depressor and its effect on towfish stability. A conservative estimate of the towing force is made and the depressor is prescribed a specific motion. The pigtail section is represented as a spring and damper between the depressor weight and the towfish. When the distance from the depressor to the nose of the towfish is less than the length of the pigtail, the force from the spring and damper is zero. See Figure 14.

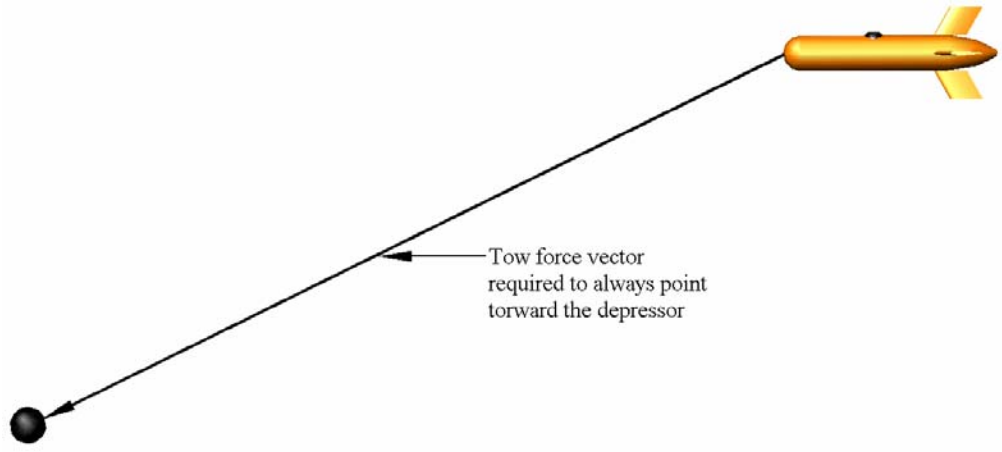

Figure 14 Tow force representation

$U_{depressor}$ and $X_{depressor}$ are the velocity and position of the depressor, respectively. The distance from the tow point of the towfish to the depressor is

$$\Delta x = X_{depressor} - \left(X_1 + R_{IB} \begin{bmatrix} l_b/2 \\ 0 \\ 0 \end{bmatrix} \right)$$

The difference in velocity of the tow point of the towfish and the depressor is

$$\Delta u = U_{depressor} - \left(R_{IB} V + R_{IB} \left(\Omega \times \begin{bmatrix} l_b / 2 \\ 0 \\ 0 \end{bmatrix} \right) \right)$$

The spring and damper coefficients are determined as follows

$$\bar{k} = EA / L$$
$$\bar{b} = M_{1,1} 2\zeta\omega_n$$

$$\omega_n = \sqrt{\frac{\bar{k}}{M_{1,1}}}$$

The damping ratio ζ was chosen to be 1. The value EA was determined from reference [7]. The length L is the nominal length of the pigtail. F_{td} is the force developed along the tether. In a coordinate frame for which the x-axis points from the towfish nose to the depressor,

$$F_{td} = \begin{bmatrix} \bar{k}\left(|\Delta x| - L\right) + \bar{b}\left(\Delta u \bullet \frac{\Delta x}{|\Delta x|} \right) \\ 0 \\ 0 \end{bmatrix}$$

This model of the tow force causes long computation time due to the large stiffness of the spring which causes very fast dynamics compared to the slow dynamics of the towfish. This stiffness can be significantly reduced without greatly affecting the disturbances passed through the pigtail from the depressor. The -3dB point of the reduced spring stiffness is at 1.38 rad/sec. This modification allows for much faster computation times.

A concern for choosing the spring stiffness is the possibility that the natural frequency of the towfish may resonate with a fundamental frequency of the pigtail. DYNTOCABS simulation suggest that the system is very well damped, making resonance issues unlikely.

Without the main catenary to tow the depressor and keep it from sinking, the depressor is modeled as a point with no weight, buoyancy or hydrodynamic forces. This depressor point is allowed to move randomly. Its random motions are described by the JONSWAP[22] wave spectrum which provides an energy density spectrum of wave amplitudes given significant wave height and wave modal period for a specific sea state. See Figure 15 for a sample JONSWAP wave spectrum.

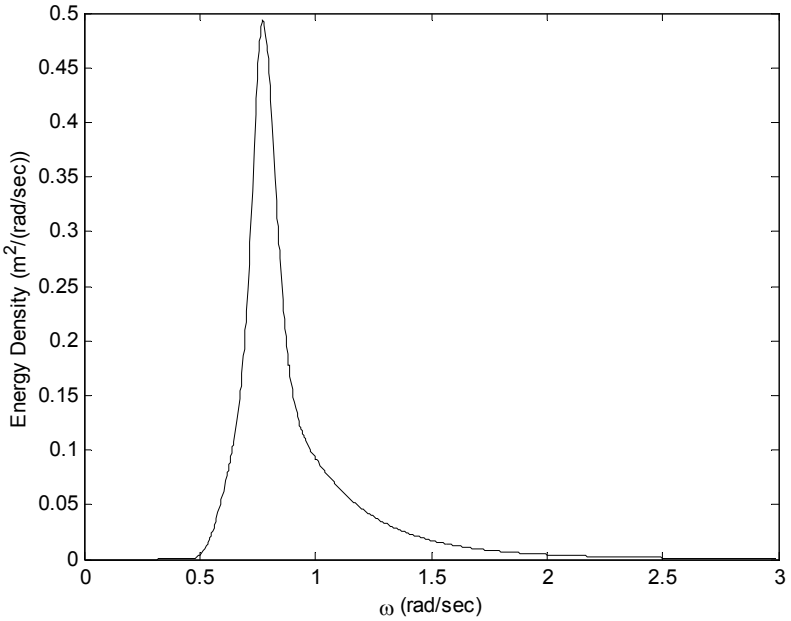

Figure 15 JONSWAP wave spectrum for significant wave height of 1.4 meters and modal period of 6.275 seconds, representative of sea state 4.

A random signal is generated from this wave spectrum by summing approximately 50[22] sinusoids at various frequencies within the significant frequency content (up to 3 rad/sec) of the JONSWAP wave spectrum. See Figure 16 for a sample random signal. This signal provides an estimate of wave heights in fully developed seas at sea state 4.

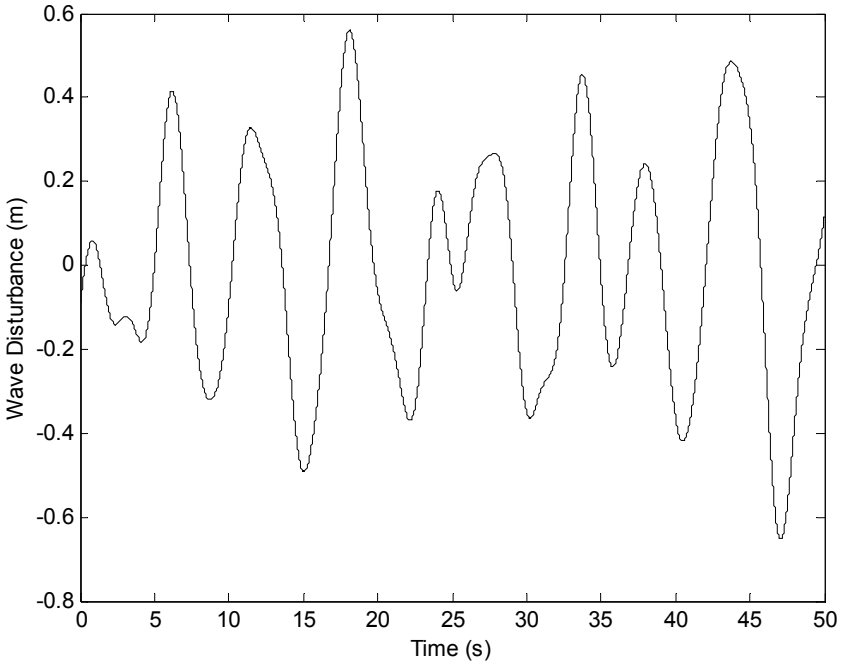

Figure 16 Random signal generated from a summation of sinusoids at various frequencies with significant energy density in the JONSWAP wave spectrum.

The ship motions that correspond to this wave history will depend on where the waves impact the ship and various parameters of the ship. It would be labor intensive to recreate the motions of the depressor due to the ship. Moreover, a variety of towing vessels may be used in a variety of conditions. A simple, highly conservative case is considered in which the wave motion is assumed to be transmitted directly to the depressor. The depressor position is

$$X_{depressor} = \begin{bmatrix} U_0 t \\ y_{random} + \frac{H}{4}\cos(\omega_{dep} t) \\ z_{random} + \frac{H}{4}\sin(\omega_{dep} t) \end{bmatrix}, \ \omega_{dep} = \sqrt{g / x_{depth}}$$

where t is time, H is the significant wave height and the frequency of oscillations is ω_{dep}

The random signal generated from the JONSWAP spectrum along the inertial y axis is y_{random} and along the inertial z axis is z_{random}. The factor of ¼ in the depressor position vector is to scale the disturbance so it is within the significant wave height. The frequency of oscillation accounts for the natural frequency of the depressor. The length, x_{depth}, is set to 200 meters in simulations. Although the actual scope of the main catenary is much greater, this is the maximum depth of the depressor. The velocity of the depressor is determined by differentiating its position. Figure 17 shows sample motion of the depressor when viewed in the y-z plane.

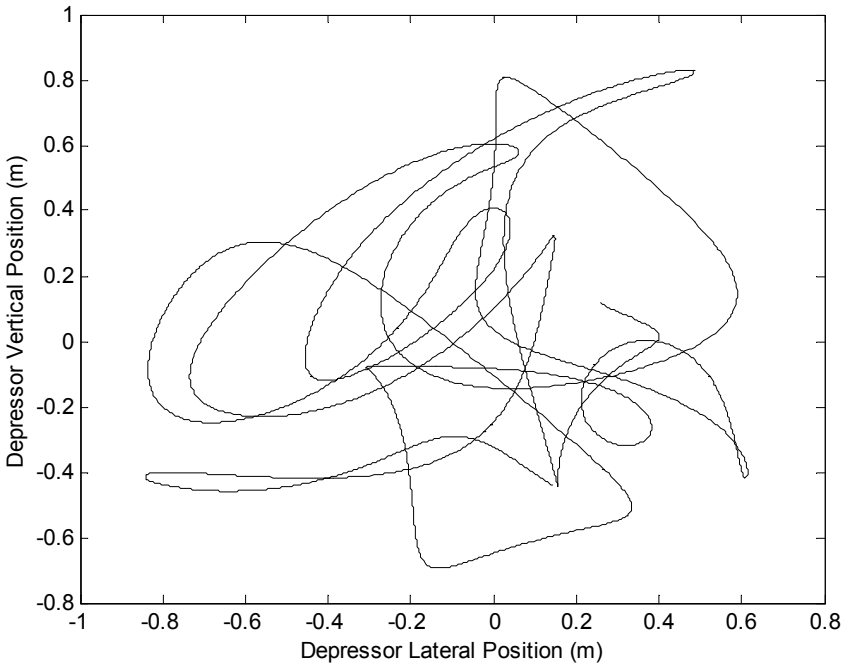

Figure 17 Depressor position viewed in the inertial y-z plane

It is important to understand that the depressor motion model does not account for surge disturbances. These would tend to pitch the towfish, since the CG is nominally below the tow point. However, this model takes the disturbance due to surface waves and transfers them unfiltered to the towfish. Thus the model is, in some sense, a worst-case scenario.

To rotate the towing force into the towfish body coordinates, a tether to inertial axes rotation matrix is defined by:

$$R_{IT} = \begin{bmatrix} \cos(\gamma)\cos(\sigma) & -\cos(\gamma)\sin(\sigma) & -\sin(\gamma) \\ \sin(\sigma) & \cos(\sigma) & 0 \\ \cos(\sigma)\sin(\gamma) & -\sin(\gamma)\sin(\sigma) & \cos(\gamma) \end{bmatrix}$$

where, similar to the aerodynamic angles in aircraft dynamics,

$$\gamma = \arctan\left(\frac{\Delta x_{3,1}}{\Delta x_{1,1}}\right)$$

$$\sigma = \arcsin\left(\frac{\Delta x_{2,1}}{|\Delta x|}\right)$$

The angles are shown in Figure 18.

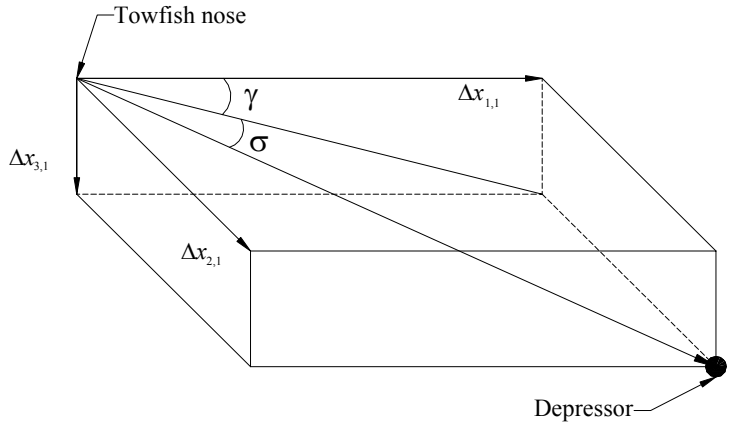

Figure 18 Tow force vector angle representation

The towing force on the body is

$$F_{tow} = R_{IB}{}^{T} R_{IT} F_{td}, \quad |\Delta x| > L$$

$$F_{tow} = 0, \quad |\Delta x| \le L$$

The moment due to the tow force is

$$M_{tow} = \begin{bmatrix} l_b / 2 & 0 & 0 \end{bmatrix}^T \times F_{tow}$$

2.5. Gravitational and Buoyant Force and Gravitational Moment

As stated before, the towfish will be 5% buoyant. The weight and buoyant forces are

$$F_{weight} = R_{IB}{}^T \begin{bmatrix} 0 \\ 0 \\ W_b \end{bmatrix}$$

$$F_{buoyancy} = -(1.05) R_{IB}{}^T \begin{bmatrix} 0 \\ 0 \\ W_b \end{bmatrix}$$

Because the CG is nominally below the CB, when the towfish pitches or rolls a restoring moment will be generated. This moment due to the offset CG is

$$M_{CG} = X_{CG} \times F_{weight}$$

2.6. Damping Moments

As the towfish pitches, rolls and yaws there will be resistance to that motion from the fluid surrounding it. The estimated roll damping moment coefficient is[23]

$$C_{lp} = -\frac{C_{L\alpha}}{12} \frac{1 + 3(c_t / c_r)}{1 + (c_t / c_r)}$$

where c_t is the tip chord and c_r is the root chord. For a tail with a constant chord the roll damping coefficient reduces to

$$C_{lp} = -2 \frac{C_{L\alpha}}{3}$$

The term is multiplied by 2 to account for both the vertical and horizontal tail section.

The estimated pitch damping moment coefficient is[23]

$$C_{mq} = -2\eta C_{L\alpha} V_t \frac{l_t}{c}$$

where

$$V_t = \frac{l_t S_t}{l_b S_b}$$

Length l_t is the distance from the hydrodynamic center of a fin to the CB of the towfish and l_b is the length of the body of the towfish. The tail chord length is c. The area S_t is the planform area of the stern plane or rudder. Typically, in aircraft dynamics, V_t, the tail volume ratio, is defined as the planform area of the tail times the moment arm of the tail divided by the planform area of the main wing times a characteristic length. Because there is no wing, length and area parameters of the body are used. In dimensional form the moments are[23]

$$L_p p = \left(C_{lp} \bar{q} S_b b \frac{b}{2U_0} \right) p$$

$$M_q q = \left(C_{mq} \bar{q} S_b l_b \frac{l_b}{2U_0} \right) q$$

$$N_r r = \left(C_{mq} \bar{q} S_b l_b \frac{l_b}{2U_0} \right) r$$

U_0 is the reference velocity. M_q and N_r are equal due to symmetry of the towfish.

2.7. Linearized Equations

The equations of motion are nonlinear but for small perturbations from the nominal motion, they can be approximated by linear equations. This approximation simplifies analysis of the towfish motion and development of a linear controller. The nominal motion or trajectory of the towfish is

$$\begin{aligned} X_{nom} &= \left[\tilde{x}(t) \;\; \tilde{y}(t) \;\; \tilde{z}(t) \;\; \tilde{\phi}(t) \;\; \tilde{\theta}(t) \;\; \tilde{\psi}(t) \;\; \tilde{u}(t) \;\; \tilde{v}(t) \;\; \tilde{w}(t) \;\; \tilde{p}(t) \;\; \tilde{q}(t) \;\; \tilde{r}(t) \right]^T \\ &= \left[U_0 t \;\; 0 \;\; 0 \;\; U_0 \;\; 0 \;\; 0 \;\; 0 \;\; 0 \;\; 0 \;\; 0 \;\; 0 \;\; 0 \right]^T \end{aligned} \tag{9}$$

$$\delta_{nom} = \left[\tilde{\delta}_2(t) \;\; \tilde{\delta}_4(t) \right]^T = \left[0 \;\; 0 \right]^T \tag{10}$$

where U_0 is the reference velocity and t represents time.

To linearize the kinematic and dynamic equations, (2), (3) and (8), the state rates are placed on the left side of the equations. For example, the body axis kinematic equation for inertial z position is

$$\dot{z} \equiv f_3(X,\delta) \equiv -u(\sin\theta) + v(\cos\theta\sin\phi) + w(\cos\theta\cos\phi)$$

The subscript 3 indicates the third equation of the set of kinematic and dynamic equations. The twelve equations are

$$\begin{aligned}
\dot{x} &\equiv f_1(x,y,z,\phi,\theta,\psi,u,v,w,p,q,r,\delta_1,\delta_2)\\
\dot{y} &\equiv f_2(x,y,z,\phi,\theta,\psi,u,v,w,p,q,r,\delta_1,\delta_2)\\
&\vdots\\
\dot{r} &= f_{12}(x,y,z,\phi,\theta,\psi,u,v,w,p,q,r,\delta_1,\delta_2)
\end{aligned}$$

Each equation is then expanded into a Taylor series and evaluated at the nominal condition, equations (9) and (10). For example,

$$\dot{z} = f_3(X,\delta)\big|_{nom} + \left.\frac{\partial f_3}{\partial x}\right|_{nom}(\Delta x) + \left.\frac{\partial f_3}{\partial y}\right|_{nom}(\Delta y)\cdots + \left.\frac{\partial f_3}{\partial \delta_1}\right|_{nom}(\Delta\delta_1)\cdots + h.o.t. \qquad (11)$$

where

$$\Delta x = x(t) - \tilde{x}(t), \text{ etc.}$$

Deviations from the nominal motion are expected to be small, so higher order terms are ignored. Noting that

$$f_3(X,\delta)\big|_{nom} = \dot{\tilde{z}}$$

and bringing it to the left hand side, one obtains

$$\frac{d}{dt}(\Delta z) = \left.\frac{\partial f_3}{\partial x}\right|_{nom}(\Delta x) + \left.\frac{\partial f_3}{\partial y}\right|_{nom}(\Delta y)\cdots + \left.\frac{\partial f_3}{\partial \delta_1}\right|_{nom}(\Delta\delta_1)\cdots$$

Repeating in a similar manner for each of the equations of motion, one obtains

$$\frac{d}{dt}(\Delta X) = A\Delta X + B\Delta\delta$$

where

$$A = \begin{bmatrix} \dfrac{\partial f_1}{\partial X_1} & \dfrac{\partial f_1}{\partial X_2} & \cdots \\ \dfrac{\partial f_2}{\partial X_1} & \ddots & \\ \vdots & & \end{bmatrix}_{nom} \quad \text{and} \quad B = \begin{bmatrix} \dfrac{\partial f_1}{\partial \delta_1} & \dfrac{\partial f_1}{\partial \delta_2} \\ \dfrac{\partial f_2}{\partial \delta_1} & \vdots \\ \vdots & \end{bmatrix}_{nom}$$

ΔX and $\Delta\delta$ represent small changes in the nominal values of the state and control variables.

$$\Delta X = X - \widetilde{X}\,,\ \Delta\delta = \delta - \widetilde{\delta}$$

After linearization it becomes apparent that the equations decouple into two sets of equations: the longitudinal and lateral-directional equations. The state vector of the longitudinal dynamics is denoted X_{long} while the state vector for the lateral-directional dynamics is denoted X_{lat}.

$$X_{long} = \begin{bmatrix} x \\ z \\ \theta \\ u \\ w \\ q \end{bmatrix},\ X_{lat} = \begin{bmatrix} y \\ \phi \\ \varphi \\ v \\ p \\ r \end{bmatrix}$$

Likewise, the A matrix is decomposed into A_{long} and A_{lat} and the B matrix is decomposed into B_{long} and B_{lat}. Noting that in the longitudinal motion, the fins deflect symmetrically and can be combined into one elevator deflection. Likewise, in the lateral/directional motion, the fins deflect antisymmetrically and can be combined into one aileron deflection. The fin deflections may also be decoupled by defining

$$\Delta\delta e = \Delta\delta 2 + \Delta\delta 4 \ \text{ and } \ \Delta\delta a = \Delta\delta 2 - \Delta\delta 4$$

Two decoupled linear systems can now be defined

$$\dot{X}_{long} = A_{long}\Delta X_{long} + B_{long}\Delta\delta e \ \text{ and } \ \dot{X}_{lat} = A_{lat}\Delta X_{lat} + B_{lat}\Delta\delta a$$

With the parameters (see Appendix A) of the final towfish design, the longitudinal and lateral-directional matrices are determined to be

$$A_{long} = \begin{bmatrix} 0 & 0 & 0 & 1 & 0 & 0 \\ 0 & 0 & -1 & 0 & 1 & 0 \\ 0 & 0 & 0 & 0 & 0 & 1 \\ 0 & -0.0002 & 0.2513 & -0.1276 & -0.0543 & 0.0861 \\ 0 & -0.0011 & 0.1144 & -0.0016 & -0.9348 & 0.6249 \\ 0 & 0.0028 & -0.5625 & 0.0115 & 0.7451 & -1.182 \end{bmatrix}$$

$$B_{long} = \begin{bmatrix} 0 \\ 0 \\ 0 \\ 0.1111 \\ -0.4735 \\ -1.5236 \end{bmatrix}$$

$$A_{lat} = \begin{bmatrix} 0 & 0 & 1 & 1 & 0 & 0 \\ 0 & 0 & 0 & 0 & 1 & 0 \\ 0 & 0 & 0 & 0 & 0 & 1 \\ -0.0006 & -0.4642 & -0.0306 & -0.8804 & -0.2455 & -0.3521 \\ -0.0047 & -10.192 & -0.2427 & -1.8458 & -6.9169 & -2.8349 \\ -0.0022 & 0.1602 & -0.1137 & -0.1140 & 0.0847 & -1.5273 \end{bmatrix}$$

$$B_{lat} = \begin{bmatrix} 0 \\ 0 \\ 0 \\ 0.6224 \\ 17.5317 \\ -0.2148 \end{bmatrix}$$

2.8. Modal Approximations

For the full 12-dimensional system, it is difficult to understand how certain parameters such as fin size or CG location affect different responses of the towfish. It is useful to reduce the order of the problem at hand by using modal approximations.[8] A mode is an eigenvalue/eigenvector pair. The approximation to the mode includes only the dominant states in that mode and clarifies the relationship between the towfish parameters and the modal response. By neglecting the effect of the less dominant modes, the system is decomposed into smaller subsystems with differing time scales. To determine an appropriate tail size, modal approximations are used. The validity of these approximations will be discussed in this section. The tail size will be determined in

Section 3.2. However, the results from that section are used here to show that the desired modes are well approximated.

It is important that the longitudinal mode approximation contain the pitch rate and the lateral/directional approximation contain the roll rate. The goal is to choose the appropriate tail size which allows for the best roll rate and pitch rate responses to fin deflections. The first approximation that is shown involves the longitudinal dynamics. It will be referred to as the pitch mode. The other approximation that follows involves the lateral/directional dynamics; it is referred to as the roll mode.

The first step in deriving the approximations is to determine which modes are fast and which are slow. If the mode that contains the desired state(s) is slow then one must consider the steady state effects of the faster states by including their steady state response in the approximation. However, if the mode that contains the desired state(s) is the fastest, then one need only consider the desired states and all other states are ignored. To determine if the desired modes are fast or slow, one examines the eigenvalues of the system. For the longitudinal states they are

$$\lambda_{long1} = -1.5149,\ \lambda_{long2,3} = -0.3015 \pm 0.4466i,\ \lambda_{long4} = -0.0050,\ \lambda_{long5} = -0.1213$$

where the units of the eigenvalues are per second. Notice there are only five eigenvalues as opposed to six. The first longitudinal state, x, was dropped due to its lack of effect on the other states. The real part of the eigenvalue indicates the relative speed of the response; the greater in magnitude, the faster the response. So it can be seen that the mode, λ_{long1} and the complex mode, $\lambda_{long2,3}$, are faster than the other longitudinal modes.

Similarly for the lateral directional states the eigenvalues are

$$\lambda_{lat1} = -4.838,\ \lambda_{lat2} = -2.125,\ \lambda_{lat3} = -1.5364,\ \lambda_{lat4,5} = -0.0387 \pm 0.0055,$$
$$\lambda_{lat6} = -0.7477$$

where the units of the eigenvalues are per second. Clearly, the first and second modes in the lateral states are the fastest relative to the other lateral eigenvalues.

Now it must be determined what, if any valid modal approximations can be made that will allow insight as to how fin span affects the pitch rate and roll rate. Therefore the sensitivity analysis procedure presented in [8] is performed. First the modal matrix is constructed. The eigenvectors, v_i, that correspond to each eigenvalue, λ_i, are arranged in columns to form the modal matrix $\mathcal{M}$. The rows of the matrix $\mathcal{M}$ are named r_i. For example if v_1 through v_n represent the eigenvectors of an n-dimensional system the modal matrix would be

$$\mathcal{M} = \begin{bmatrix} & & & & \\ v_1 & v_2 & v_3 & \cdots & v_n \\ & & & & \end{bmatrix} = \begin{bmatrix} r_1 \\ r_2 \\ r_3 \\ \vdots \\ r_n \end{bmatrix}$$

The elements of the inverse of the matrix $\mathcal{M}$ are defined as follows:

$$\mathcal{M}^{-1} = \begin{bmatrix} c_{1,1} & c_{1,2} & c_{1,3} & \cdots & c_{1,n} \\ c_{2,1} & & & & \\ c_{3,1} & & & & \\ \vdots & & & & \\ c_{n,1} & & & & \end{bmatrix}$$

Next, each column of $\mathcal{M}^{-1}$ is made into a diagonal matrix. For example the first column of the matrix will be put into its own diagonal matrix as follows

$$C_1 = \begin{bmatrix} c_{1,1} & 0 & 0 & 0 & 0 \\ 0 & c_{2,1} & 0 & 0 & 0 \\ 0 & 0 & c_{3,1} & 0 & 0 \\ 0 & 0 & 0 & \ddots & \vdots \\ 0 & 0 & 0 & \cdots & c_{n,1} \end{bmatrix}$$

The sensitivity matrix, S, is formed from multiplication of the rows of the modal matrix, r_n, and the C_n matrices.

$$S = \begin{bmatrix} r_1 C_1 \\ \vdots \\ \\ \\ r_n C_n \end{bmatrix} = \begin{bmatrix} s_{1,1} & \cdots & s_{1,n} \\ \\ \vdots & \ddots & \vdots \\ \\ s_{n,1} & \cdots & s_{n,n} \end{bmatrix}$$

Next, the rows of the matrix are normalized. To normalize the rows, the magnitude of each entry of S is divided by the sum of the magnitudes of each element in the corresponding row.

$$S = \begin{bmatrix} \dfrac{|s_{1,1}|}{\sum_{i=1}^{n}|s_{1,i}|} & \cdots & \dfrac{|s_{1,n}|}{\sum_{i=1}^{n}|s_{1,i}|} \\ \vdots & \ddots & \vdots \\ \dfrac{|s_{n,1}|}{\sum_{i=1}^{n}|s_{n,i}|} & \cdots & \dfrac{|s_{n,n}|}{\sum_{i=1}^{n}|s_{n,i}|} \end{bmatrix}$$

The columns of the normalized sensitivity matrix correspond to a specific eigenvector and the rows correspond to a specific state.

For the longitudinal states of the towfish, the sensitivity matrix is

$$S_{long} = \begin{bmatrix} 0 & .004 & .004 & .989 & .018 \\ .119 & .435 & .435 & .006 & .005 \\ 0 & .007 & .007 & .001 & .986 \\ .570 & .215 & .215 & 0 & 0 \\ .421 & .289 & .289 & 0 & .002 \end{bmatrix}$$

The first three columns represent the pitch mode. The bottom two entries of the first three columns have the greatest magnitude. They correspond to the states w and q. It seems from the second row of the first three columns that the state θ, contributes to this mode also. This is expected as the direction of the towing force on the towfish is dependent on the towfish orientation. So it is also included in the pitch mode approximation. The approximation becomes

$$\begin{bmatrix} \dot{\theta} \\ \dot{w} \\ \dot{q} \end{bmatrix} = A_{pitch} \begin{bmatrix} \theta \\ w \\ q \end{bmatrix} + B_{pitch}\delta e$$

where

$$A_{pitch} = \begin{bmatrix} 0 & 0 & 1 \\ 0.114 & -0.935 & 0.625 \\ -0.563 & 0.745 & -1.182 \end{bmatrix}, \; B_{pitch} = \begin{bmatrix} 0 \\ -0.474 \\ -1.524 \end{bmatrix}$$

To get a measurement of the accuracy of the approximation, the pitch mode eigenvalues are compared to the original. The eigenvalues of A_{sp} are

$$\lambda_{pitch1} = -1.516\,,\ \lambda_{pitch2,3} = -0.301 \pm 0.448i$$

It can be seen that they compare well with the original eigenvalues of

$$\lambda_{long1} = -1.515\,,\ \lambda_{long2,3} = -0.302 \pm 0.447i$$

For the lateral/directional states, the sensitivity matrix is:

$$S_{lat} = \begin{bmatrix} 0 & 0 & 0 & .5 & .5 & 0 \\ .304 & .690 & 0 & 0 & 0 & .006 \\ 0 & 0 & .007 & .496 & .496 & .001 \\ .030 & .027 & .501 & 0 & 0 & .892 \\ .688 & .302 & .007 & 0 & 0 & .004 \\ .017 & .035 & .757 & .074 & .074 & .043 \end{bmatrix}$$

The roll rate is dominant in the first two modes along with the roll angle. Therefore, these two states will be used to create the roll mode

$$\begin{bmatrix} \dot{\phi} \\ \dot{p} \end{bmatrix} = A_{roll} \begin{bmatrix} \phi \\ p \end{bmatrix} + B_{roll}\delta a$$

where

$$A_{roll} = \begin{bmatrix} 0 & 1 \\ -10.192 & -6.917 \end{bmatrix},\ B_{roll} = \begin{bmatrix} 0 \\ 17.532 \end{bmatrix}$$

The eigenvalues of the roll mode are

$$\lambda_{lat1} = -4.788\,,\ \lambda_{lat2} = -2.129\,.$$

which compare well to the eigenvalues of the original system

$$\lambda_{lat1} = -4.838\,,\ \lambda_{lat2} = -2.125\,.$$

These approximations will be used in Section 3.2.

3. Critical Design Parameters

3.1. Servo Actuator Sizing

Critical to an effective controller is the ability of the actuators to fulfill the command inputs from the computer. Three important design parameters that are considered for the servo-actuators are:

1. Bandwidth
2. Maximum angular rate
3. Resolution error

To achieve efficient disturbance rejection, a rule of thumb is that the control system bandwidth should be 5 to 10 times greater than the highest disturbance frequency and the actuator bandwidth should be 5 to 10 times higher than the control bandwidth.[29] The greatest disturbance frequency is expected to be 0.318 Hz (2 rad/sec). Appling the rules of thumb gives a minimum of 1.6 Hz for controller bandwidth and 8 Hz for actuator bandwidth. The author of [29] claims that, for a well-performing control system, most fin deflections are within 8 degrees. Knowing that the control bandwidth should be about 1.6 Hz, the dominant response time constant is

$$\tau_a = \frac{1}{2\pi(1.6)} = 0.1 \text{sec/ rad}$$

Assuming the control response settles in 3 time constants,[29] the fin must reach 95% of its commanded position within 0.3 seconds. To travel 8 degrees in 0.3 seconds, the actuator rate must be at least 27 degrees per second. The actuators which were selected for this design are the Tecnadyne Model 60 rotary actuators. The maximum angular rate available for the purchased actuators is 90 degrees per second, certainly more than is required.

The maximum angle resolution error is one-half of the encoder resolution. This error can cause the actuators to either overshoot or undershoot the desired shaft angle. If the resolution error is small enough, this effect will be minimized. Assuming the towfish is towed through a quiescent fluid, the actuators should remain at some steady angle to maintain correct attitude, however, the resolution error can cause some offset in attitude. This offset should certainly be less than $\pm 1^o$ and preferably much smaller.

3.2. Tail Fin Sizing

Several factors considered for tail fin sizing are:

1. Longitudinal and lateral-directional characteristics
2. Actuator resolution error
3. Fin effectiveness at low velocities

4. Manufacturability/Repairability
5. Proper sizing to fit flasher/pinger

The NACA 0012 airfoil is the chosen stern plane and rudder profile. The upper rudder must house a VHF pinger/flasher which imposes a minimum thickness. Requiring that all four fins be the same size for manufacturing ease, the fins are designed to have a constant chord of 0.4 meters (1.31 ft). To properly size the tail fins to ensure desirable longitudinal and lateral/directional characteristics, certain mode approximations are used.

Recall the mode approximations presented in Section 2.8. The tail span, *b*, is left as a free parameter and the transfer function from elevator to pitch rate is obtained from the pitch mode approximation and the transfer function from aileron to roll rate is obtained from the roll mode approximation. The tail span is then varied from 0.5 meters to 1 meter at increments of 0.1 meter and the Bode plots and step responses are created for each transfer function at the given span. The Bode plots can be seen in Figure 19 and Figure 20. The step responses can be seen in Figure 21 and Figure 22.

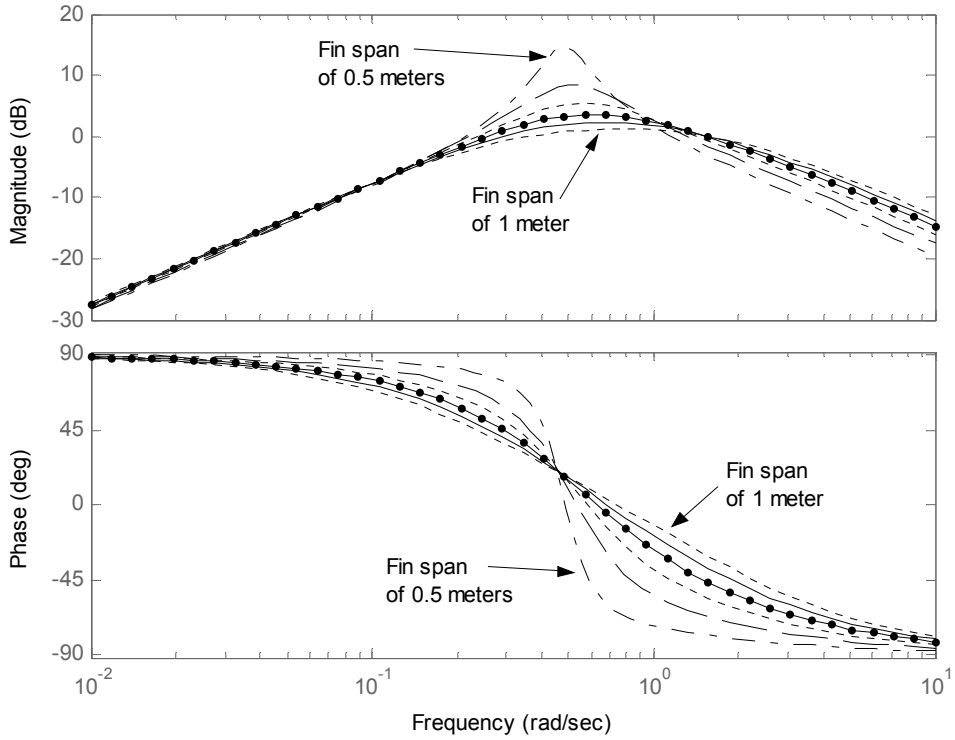

Figure 19 Bode plots of the elevator to pitch rate transfer function

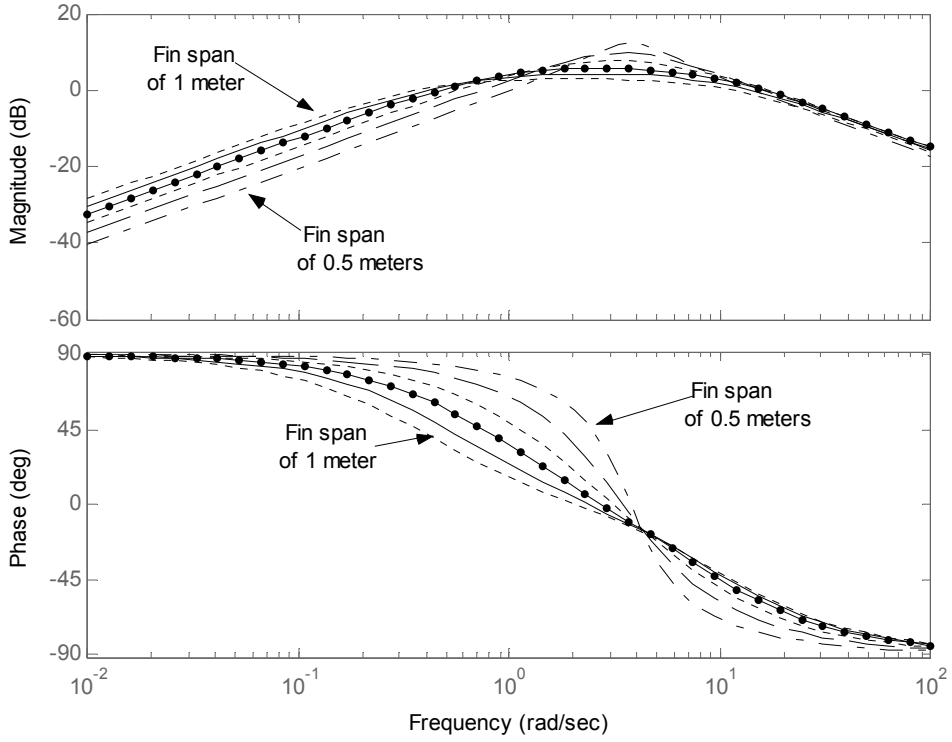

Figure 20 Bode plots of the aileron to roll rate transfer function

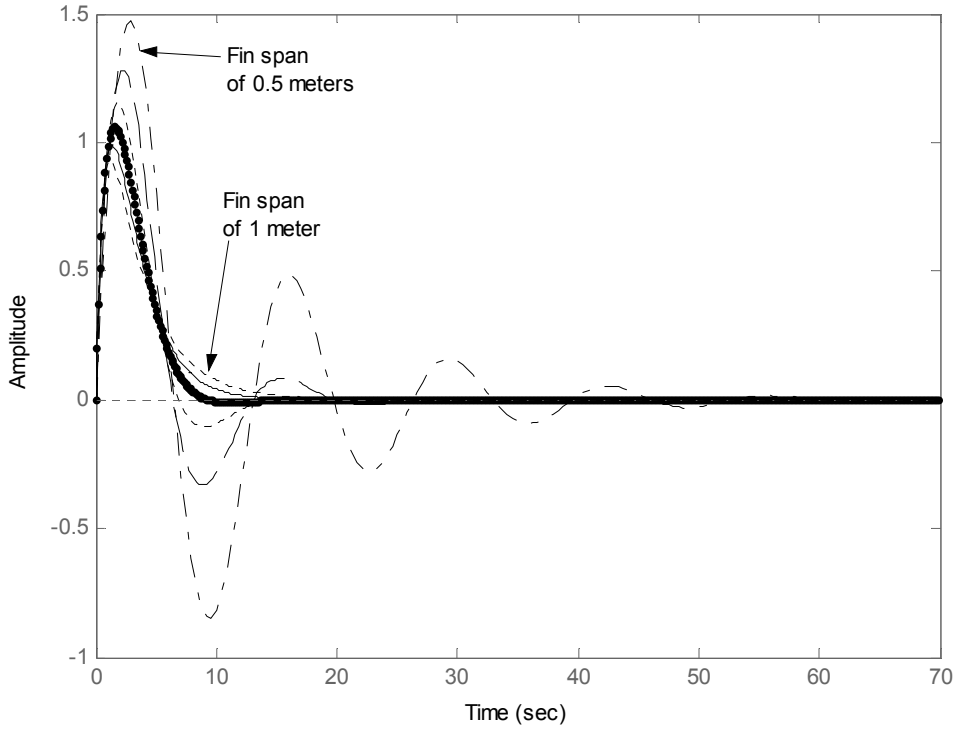

Figure 21 Step response of the elevator to pitch rate transfer function

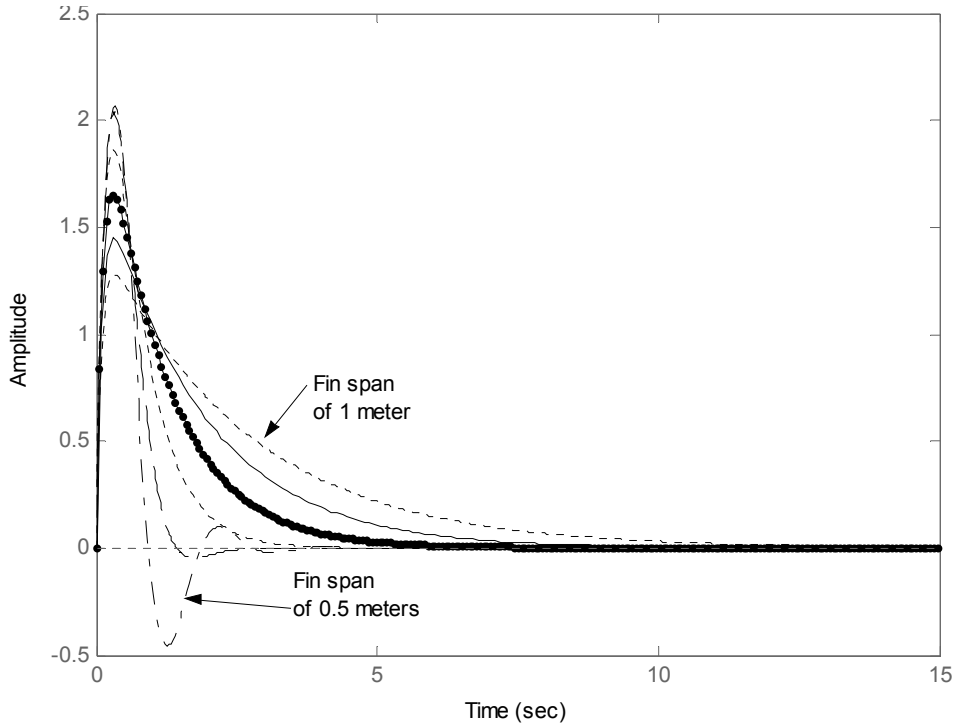

Figure 22 Step response of the aileron to roll rate transfer function

Too much overshoot and large oscillations in the step response is not desirable because this translates into possible overshoot and oscillations of the desired tilt angle. However a response that is too damped is also not desirable since it can be rather slow and unable to deal with higher frequency inputs. With this in mind the span is chosen to be 0.68 meters. With this span there are little oscillations in both pitch rate and roll rate step response and both seem to settle out rather quickly. A schematic of the rudder can be seen in Figure 23. The remaining fins are identical, except that they do not house VHF pingers. All fins have 2 stainless steel rods for mounting to the towfish. The exposed end of the rod is threaded to fit a ¼”-20 nut.

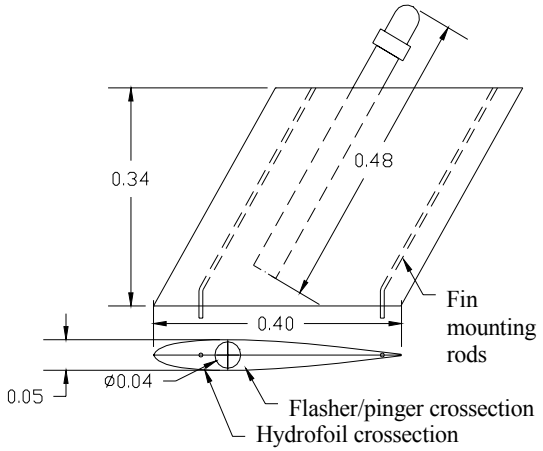

Figure 23 Views of the rudder with the imbedded VHF pinger/flasher Units in meters

The actuators for the towfish have a resolution of 0.225° which means a resolution error of 0.1125°. When simulations are performed for a neutrally buoyant towfish with fins shown in Figure 23, the resolution error causes less than 1° of roll for a CG that is three inches below the CB.

Another practical design consideration is the amount of torque required to turn the fin. The available torque from the chosen actuators is a rather large 81 Nm (60 ft-lbs). Assuming that the fins will be actuated at the hydrodynamic center then the theoretical pitching moment is zero and independent of angle of attack.[1] Therefore the equation of motion for the fin is

$$\left(I_{yplate} + M_{\dot{q}plate}\right)\dot{q}_{fin} = T_{fin}$$

where I_{yplate} is the moment of inertia of the fin approximated as a flat rectangular plate, $M_{\dot{q}plate}$ is the added inertia for a flat plate, T_{fin} is the torque placed on the fin and q_{fin} is the pitch rate of the fin. The inertia is determined from

$$I_{yplate} = \frac{1}{12} m_{fin} c^2$$

Where m_{fin} is the mass of a fin which will be about 6.8 kg and c is the chord length.

The added inertia is estimated from Fossen[10] as

$$M_{\dot{q}plate} = \int_{-b/4}^{b/4} M_{\dot{q}plate}^{2D} dy = M_{\dot{q}plate}^{2D} \, b/2$$

where the two-dimensional added mass coefficient is taken from Newman[24]

$$M_{\dot{q}plate}^{2D} = \frac{1}{8}\pi\rho\frac{c}{2}$$

From simulations presented in Section 5.1, it is determined that the maximum fin deflection acceleration is about10 rad/sec^2. From this value it is calculated that the average torque required by the actuator is 3.04 Nm, well within the available torque range.

3.3. Buoyancy Consideration

Due to changes in salinity of ocean water, buoyancy can vary up to 3%. To ensure the towfish is always buoyant, the buoyancy factor of the towfish is chosen to be 5% of the towfish weight. In case if the towfish broke away from the tow tether at the tow point, the towfish would float to the surface. It is necessary for the towfish to ascend to the surface quickly enough so it is not carried too far away from the towing vessel because the VHF flasher/pinger embedded in the rudder has a transmitter range of around 5 to 10

kilometers. It is important that the ship be within that range when the towfish surfaces. A simple simulation shows that it would take approximately 800 seconds for the towfish to float to the surface in a bluff position (meaning along its *z* axis). If the tow vessel was traveling at 3 m/s and the towfish broke off, the vessel would be approximately 2400 meters away plus the cable scope. This distance is within the recovery range of the VHF pinger. The simulations assume that the vessel doesn't stop and there are no currents.

4. PID Control Design

4.1. Controller Design Motivation

For the two stage towfish, the plant dynamics are stable; all that is required is to enhance stability. Even with a non-hydrodynamic platform without fins, pitch and roll angles have been maintained to within $\pm 2^o$. The goal is to narrow that stability to within $\pm 1^o$ and have the ability to remove mean biases in both pitch and roll. For recovery purposes, in the event that the tether breaks at the tow point, the towfish must be 5% positively buoyant. This will cause the towfish to float above the depressor, thus a downward towing force at the nose causing it to pitch down. Feedback control can provide active disturbance rejection and removal of mean biases.

Simple proportional feedback may enhance stability to within the given requirements. However, the sensing equipment used to feed back pitch and roll will not be perfect and is subject to vibrations and electromagnetic interference. The actuators have resolution error and magnitude and rate limits. The balancing of the CB and CG will not be perfect and the water may have changes in salinity which affects buoyancy. Integral control is necessary to remove small errors in pitch and roll. Higher frequency disturbances from either the towing vessel or from cable modes[5] must also be removed and therefore derivative control is useful. A proportional-integral-derivative (PID) control structure seems appropriate; see Figure 24.

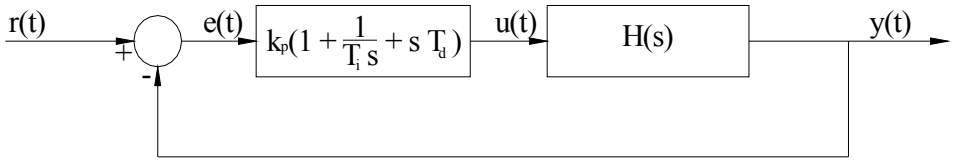

Figure 24 PID controller structure. T_i is the integral time, T_d is the derivative time, k_p is the proportional gain. Sensor noise and disturbances are not shown

4.2. Pitch Channel PID Tuning

For the purpose of tuning the gains it is necessary to define what an acceptable response would be for a given scenario. The scenarios are based around the design criterion of pitch and roll regulation to within ±1 degree. Due to the complexity of the pitch and roll transfer functions, root locus techniques are not very helpful. Each channel has poles and zeros all in close proximity to each other. It is difficult to firmly say that one set of poles dominate. Also, root locus techniques do not take into account the effect of zeros. A Bode plot can give a better idea of how a system will perform but it is difficult to say what phase and gain margin will provide acceptable results. The best way to do so is to simulate. Therefore when gains are chosen, an initial condition response will be used to determine their acceptability. The initial condition response will be of a *neutrally buoyant* towfish to a 1 degree initial pitch or roll angle. The controller should be able to bring the pitch or roll angle back to 10% of the design criteria of 1 degree in a reasonable time with little oscillation. Fin deflections should be reasonable. Then the controller

performance will be tested in a more realistic simulation; the gains must maintain pitch and roll to within ±1 degree subject to the random disturbance model.

There are many different ways to tune the gains of a PID controller. The authors of [6] provide a way to search for the set of all stabilizing gains for an open loop plant that can be either stable or unstable. They suggest a way to search for a range of k_p (proportional gain) so that the closed loop polynomial is Hurwitz and then sweep over this range obtaining values of k_i (integral gain) and k_d (derivative gain) that make the closed loop polynomial Hurwitz for a fixed k_p. However, this method introduces greater complexity than is necessary for the problem at hand.

A simpler and more appealing way of tuning the gains of a PID controller is Zeigler-Nichols frequency response method.[6][25][3] The frequency response method requires the designer to increase the proportional gain to a point where the system has sustained oscillations while setting integral and derivative gain to zero. This critical gain, k_{cr}, and the period of oscillations, P_{cr} are used to determine the three gains. See Figure 25 for determination of the pitch critical period.

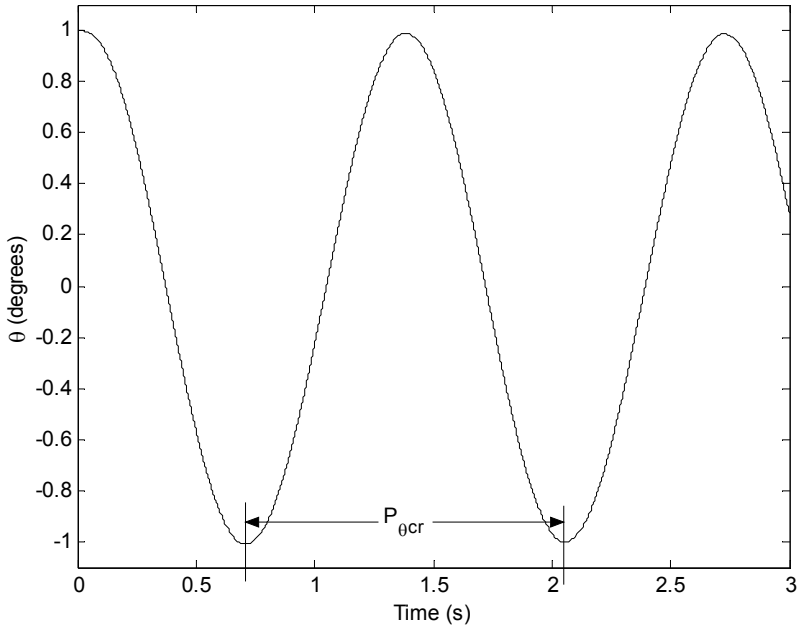

Figure 25 Pitch response to an initial condition of $\theta_0 = 1^o$ with proportional gain set to $k_{\theta p} = k_{\theta cr} = 15$

The simulation was run for a neutrally buoyant towfish with the CG at $[0\ 0\ 3]^T$ inches in body coordinates (i.e. below the CB). The Zeigler-Nichols frequency response gives the following equations for the proportional gain, integral and derivative time

$$k_p = 0.6k_{cr}$$

$$T_i = 0.5P_{cr}$$

$$T_d = 0.125P_{cr}$$

The pitch channel critical period and gain are respectively

$$P_{\theta cr} = 1.35 \text{ seconds}$$

$$k_{\theta cr} = 15$$

Therefore proportional gain and the integral and derivative times are determined to be

$$k_{\theta p} = 9$$

$$T_{\theta i} = 0.475 \text{ seconds}$$

$$T_{\theta d} = 0.1688 \text{ seconds}$$

In Figure 26 an initial condition response of 1 degree shows a rather oscillatory response. The stern plane deflections also seem large for such a small initial condition.

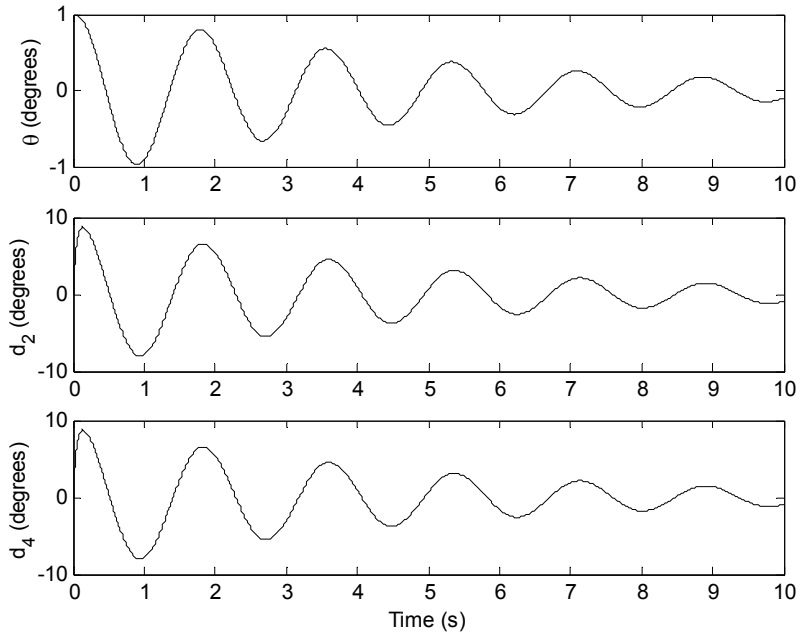

Figure 26 1^0 pitch initial condition response using the initial set of gains

Therefore an attempt is made to improve the performance.

The integral control gain is defined as

$$k_i = k_p / T_i$$

and the derivative control gain is

$$k_d = k_p T_d$$

Given the values for the integral and derivative time, it can be seen that the integral control gain is strong while the derivative control gain is relatively weak. The controller is tuned until a less oscillatory initial condition response is reached. The following proportional gain, integral time and derivative time are obtained.

$$k_{\theta p} = 4$$

$$T_{\theta i} = 0.6 \text{ seconds}$$

$$T_{\theta d} = 1 \text{ seconds}$$

With the new gains the 1 degree initial condition response is simulated. It can be seen that the pitch angle settles out within 7 seconds with few oscillations. The maximum fin deflection is about a third of what it was previously. See Figure 27.

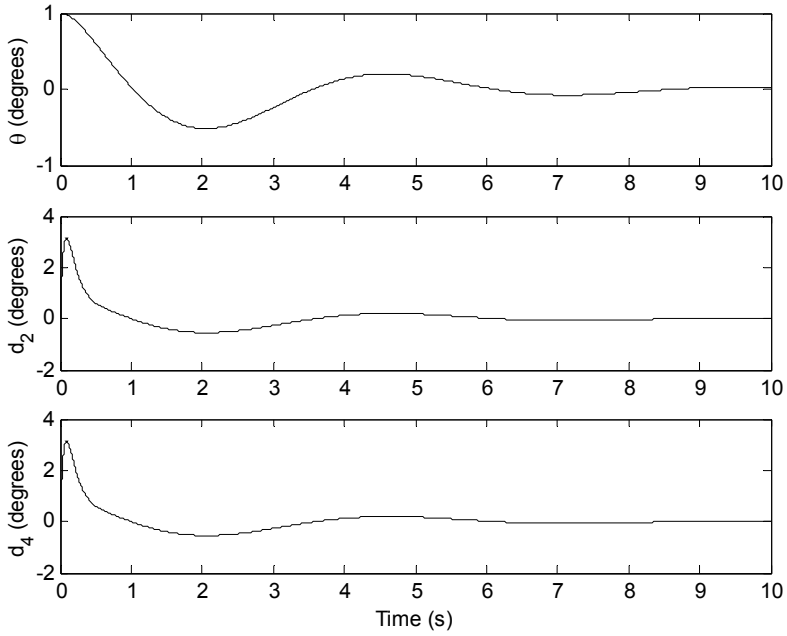

Figure 27 1^0 pitch initial condition response using the revised set of gains

The pitch channel Bode diagram of both the compensated and uncompensated system can be seen in Figure 28.

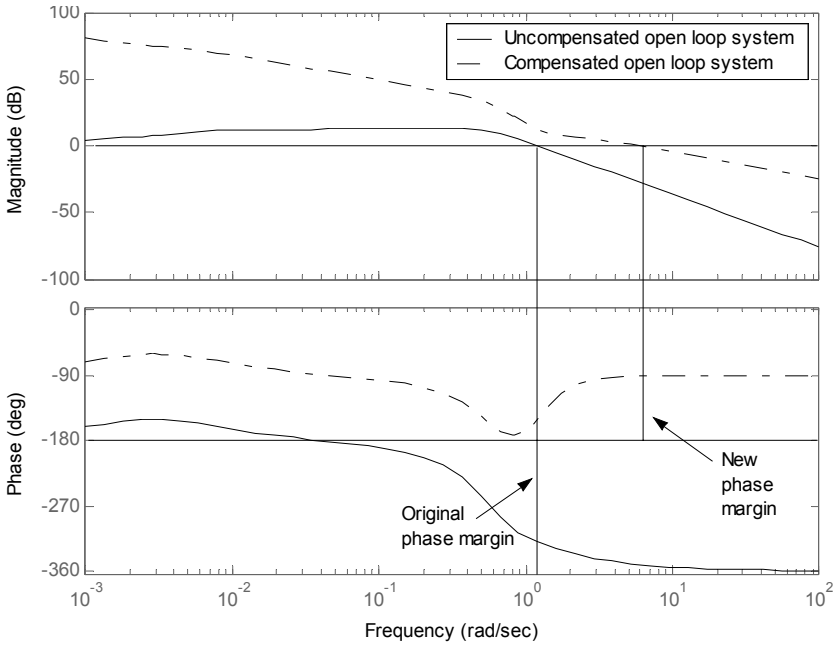

Figure 28 Pitch channel Bode plot

The appearance of a negative phase margin in Figure 28 is an artifice of sign convention. A positive fin deflection has been defined to give a negative pitching moment. One can redefine the fin deflection so that a positive fin deflection gives a positive pitching moment. The sign on the PID gains must also be changed and the Bode plot becomes that in Figure 29. The closed loop phase margin is greater then the open loop phase margin; both are positive, as one would expect.

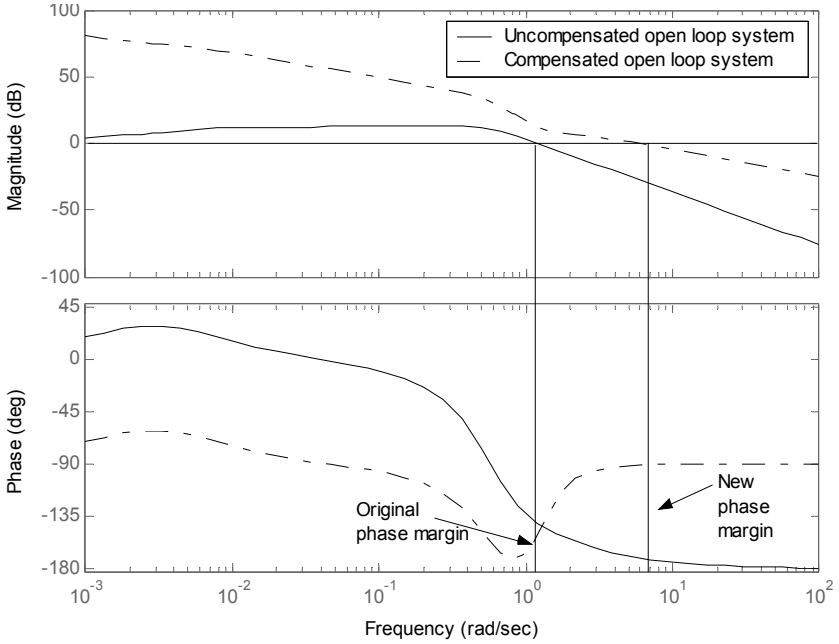

Figure 29 Pitch channel Bode plot with redefined fin deflection

So from Figure 29 it appears that there is additional phase margin gain.

4.3. Roll Channel PID Tuning

The roll channel is tuned using the Zeigler-Nichols frequency response. A nonlinear simulation is run with roll proportional gain set to achieve sustained oscillations in roll. The oscillations have amplitudes of about ±0.9° with very slight decay. See Figure 30.

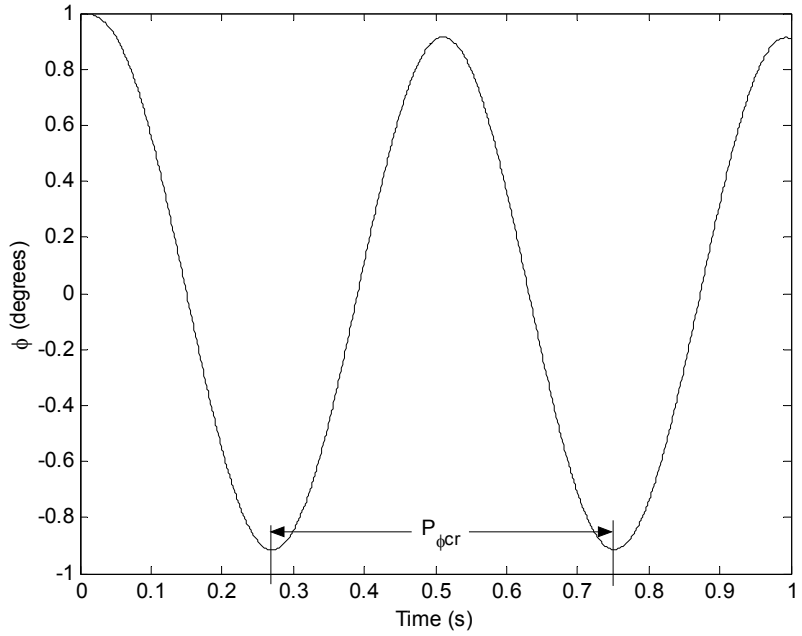

Figure 30 Roll response to an initial condition of $\phi_0 = 1^o$ with proportional gain set to $k_{\phi p} = k_{\phi cr} = 12.2$

The critical period and gain are respectively

$$P_{\phi cr} = 0.48 \text{ seconds}$$

$$k_{\phi cr} = 12.3$$

Therefore the proportional gain, integral and derivative time from the Ziegler-Nichols rules are

$$k_{\phi p} = 7.38$$

$$T_{\phi i} = 0.24$$

$$T_{\phi d} = 0.06$$

Using these gains, a 1 degree initial condition shows that fin deflections are somewhat large for such a small initial condition and there are rather large oscillations in the beginning of the response. See Figure 31.

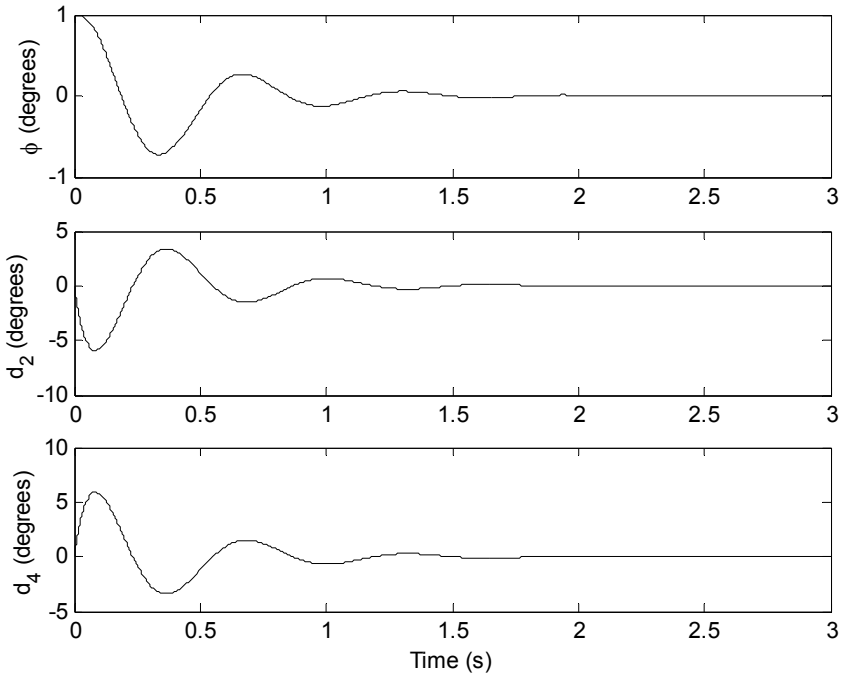

Figure 31 1^0 roll initial condition response using the original set of gains

As with the pitch control, the roll control has strong integral and weak derivative control, respectively. The proportional gain and the integral and derivative time are tuned to the following values

$$k_{\phi p} = 2$$

$$T_{\phi i} = 0.5$$

$$T_{\phi d} = 0.3$$

An initial condition response of 1 degree shows the towfish settles more quickly while the maximum fin deflection is about 1.5 degrees. See Figure 32.

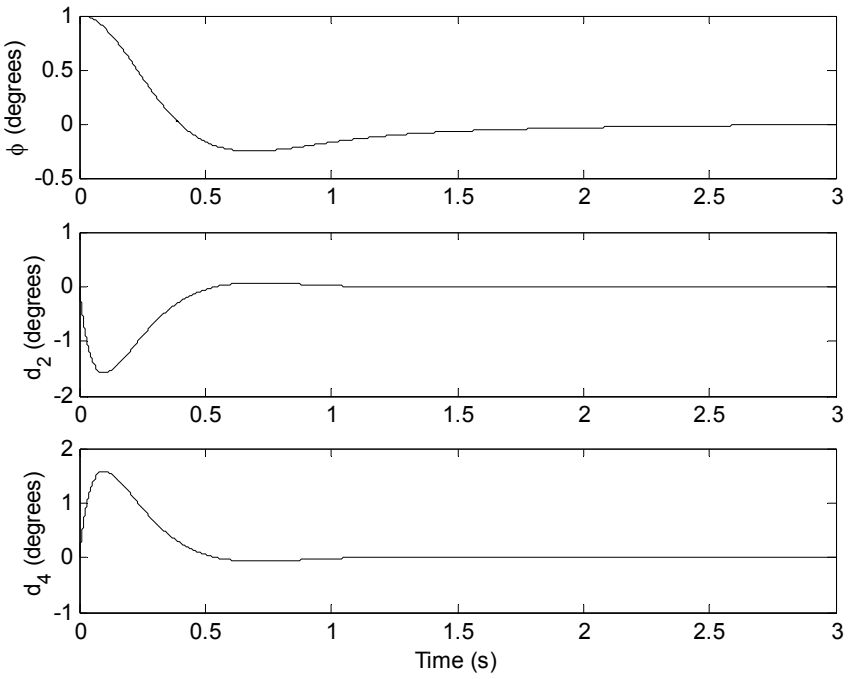

Figure 32 1^0 roll initial condition response using the revised set of gains

The roll channel Bode diagram of both the compensated and uncompensated open loop systems can be seen in Figure 33. Notice the small increase in phase margin.

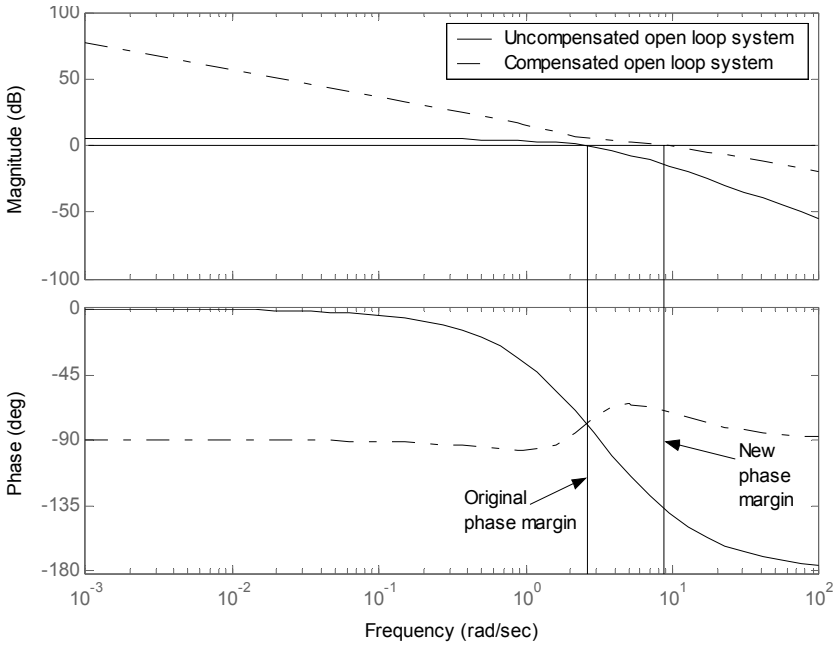

Figure 33 Pitch channel Bode plot

4.4. Discrete Control

To execute control in a digital computer the controller must be discretized. To evaluate its performance after discretization, the discrete controller can be combined with the zero order hold transfer function and the original plant. The zero order hold is a sampling method which holds constant the last sampled value until it is resampled. Bode plots of both the discrete system and continuous system can be compared to determine at what frequency performance begins to degrade. The discrete time block diagram can be seen in Figure 34. The Tustin[12] method is used to discretize the controller and the zero order hold (ZOH) is used to create the equivalent plant. The Tustin method is valuable because it maintains the stability of the controller and makes its transfer function representation proper. The output rate of the serial information of the vertical gyroscope is a maximum of 74 Hz. However when used in conjunction with Labview™ data acquisition software, the sample rate is 70 Hz. This is the frequency at which the controller will be receiving data so this is the effective sample rate. The Bode plots of the pitch and roll channel can be seen in Figure 35 and Figure 36.

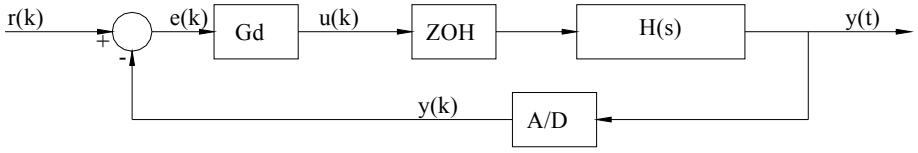

Figure 34 Block diagram of the discrete time system. Noise and disturbances are not shown. Gd is the controller, H(s) is the plant and A/D is an analog to digital converter.

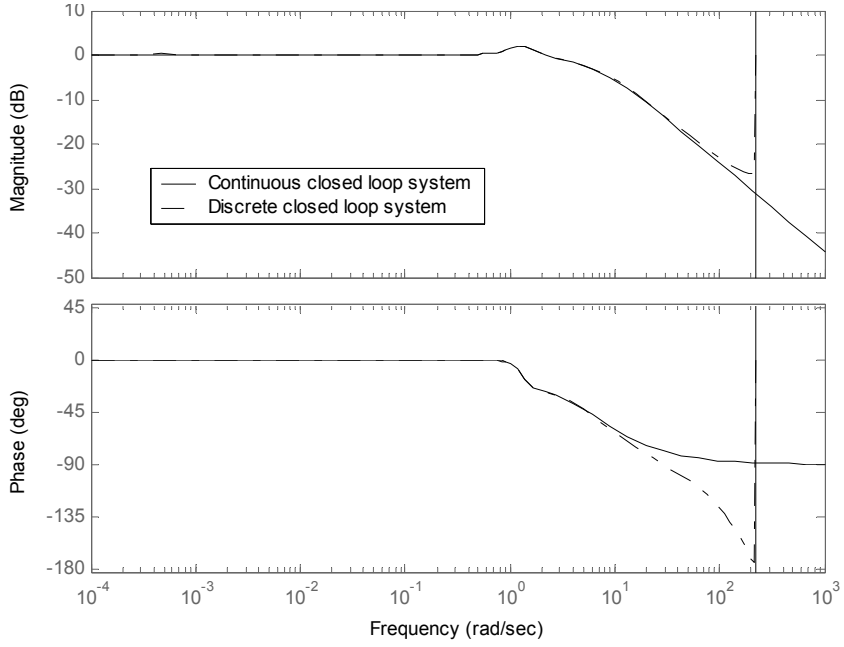

Figure 35 Comparison of the discrete and continuous pitch closed loop Bode plots

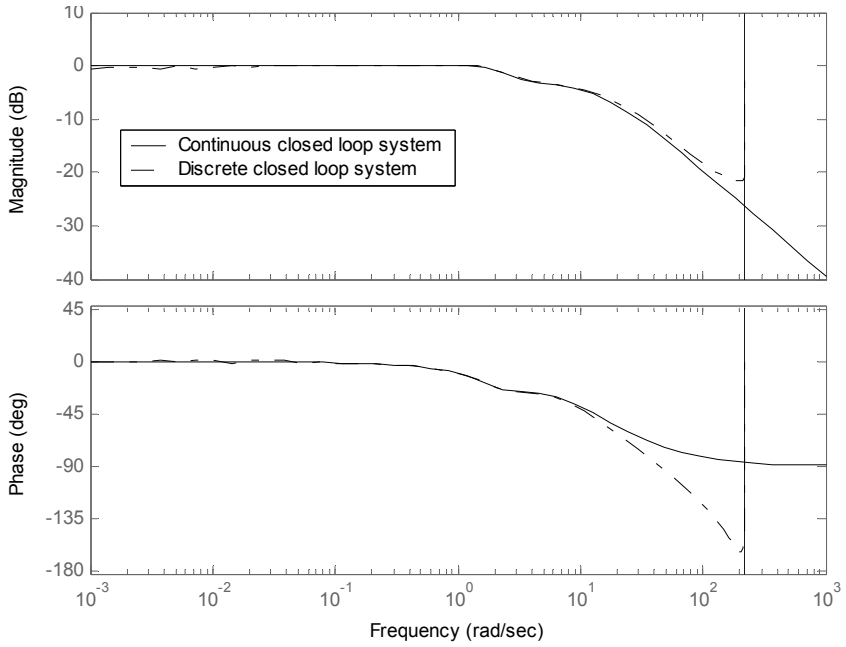

Figure 36 Comparison of the discrete and continuous roll closed loop Bode plots

It can be seen that for both systems the discrete approximation begins to deviate at about 10 rad/sec. The expected disturbances will be 2 rad/sec at most and therefore the controller should perform as predicted by the continuous system. Also, since the controller bandwidth is about 5 times greater than the expected maximum disturbance frequency, sufficient disturbance rejection is expected.

5. Attitude Control Simulations

5.1. Low Speed Control

Presented here are nonlinear simulations of a 5% buoyant towfish that has a dry weight of 250 lbs. The CG is set 3 inches below the CB. All initial conditions are set to zero except for the towfish axial velocity, which is 1 m/s. Because 1 m/s is the slowest anticipated speed, these simulations represent a "worst case" scenario. The tether is 50 meters long with the tow point at the nose of the tow fish and the free end (depressor end), traveling at a constant forward velocity with random lateral and vertical motion. Refer to Figure 14. Typically in simulation, the lateral and vertical position of the free end may change by ±1 meter. The attitude response of an uncontrolled towfish is presented in Figure 37. The position of the towfish can be seen in Figure 38.

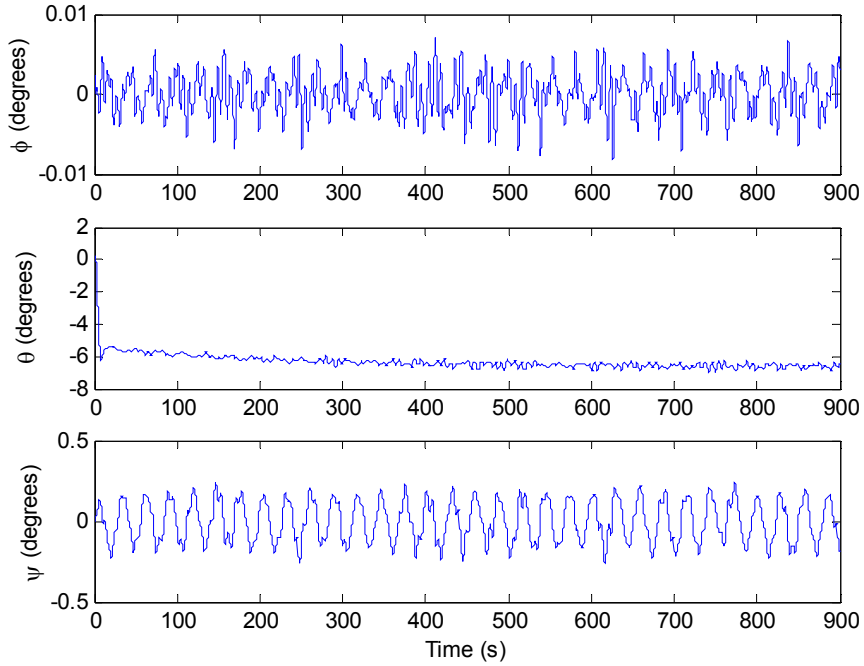

Figure 37 Attitude of the uncontrolled towfish subject to random depressor motions

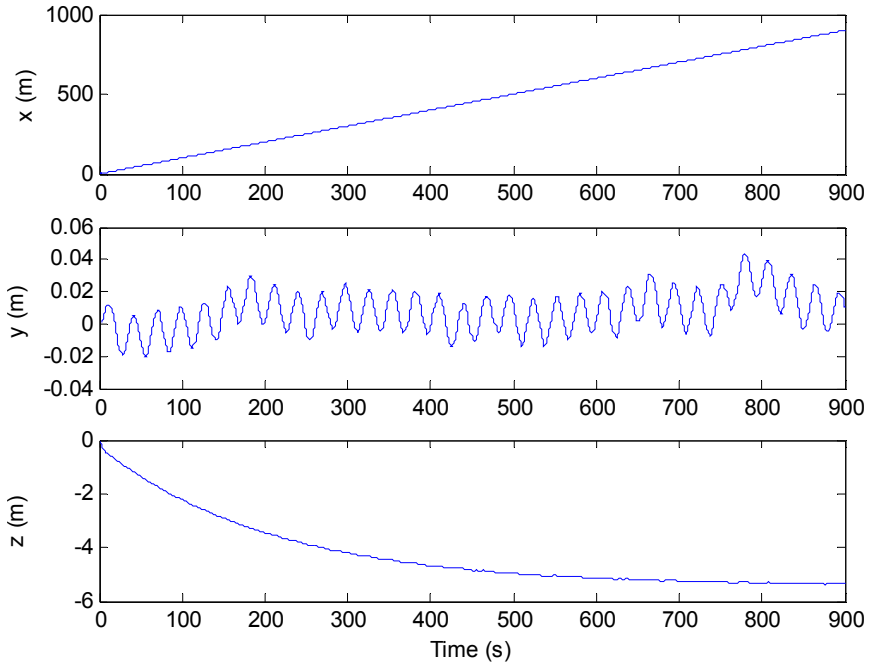

Figure 38 Position of the uncontrolled towfish subject to random depressor motions

Notice that, at steady state, the towfish is pitched downward due to its height above the depressor. The towfish floats up to about 5 meters above the depressor. The simulations show the pitch angle is nominally -6.5 degrees and ranges by ±1 degree. However there is little deviation in the roll or yaw angle. This is due to the assumption of a quiescent fluid and the CG being directly below the CB.

Now the gains that were developed in Section 4 are applied with the towfish in the same configuration. To better reject disturbances, the pitch derivative time was raised to 4 seconds and the buoyancy was lowered to 3%. A buoyancy of 5% caused the towfish to float too high when the pitch angle was regulated. This caused the tether to make a rather sharp angle with the towfish and thus increased the disturbances seen by the towfish. Note the change in time scale. The results can be seen in Figure 39 and Figure 40.

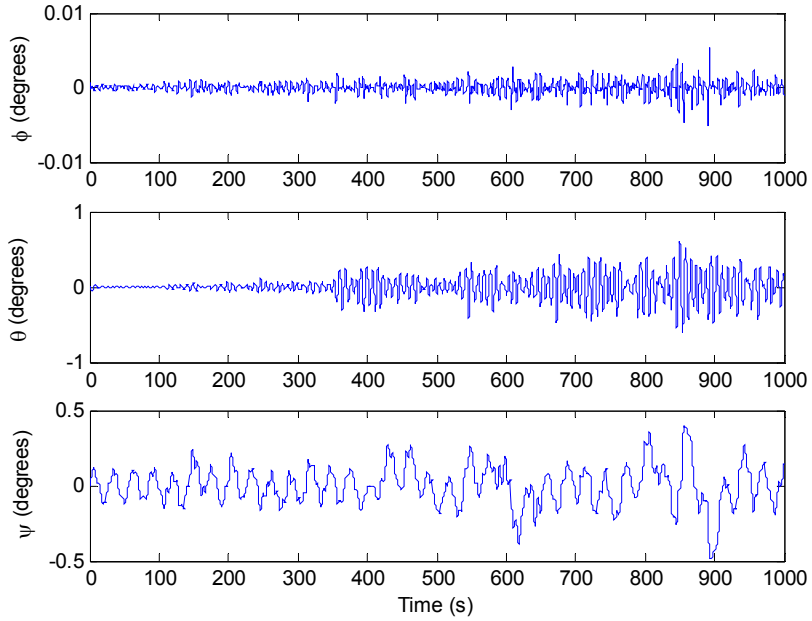

Figure 39 Attitude of the controlled towfish

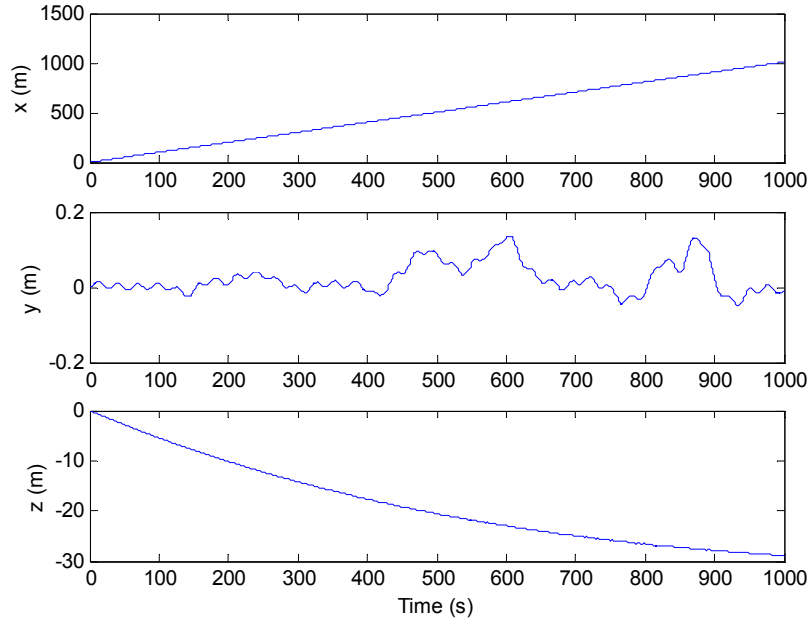

Figure 40 Position of the controlled towfish

It can be seen that the pitch angle is controlled to within ±0.6 degrees even as the towfish floats up to its steady-state depth. The roll angle barely deviates from 0 degrees. Most of the effort of the controller involves controlling pitch since the roll angle experiences few perturbations. Notice in Figure 40 that the towfish takes much more time to float to its nominal depth because it remains horizontal. The stern plane deflections can be seen in Figure 41.

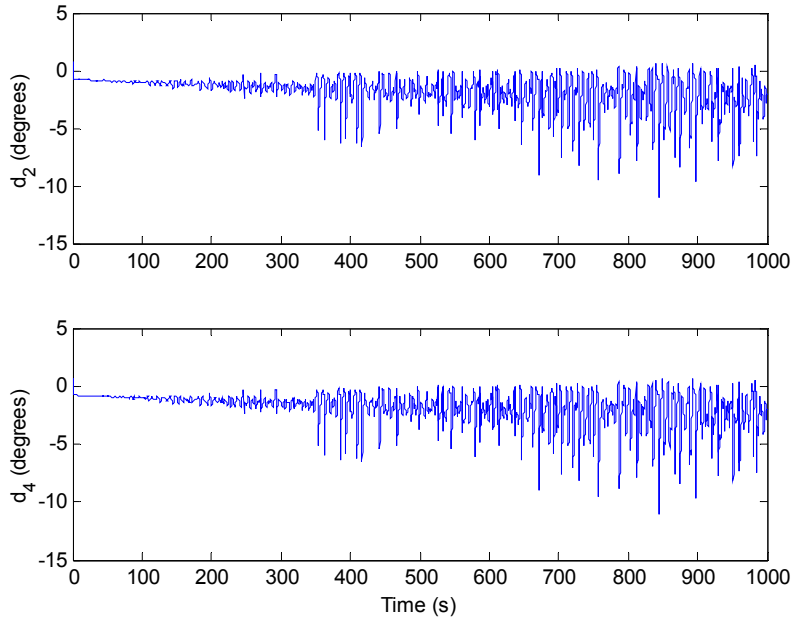

Figure 41 Stern plane deflections

The deflections are kept within ±10 degrees, well within the ±20 degree limit.

Realistically, the CG will not be exactly where it is designed to be. Therefore, for simulation purposes, it is arbitrarily placed 1 inch forward and 1 inch to the right side of the towfish. (The CG of the actual towfish should be able to be trimmed to within one centimeter.) Therefore the location of the CG with respect to the body axes origin is

$$X_{CG} = \begin{bmatrix} 1 \\ 1 \\ 3 \end{bmatrix}$$

Buoyancy of the towfish is set to 3%. The uncontrolled simulation is seen in Figure 42 and Figure 43.

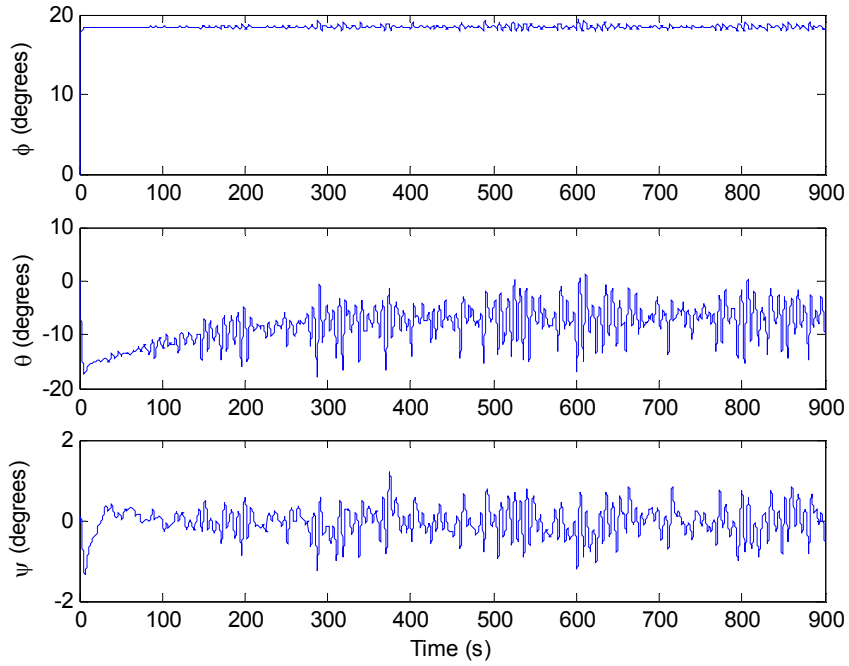

Figure 42 Attitude of the uncontrolled towfish with $X_{CG} = [1 \;\; 1 \;\; 3]^T$ inches

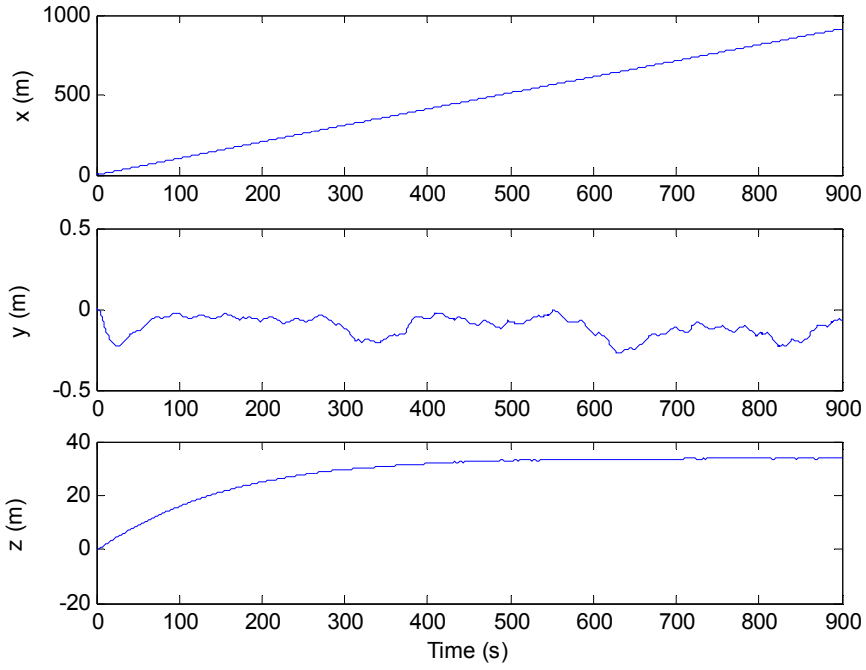

Figure 43 Position of the uncontrolled towfish with $X_{CG} = [1 \;\; 1 \;\; 3]^T$ inches

Notice that only placing the CG two inches off to the right causes the towfish to roll about 18 degrees. It can also be seen that moving the CG forward causes the towfish to have a steady-state pitch of about -6 degrees. This gravitational pitch moment actually

causes the towfish to sink to 37 meters below the nominal position of the depressor. If a mission required the towfish to be in close proximity to the ocean floor, then the effect from the CG may cause it to run into the bottom. Now the controller is turned on with the gains developed in Section 4 with the pitch derivative time turned up to 4 seconds and the roll proportional control turned up to 7 to better reject the initial roll disturbance from the off set CG. Figure 44 shows the attitude of the towfish for 3% buoyancy.

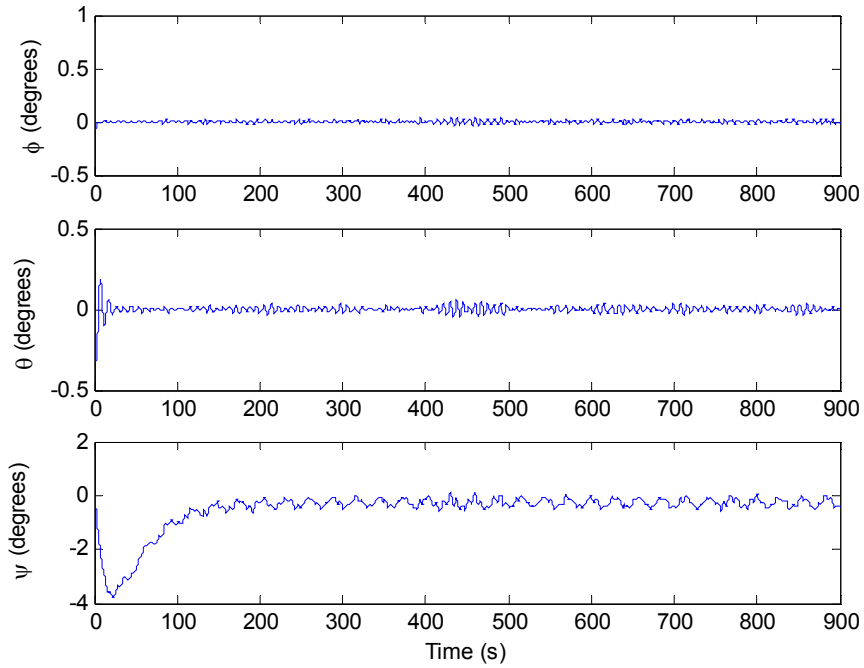

Figure 44 Attitude of the controlled towfish with $X_{CG} = [1 \;\; 1 \;\; 3]^T$ inches

It appears that with the CG in the given location the pitch angle is more easily controlled. There is a bit more deviation in roll, however the attitude remains well within specification. Notice the position of the towfish. With it now being regulated to zero degrees in attitude, it floats to about 5 meters and sways to about -4 meters. See Figure 45. The controller deflections can be seen in Figure 46. Notice that the deflections are no longer symmetric in order to restore the roll angle although this scenario seems to be easier to control. Note the small deviations in the nominal fin deflections.

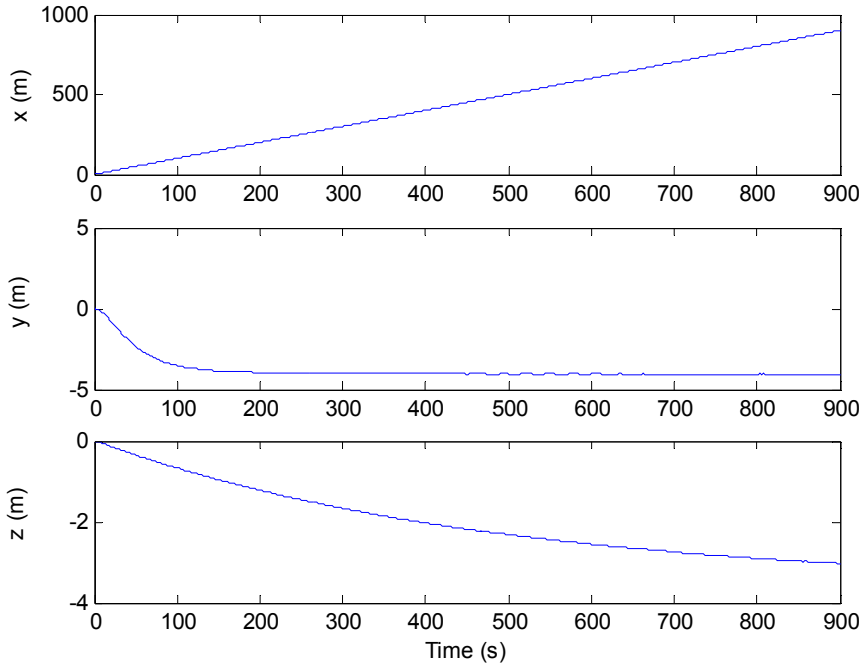

Figure 45 Position of the controlled towfish with $X_{CG} = [1 \;\; 1 \;\; 3]^T$ inches

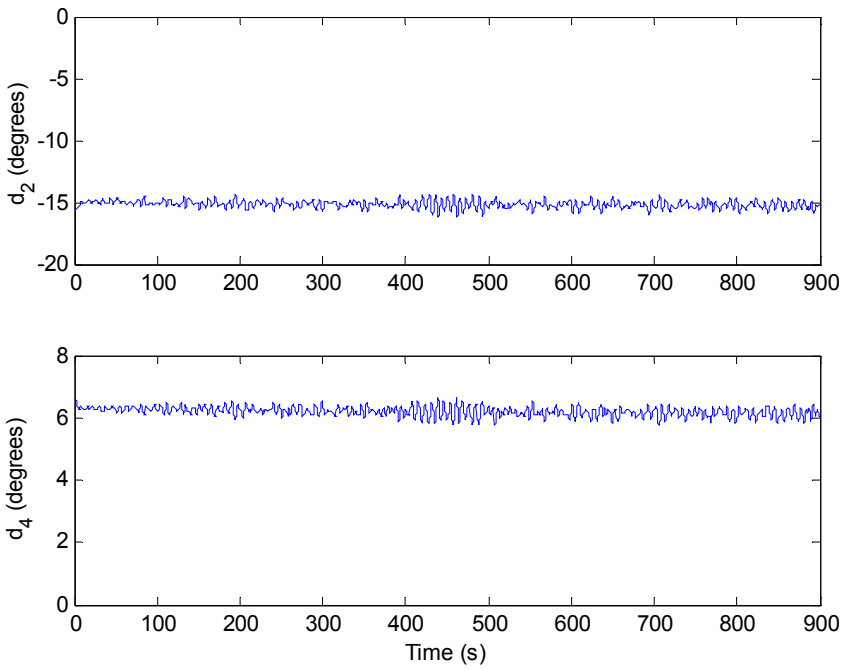

Figure 46 Stern plane deflections of the controlled towfish with $X_{CG} = [1 \;\; 1 \;\; 3]^T$ inches

5.2. High Speed Control

The towfish controller has shown good results at its slowest speed of 1 m/s. At higher speeds the fins become more effective. Therefore the current selection of gains may cause the stern planes to overcompensate and violate the design criteria. The set of gains developed in Section 4 is tested here for its maximum tow velocity of 3 m/s with random disturbances and a CG at $[0 \;\; 0 \;\; 3]^T$ inches with 3% buoyancy. The results can be seen in Figure 47 and Figure 48. The control deflections can be seen in Figure 49. Notice that the controller performs even better than in the low speed case. As expected the fins are much more effective at higher speeds. It can be seen that traveling at a faster speed causes greater drag on the towfish and therefore its nominal height is lower than in the 1 m/s case. This provides verification that a given set of gains can be used at various speeds. Gain scheduling for various speeds is therefore not necessary.

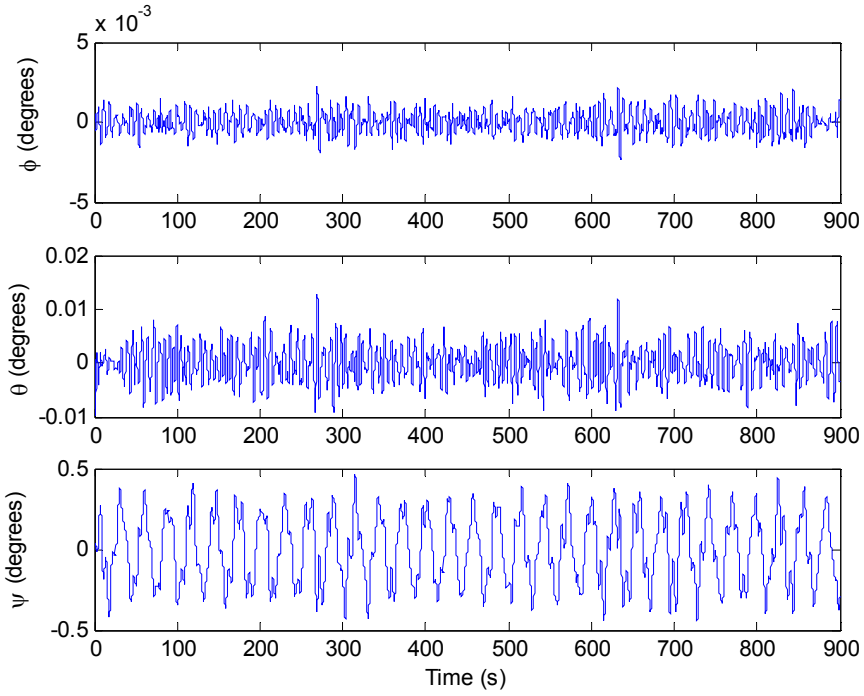

Figure 47 Attitude of the controlled towfish traveling at 3 meters per second with $X_{CG} = [0 \;\; 0 \;\; 3]^T$ inches

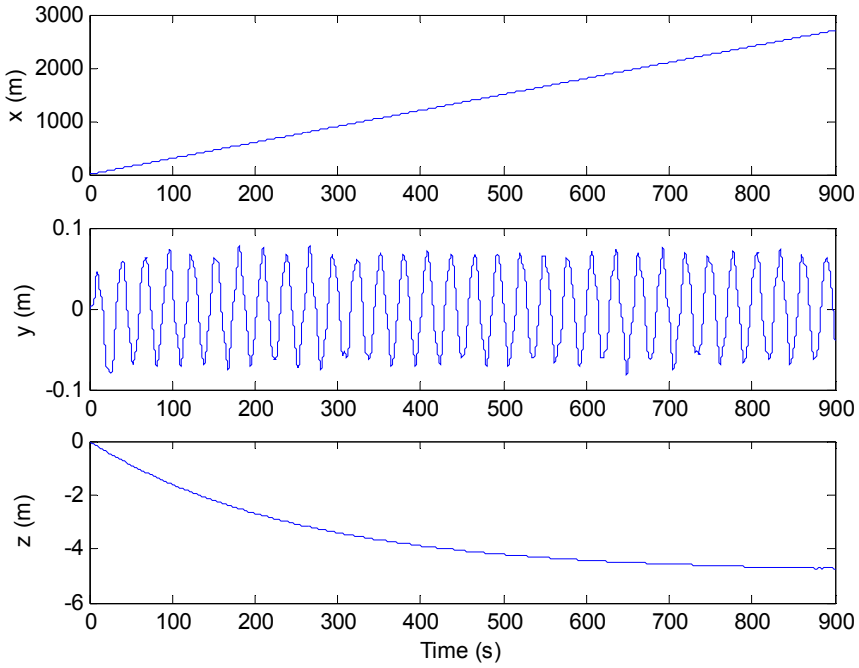

Figure 48 Position of the controlled towfish traveling at 3 meters per second with $X_{CG} = [0 \quad 0 \quad 3]^T$ inches

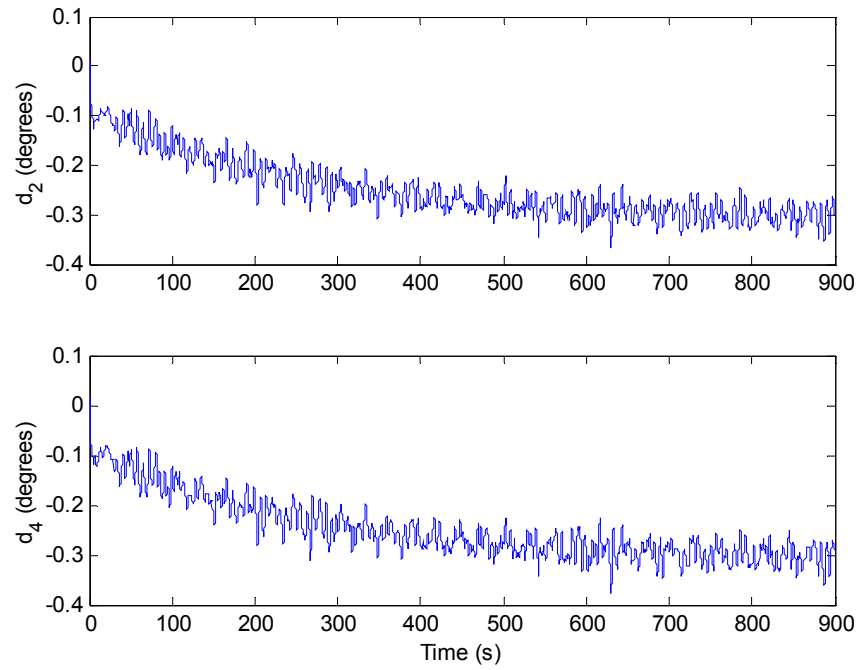

Figure 49 Stern plane deflections of the controlled towfish traveling at 3 meters per second with $X_{CG} = [0 \quad 0 \quad 3]^T$ inches

5.3. Pigtail Length Variation

Another factor for the performance of the towfish is the length of the pigtail. The towfish will respond more to disturbances with a shorter pigtail. However a shorter length may be desirable as it would allow for less variation in height for a given buoyancy or nominal stern plane deflection and would allow the towing vessel to be more maneuverable. The pigtail length is shortened to 20 meters and the speed of the towfish is set to 1 m/s with the CG at $[0 \;\; 0 \;\; 3]^T$ inches in body coordinates. The uncontrolled response can be seen in Figure 50 and Figure 51.

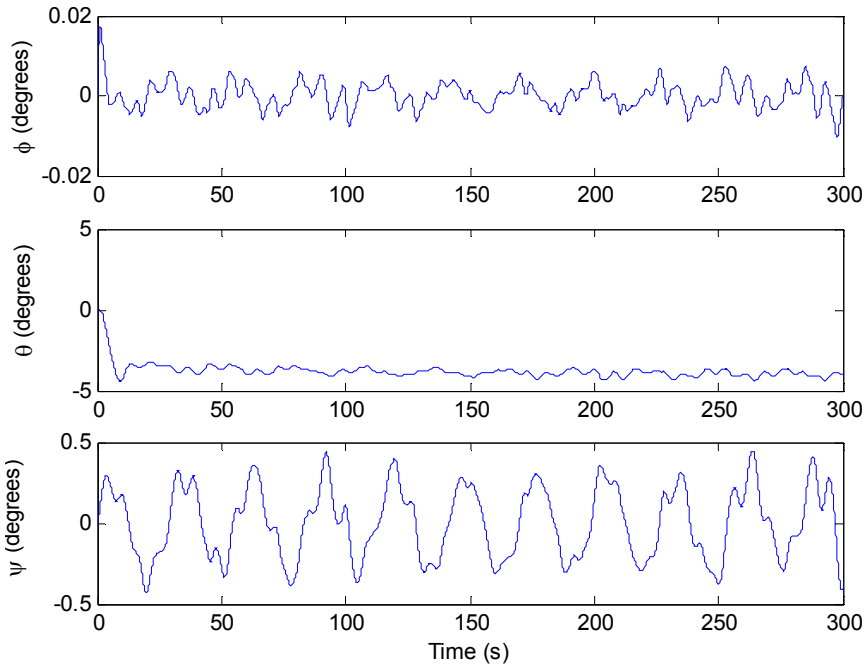

Figure 50 Attitude of the uncontrolled towfish with a pigtail length of 20 meters

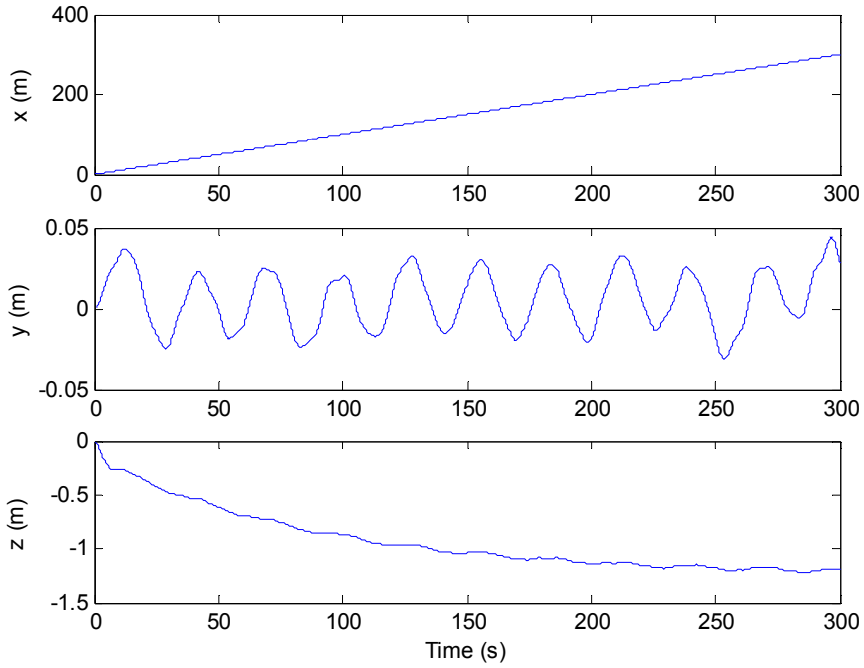

Figure 51 Position of the uncontrolled towfish with a pigtail length of 20 meters

It can be seen that the pitch angle is nominally at about -4.5 degrees and ranges by 1 degree. The roll angle deviations have also slightly increased but are still well within the design criterion. The yaw angle also sees greater disturbances within ± 0.5 degrees. There is a bit of a difference in the nominal height of the towfish. Previously it would float to about 5 meters while with a pigtail length of only 20 meters it floats to about 1.2 meters.

To control this more difficult case the pitch derivative time is raised to 6 seconds otherwise the controller would have failed. The results can be seen in Figure 52, Figure 53 and Figure 54. Although the towfish is controlled within the criterion, the fins break the ±20 degree limit several times.

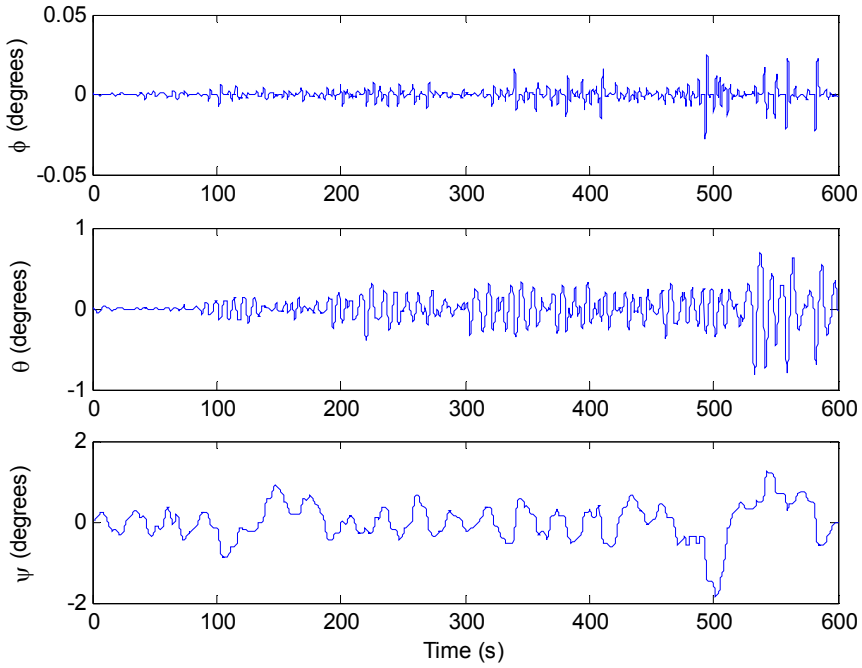

Figure 52 Attitude of the controlled towfish with a pigtail length of 20 meters

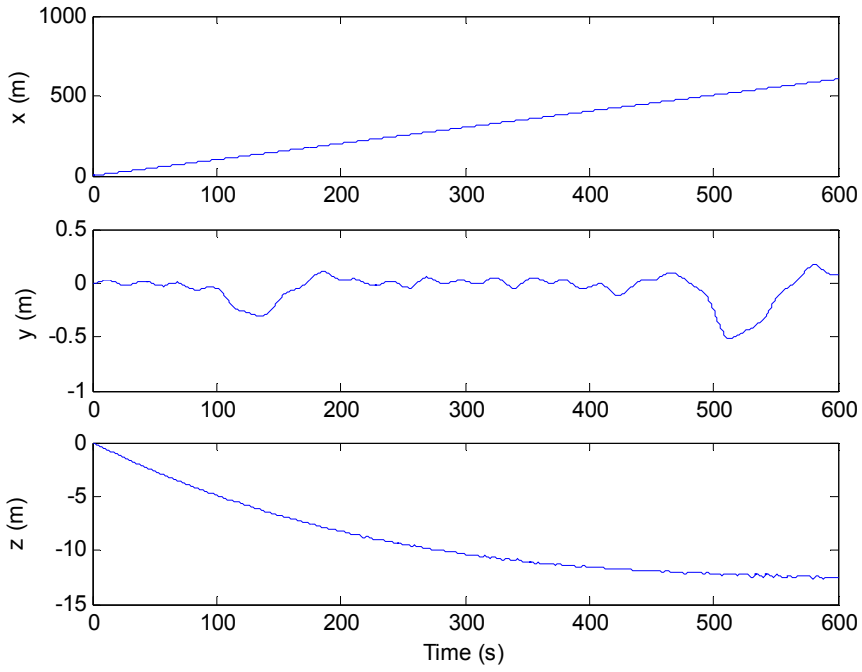

Figure 53 Position of the controlled towfish with a pigtail length of 20 meters

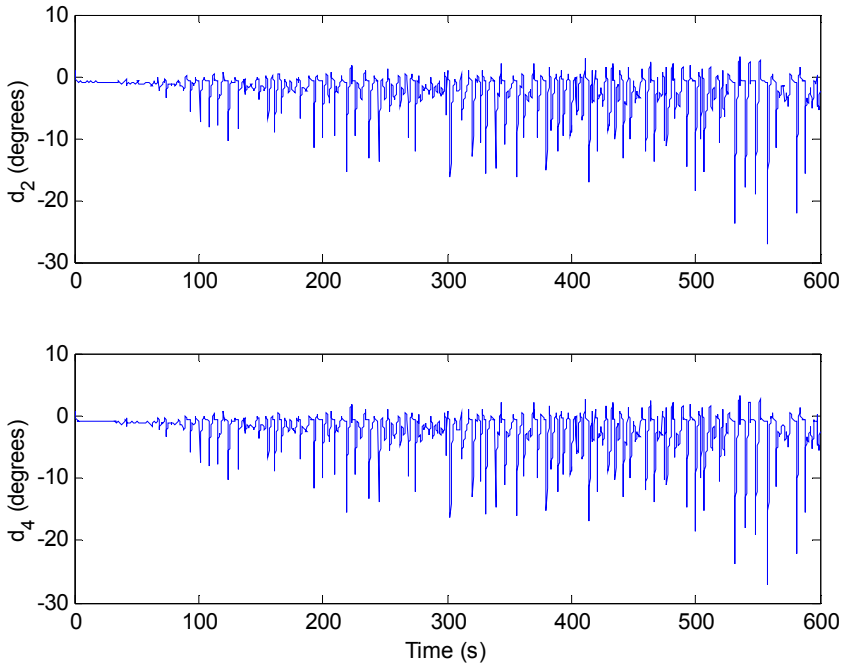

Figure 54 Stern plane deflections of the controlled towfish with a pigtail length of 20 meters

Simulating a neutrally buoyant towfish with the revised gains, pigtail length of 20 meters and an initial condition of 1 degree of pitch shows a slightly degraded response when compared to the initial condition response in Section 4.2. See Figure 55.

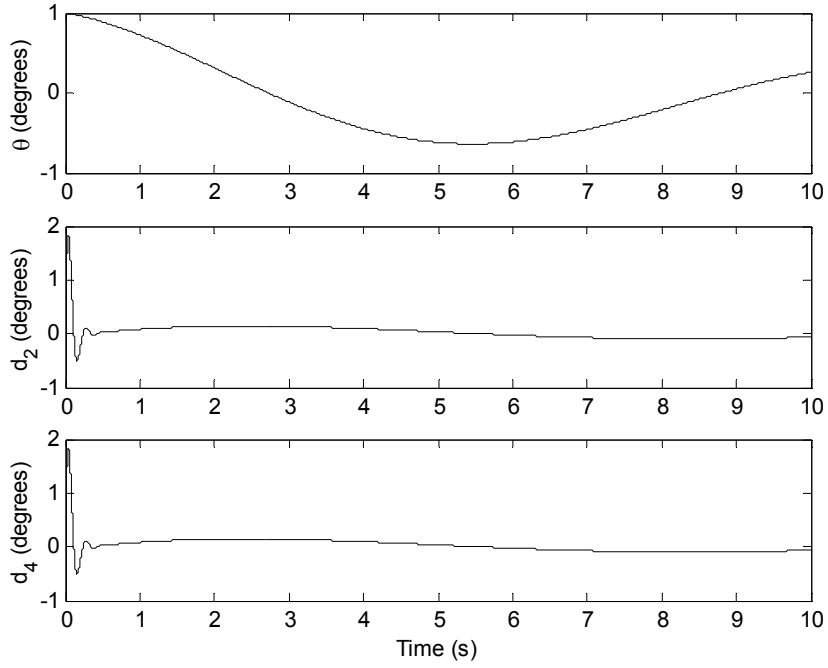

Figure 55 1^0 initial condition pitch response with revised gains

There is a trade off between tilt regulation to within the design criteria and the ability of the controller to return the towfish from a large initial pitch angle. Strong derivative control is useful for the random disturbances but too much degrades the initial condition response. The original set of gains that were tuned to meet the design criteria for a pigtail length of 50 meters were not able to perform well enough when the pigtail length was reduced to 20 meters. This would suggest that gain scheduling would be advisable if one would want to vary the pigtail length.

It is apparent that the PID control structure is very well suited for the control of the towfish and can be easily adjusted to meet differing conditions. The controller showed some robustness for different speeds, CG locations and pigtail lengths. The simulations made it apparent how these three factors can affect nominal height.

6. Design Overview

There are many parameters that play a role in the design of the towfish. The towfish size needs to be manageable; it must be suitable for use on a small research vessel. For example, it must be light enough to be handled by two people, when dry, and to be recovered with a small shipboard winch when flooded. The components are placed in such a way as to limit length and to achieve approximately a 6 to 1 fineness ratio. It is necessary that the towfish frame be modular for trimming purposes and corrosion resistance; sacrificial zinc or magnesium buttons and trim weights need to be bolted to the frame in various spots. The hull was chosen to be fiberglass due to its strength and repairability. A limited production tool supplied by Vectorworks was used to mold the fiberglass hull and can be used to make additional hulls if necessary. Figure 56 shows an annotated schematic. To protect the actuators from bending moments from the fins, a stainless steel ring leader sprocket/chain assembly is used to actuate the fins and can be seen in Figure 57. Throughout this section, all units are in inches.

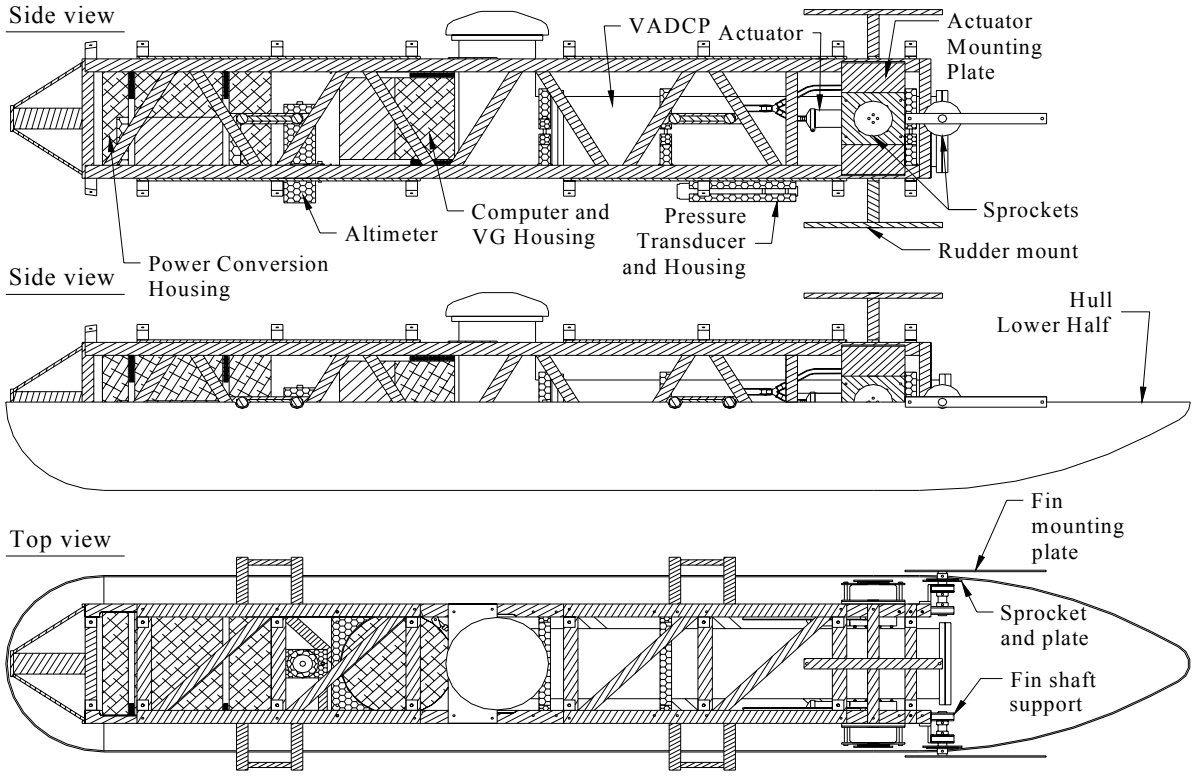

Figure 56 Towfish assembly schematic

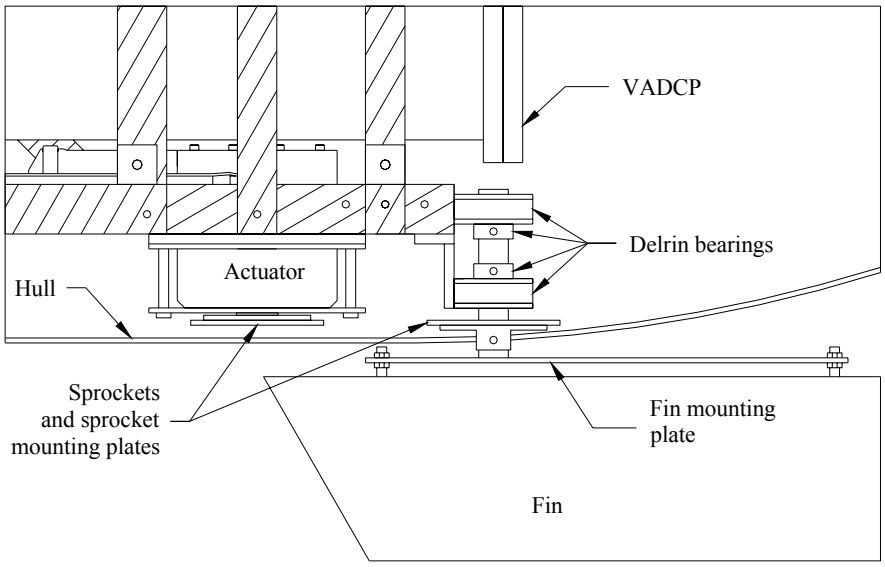

Figure 57 Actuator gear and bearing system. Chain not shown

The six main components of the towfish are:

1. Sensor pressure housing
2. Power conversion pressure housing
3. Free flood devices
4. Servo actuators
5. Frame
6. Free flood hull

6.1. Sensor Pressure Housing

The sensor pressure housing supplied by Prevco contains both the attitude sensor and the computer. The vertical gyro (VG) chosen to perform attitude and angular rate sensing is the Crossbow VG400-CC-100. This sensor allows one to determine both pitch and roll within approximately a half of a degree of accuracy. Pitch and roll rate are also supplied. The yaw rate signal will not be utilized for feedback control. All equipment on the towfish communicates serially. Therefore, a reliable, compact, modular and fast computer is necessary. To fulfill the requirements, a PC-104 computer running LabVIEW™ over Linux is utilized for data collection and control. The computer includes the CPU module (a Micro 886ULP from Advanced Micro Peripherals), the power board (a HE512-V512-T from Diamond Systems), a serial expansion card (an Emerald-MM-8, also from Diamond Systems) and a two-axis motor control card (a 4I27A from Mesa Electronics). The housing, vertical gyro and computer can be seen in Figure 58.

The PC-104 is mounted to a bracket in the shape of a “U”. The bracket is mounted to the upper end cap of the pressure housing housing. To save space, some of the cards that

make up the PC-104 are mounted to the sides of the "U" bracket. The Crossbow vertical gyro is mounted directly to the lower end cap. Both the upper and lower end cap use Impulse brand underwater right angle connectors. The right angle is necessary to conserve space outside of the housing. See Figure 58. This pressure housing is mounted upright so the right angle connectors must be oriented in a specific way to avoid the upper and lower frame cross members. See Figure 56 and Figure 64.

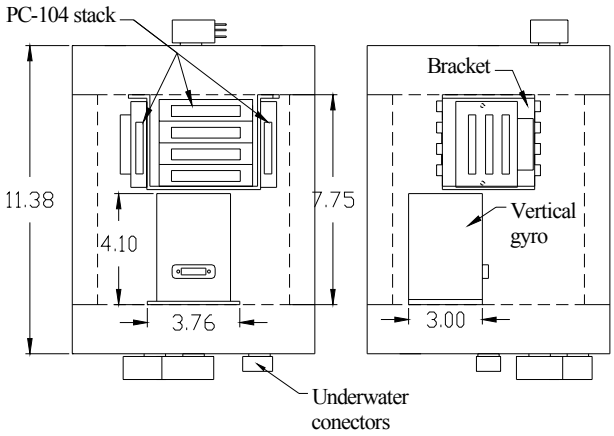

Figure 58 Crossbow vertical gyro and PC-104 housing. Units in inches

6.2. Power Conversion Housing

The power conversion pressure housing supplied by Prevco contains three power conversion units. For safety concerns and to minimize losses, 110 VAC is supplied from the research vessel. The 110 VAC is supplied along the umbilical tether into the power conversion pressure housing. The supply voltage is converted into 144 VDC using an AC to DC power converter (model number VI-RU44H-EUUU from Vicor). The 144 VDC is dropped down to 48 VDC using a VI-254 and then once again to 12 VDC using a VI-231, both units supplied by Vicor. The housing will be filled with an organic oil to facilitate heat dissipation. An air bubble is left in the housing to allow the oil to expand. Given the temperature range the pressure housing will experience (ΔT) and the volume of the housing (V_{PH}), the minimum volume required for the oil to expand (V_{req}) can be determined by

$$V_{req} = \alpha_{TE} V_{PH} \Delta T$$

where α_{TE} is the coefficient of thermal expansion. As a safety measure, twice the required volume is allowed for expansion. The housing is also fitted with a pressure release valve as an additional safety measure. There are also two vent ports for filling the housing with oil and allowing air to escape.

All three power converters are secured to a rectangular bracket which is cantilevered. The AC to DC converter is placed on the upper side of the bracket and its heat exchanger

faces away from the DC to DC converters which are secured below it; see Figure 59 and Figure 60.

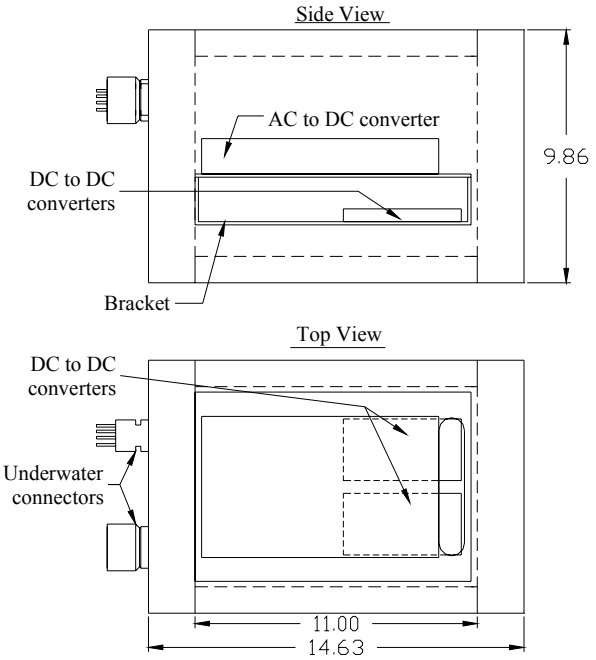

Figure 59 Power conversion housing. Units in inches

The housing is mounted on its side. Therefore, inline connectors rather than right angle connectors can be used.

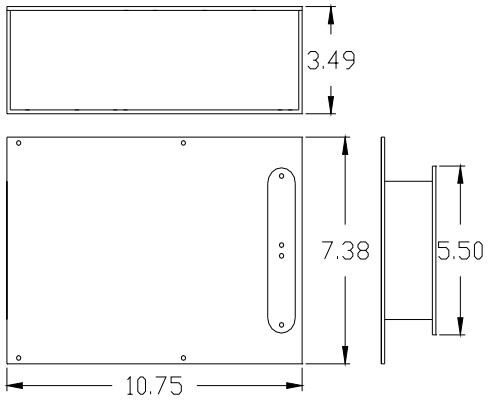

Figure 60 Power conversion housing bracket

The pressure housings are both secured with a 10.75 inch long aluminum plate that is 1/8 inch thick. It is curved to the shape of a half circle. It is then fastened to a Starboard™ clamp, one at each end. The 1 inch thick Starboard™ clamp is fastened to an aluminum "L" bracket which is welded to the frame. See Figure 61. The pressure housing lies in the half circle aluminum piece and is secured in place with quick-release hose clamps. The steel hose clamps are isolated from the aluminum housing with strips of neoprene.

The power conversion pressure housing is closest to the nose of the towfish and lies on its side in the clamp. The vertical gyro/pc-104 pressure housing is also strapped to its clamp but is standing up. From Figure 64 you can see that above the pressure housings some of the frame has been cut away so the housings may be easily inserted and removed from the frame. In between the two housings is the altimeter. It is seated in a Starboard™ clamp that is fastened to the underside of the frame.

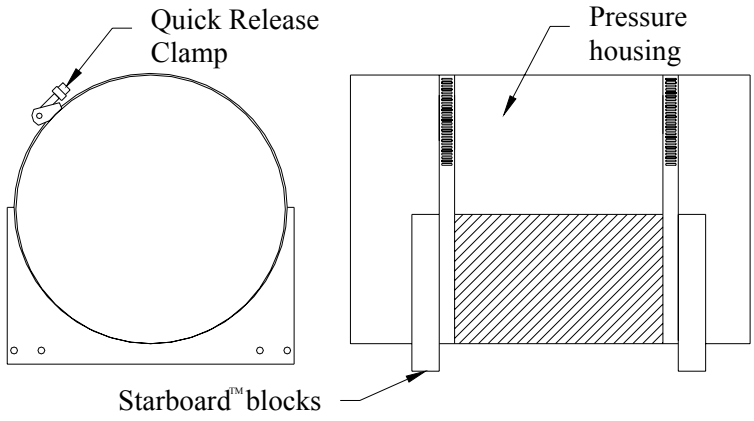

Figure 61 Pressure housing mounting bracket

6.3. Free Flood Devices

The free flood devices include the VADCP, a Seabird SBE 50 pressure transducer, a Benthos Datasonics PSA-916 altimeter and a Novatech Designs RF-700C1 light beacon and VHF pinger. The VADCP is the main sensor which is used to gather water velocity data. Because the towfish will be operated in the coastal oceans it may at times be close to the ocean floor, as little as 20 meters away. The altimeter is used to determine the altitude of the towfish to avoid collision. The light beacon/VHF pinger will be used for recovery purposes and is mounted in the upper vertical fin.

The VADCP has a shaft of approximately 33.75 inches in length and 6.75 inches in diameter. At the end of the shaft is a right angle head that terminates approximately 15 inches in length. At the end of the right angle head are the five transducers. The VADCP sits in three clamps made from Starboard™. See Figure 62. Each clamp is 1 inch in width and 10.5 inches in length. The upper and lower clamps are identical and attach to each other with a ¼-20 aluminum bolt and nut. The clamps are secured to the frame via an aluminum "L" bracket that is welded to an aluminum plate which is fastened to the frame. See Figure 56. The VADCP is allowed to be either upward or downward pointing. Under the VADCP lies the pressure sensor. It is secured in a clamp constructed from Starboard™ that is fastened to the underside of the frame.

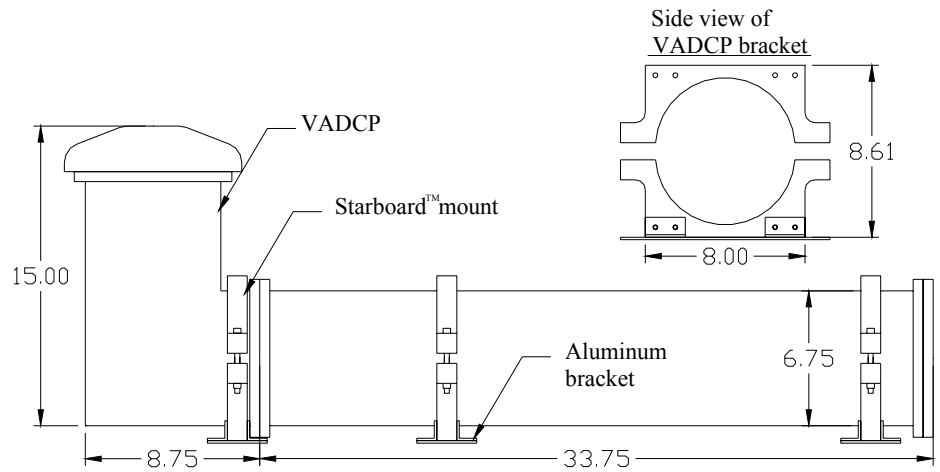

Figure 62 VADCP and mounting brackets. Units in inches

6.4. Servo Actuators

The servos chosen to actuate the stern planes are Tecnadyne Model 60 rotary actuators. They each are provided with eight hall sensors on the input shaft. Combined with a 200 to 1 gear ratio one obtains 1600 pulses per revolution of the output shaft. This gives a resolution of 0.23 degrees. They provide 60 ft-lbs of torque and can rotate at speeds from 0 to 90 degrees per second. There will be 2 reed switches offset from the actuators, mounted approximately at the stall angle of the fins. The fins will not be able to rotate beyond the switches. These switches will also initialize the actuators. See Figure 63.

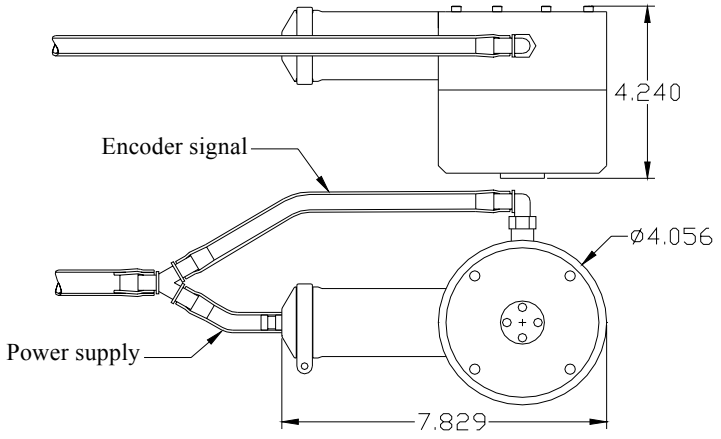

Figure 63 Actuator schematic, units in inches. Drawing courtesy of Tecnadyne, Inc

6.5. Frame

The frame is rectangular and is 80 inches in length and 11.5 inches in height and width. It is constructed from 6061 aluminum for its good strength and corrosion resistance. Four angle aluminum bars form the corners of the frame. They are a quarter inch thick

with equal legs of 1.25 inches and are approximately 73 inches long. The lateral sides of the frame are constructed from one inch wide and quarter inch thick aluminum bar stock that is welded to the upper and lower angle aluminum bars in a truss-like pattern. The lower normal side has two square frame sections constructed from 1.25 inch wide and quarter inch thick bar stock. Both square frame sections are welded to the lower normal surface. Similar square frame sections are fastened (not welded) to the top normal surface. This allows them to be removable so that the VADCP and the two pressure housings may be removed from the frame. See Figure 64.

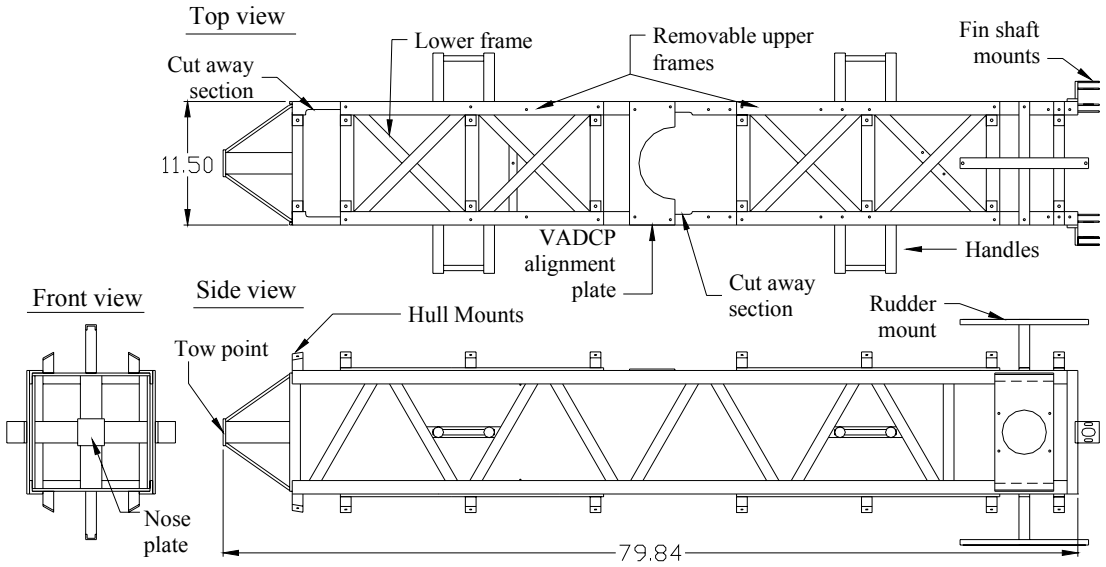

Figure 64 Frame schematic Units in inches

The lateral sides of the frame have handles welded to the truss-like structures to facilitate lifting and handling. The upper and lower normal surfaces of the frame have one inch by one inch square mounting blocks to facilitate attachment of the hull. The nose of the frame is formed with four, 2 inch wide by 0.25 inch thick by 7.25 inch long aluminum bars set at a 35 degree angle. The four bars are welded to four cross members that span across the lateral and normal sides. They meet a 2 inch by 2.5 inch by 0.25 inch plate which forms the top of the nose. In the nose plate, an I-bolt is fastened to secure the tether. Because the I-bolt is made from steel it is isolated from the aluminum with a plastic collar. If not done, the aluminum and steel will quickly corrode in salt water. Near the rear of the frame there are two 5.5” X 11.5” X 0.13” plates welded to both lateral sides. The plates have a 4.13” diameter hole in the center. This allows the cylindrical head of the actuators to fit through.

6.6. Free Flood Hull

The hull is manufactured with Owens Corning glass using a limited production tooling fabricated by Vectorworks Marine Inc. The hull is 103 inches long, 17 inches in diameter and 0.25 inches wall thickness. It is split into two sections, an upper and lower half. The nose is spherical with 17 inches outer diameter. The cylindrical main body is

66.75 inches long, 17 inches in outer diameter. The tail section is 27.5 inches long, 17 inches in diameter and is in the shape of an elliptic paraboloid. There is an 8.9 inch diameter hole in approximately the center of the hull on both the upper and lower normal sides. This allows the VADCP head to protrude from the hull. At the end of the body section there are four holes of radius 0.63 inches. One hole is on the upper and another on the lower normal surface of the body to allow the rudder shafts to protrude from the hull. The third and fourth holes are on the left and right sides to allow the stern plane shafts to protrude from the hull.

The upper and lower halves have two aluminum bars running along the length of the hull which are molded into the hull. The bolts that attach the hull to frame run through these aluminum bars. Holes are counter-sunk in the hull outside of the aluminum bars to accept the bolts. Along the seam where the upper hull section and lower hull section meet there is an aluminum H-channel to secure the upper and lower halves together. See Figure 65.

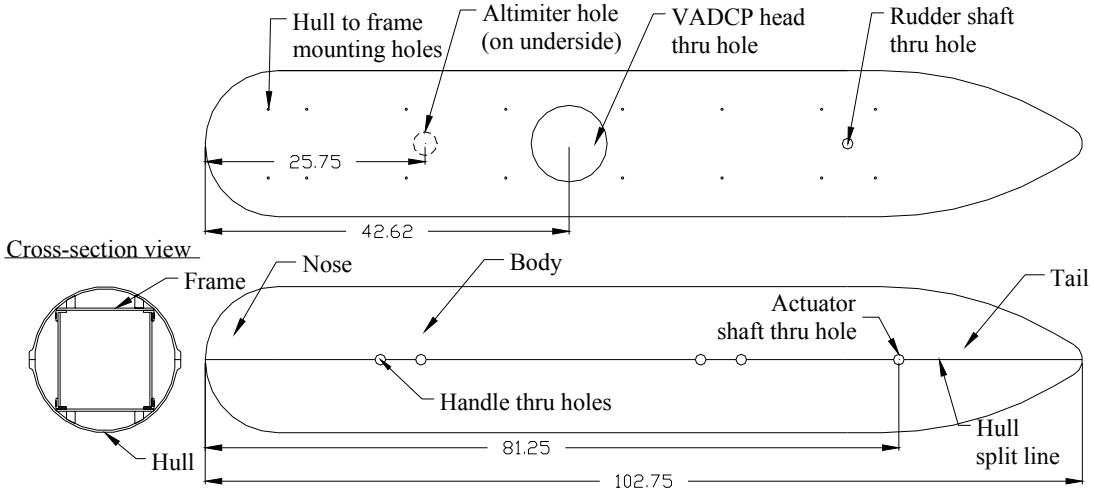

Figure 65 Hull schematic. Units in inches

The streamlined shape of the hull was chosen to minimize any asymmetric hydrodynamic effects. The nose shape was chosen to be a blunt sphere for ease of manufacturing and to avoid large shed vortices when the towfish pitches or yaws; this effect is seen in vehicles which have sharper noses. The tail was chosen to have a general streamlined shape and to allow room for the large underwater connector at the end of the VADCP. There are various holes placed along the body to facilitate draining when being lifted out of the water. Because drag and lift is not an important issue to the hull design, it was not necessary to optimize the design for hydrodynamic purposes.

6.7. Electronics and Underwater Connectors

It is important that the power and communications be connected with waterproof connectors. All connectors are supplied by Impulse, except for the Seacon connectors which fix to the actuators. An electronics schematic can be seen in

Figure 66. Table 3 describes the Impulse and Seacon connectors being used and the signals they carry. Because the tether is limited to 7 conductors, towfish communication must use as few conductors as possible. Two conductors are to be used for power and one is used for ground. Four conductors are used for data and communication. RS-485 is preferred due to the length of tether that will need to be used.

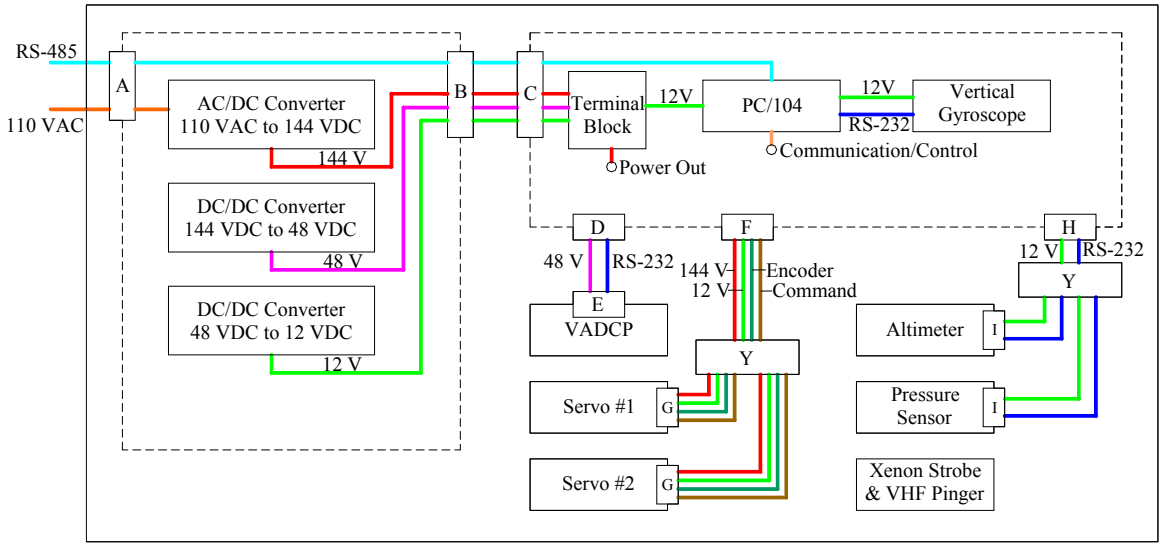

Figure 66 Electronic and connector schematic. "Y" represents a Y-split in the cable

Table 3 Bulkhead and inline connectors. All supplied by Impulse unless otherwise stated

Terminal	Inline Connector	Bulkhead Connector	Signals Carried
A	IL-8-FS	BH-8-MP	110VAC, RS-485
B	IL-12-MP	BH-12-FS	144VDC, 48VDC, 12VDC, RS-485
C	LPIL-12-FS	LPBH-12-MP	144VDC, 48VDC, 12VDC, RS-485
D	LPIL-5-MP	LPBH-5-FS	48VDC, RS-232
E	XSL-20 CCP-RA	N/A	48VDC, RS-232
F	LPIL-12-MP	LPBH-12-FS	144VDC, 12VDC, (2) Analog input, (2) Quadrature encoder pair
G	SEA-CON XSJ-9-CCP	N/A	144VDC, 12VDC, Analog input, Quadrature encoder pair
H	LPIL-9-MP	LPBH-9-MP	12VDC, (2) RS-232
I	In hand	N/A	12VDC, RS-232

7. Conclusions

A hydrodynamic model of a towed underwater vehicle with actuated stern planes and a fixed rudder has been presented. Simple but conservative models of disturbances were used. A conventional PID controller was developed according to desired response characteristics to regulate both pitch and roll angle. The control law was validated for different towing speeds and CG locations. A pigtail length variation was also investigated and required the control gains to be retuned. Although the new gains were able to meet the pitch and roll angle criteria with a shortened pigtail, the initial condition response of the towfish was degraded. Mode approximations were shown to have acceptable accuracy and proved to be a useful tool for the stern plane design.

The design of the towfish was also discussed. Characteristics of the towfish design that were taken into consideration were buoyancy, dry weight and size. The main aspects of the design that were covered include actuators, pressure housings, the frame and the hull.

Future work includes assembly of the towfish and trimming and balancing of the CG and CB. Once it is completely assembled, there will be preliminary sea trials to fine tune the controller gains. Shortly thereafter, the towfish is scheduled to be used aboard the *R/V Hatteras* to search for and characterize ocean turbulence off the mid-Atlantic coast of North America.

Appendix A – Towfish Parameters

Below are the parameters of the towfish that are used for simulation and linearization. The dry weight including the hull, frame and other components is approximated to be 1112 N (250 lbs). The mass of the towfish is approximated to be the mass of the water the towfish displaces. Moments of inertia are approximated for a cylinder of length l_b and diameter D_b. Body hydro dynamic coefficients were approximated from NACA report 432.[13] Fin chord length was chosen so that, with an airfoil shape of a NACA 0012, the maximum fin thickness would be able to accommodate the xenon flasher/pinger. The fin span and aspect ratio were chosen such that certain pitch and roll mode performance was achieved. The span efficiency factor, ε, was determined from reference [1], page 340, Figure 5.18 for a taper ratio of 1. The tail efficiency factor, η, was assumed to be 0.8. The pigtail parameters were approximated from a second order system model where the damping ratio, ζ, was assumed to be 1. The value or EA was originally 45×10^6 [7] but is reduced to 5000 to speed up simulation. The length of the pigtail is chosen to be nominally 50 meters.

Towfish parameters	
W_b	1112.1 N
I_x	5.9849 kg m^2
I_y	87.2438 kq m^2
I_z	87.2438 kq m^2

Body parameters	
D_b	0.4318 m
l_b	2.5908 m
S_b	0.1464 m^2
Vol	0.2529 m^3
$C_{D\alpha b}$	0.3511
$C_{L\alpha b}$	0.3508
$C_{m\alpha b}$	1.3076
C_{D0}	0.0194
C_f	0.004[17]
X_{CG}	[0 0 0.0762] m

Tail parameters	
c	0.4 m
b	0.68 m
l_c	0.9715 m
l_f	0.9144 m
ε	0.971
η	0.8

X_{ac1}	$\left[-l_t \quad 0 \quad \left(b/4+D_b/2\right)\right]^T$
X_{ac2}	$\left[-l_t \quad -\left(b/4+D_b/2\right) \quad 0\right]^T$
X_{ac3}	$\left[-l_t \quad 0 \quad -\left(b/4+D_b/2\right)\right]^T$
X_{ac4}	$\left[-l_t \quad \left(b/4+D_b/2\right) \quad 0\right]^T$

Depressor parameters	
x_{depth}	200 m

Pigtail parameters	
EA	5000N/m
ζ	1

Other constants	
ρ	1000 kg/m^3
g	9.81 m/s^2

Other linearization parameters	
F_{td}	21 N
U_0	1 m/s
L	50 m

Appendix B – Towfish Matlab™ Code

Simulation File

```
clear
close all

global rho lb Sb St U0 MII M Mcg Icg Volb CLalpha Cybeta Weight Buoyancy kbar bbar StaticDeflection
epsilon AR b L X0 lt...
    Xac1 Xac2 Xac3 Xac4 Kpitch Kroll CDo CDbo CLalphab CMalphab Clp Cmq Cnr omega_Depressor
RandomSignal Deltat Xcg tspan

% NOTE: All units are metric unless otherwise specified!

% Compute rigid body and potential flow hydrodynamic parameters for a 6:1 ellipsoid
D = 17*0.0254;
FinenessRatio = 6;
lb = FinenessRatio*D;
Sb = pi*(D^2)/4;
Volb = (4/3)*pi*(D/2)*(D/2)*(lb/2); % Volume of an ellipse

rho = 1000;
g = 9.807;
DepressorDepth = 200;
omega_Depressor = sqrt(g/DepressorDepth);
%%%%%%%%%%%%%%%%%%%%%%%%%%%%%%%%%%%%%%%%%%%%%%%%%%%%%%%%%%%%%%%%%%%%%%%%%%%%%%%%


%%%%%%%%%%%%%%% State the tail parameters %%%%%%%%%%%%%%%%%%
cr = 1.31*0.3048; % Constant chord of tail necessary to fit pinger
b = 0.68; % Tip-to-tip tail fin span of fins only, not including body
AR = b/cr;
St = b*cr; % Tip-to-tip fin area
CLalpha2D = 2*pi; % From Anderson Pg 277 Eq 4.58
CLalpha = CLalpha2D/(1+(CLalpha2D/(pi*AR))); % From Anderson Pg 343 Eq 5.68
CDo = 0;
epsilon = 0.971; % From Anderson Pg 340 Fig 5.18
lt = (3/8)*lb; % Length from tail AC to tow fish CG/CB, approximate
Vt = (lt*St)/(Sb*lb); % Tail volume
eta = 0.8; % Tail effency factor
lf = 3*0.3048; %Distance from the body axis origin to fin center
%%%%%%%%%%%%%%%%%%%%%%%%%%%%%%%%%%%%%%%%%%%%%%%%%%%%%%%%%%%%%%%%%%%%%%%%%%%%%%%%


%%%%%% Mass, inertia, added mass and added inertia %%%%%%%
Weight = 250/0.2248; % Dry (Newtons), estimated weight
m = Volb*rho; % Mass of body plus fluid inside hull approximation(kg)

Ix = 0.5*m*(D/2)^2; % Approximated from cylinder
Iy = (m/5)*((lb/2)^2+(D/2)^2);
Iz = (m/5)*((lb/2)^2+(D/2)^2);

Ixy = 0;
```

```
Ixz = 0;
Iyz = 0;

% Added mass parameters for the fins from Newman and Lewis
Yvdot = pi*rho*b*(cr/2)^2;
Zwdot = Yvdot;

Nvdot = lf*Yvdot;
Mwdot = Nvdot;

Nrdot = (lf^2)*Yvdot;
Mqdot = Nrdot;
Kpdot2D = (2/pi)*rho*(b/2)^4;
Kpdot = Kpdot2D*cr;

% Added mass parameters for ellipsoid from Fossen
e = sqrt(1-(D/lb)^2);
alphao = (2*(1-e^2)/(e^3))*((1/2)*log((1+e)/(1-e))-e);
betao =(1/(e^2))-((1-e^2)/(2*e^3))*log((1+e)/(1-e));
k1 = alphao/(2-alphao);
k2 = betao/(2-betao);
k3 = (betao-alphao)*e^4/((2-e^2)*(2*e^2-(2-e^2)*(betao-alphao)));

% Location of CG
xcg = 1*0.0254*0;
ycg = 1*0.0254*0;
zcg = 3*0.0254;

Xcg = [xcg;ycg;zcg];

% Mass and inertia matricies
Mcg = m*hat(Xcg) + [0 0 0;0 0 Mwdot;0 Nvdot 0];
M = diag([1+k1;1+k2;1+k2])*m + diag([0;Yvdot;Zwdot]);
I = diag([1;1+k3;1+k3])*diag([Ix;Iy;Iz]) + diag([Kpdot;Mqdot;Nrdot]);
Icg = I+[0 -Ixy -Ixz;-Ixy 0 -Iyz;-Ixz -Iyz 0];

MII = [M Mcg';Mcg Icg];
%%%%%%%%%%%%%%%%%%%%%%%%%%%%%%%%%%%%%%%%%%%%%%%%%%%%%%%%%


%%%%% State the body viscous hydrodynamic parameters %%%%%
CLalphab = 0.3508; % From NACA Report No. 432 Table 1 using linear fit from 0 deg to 12 deg pitch
CMalphab = 1.3076; % From NACA Report No. 432 Table 1 using linear fit from 0 deg to 12 deg pitch
Cf = 0.004; % From Hoerner FDD Section 3-12 for supercritical flow.
CDbo = 0.44*(D/lb)+4*Cf*(lb/D)+4*Cf*sqrt(D/lb); % From Hoerner FDD Section 3-12 for supercritical flow.
%%%%%%%%%%%%%%%%%%%%%%%%%%%%%%%%%%%%%%%%%%%%%%%%%%%%%%%%%


%%%%%%%%% Hydrodynamic damping moment from Nelson %%%%%%%%
Clp = -2*(CLalpha/3); % Taper ratio of 1, multiplied by 2 for both horizontal and vertical sections
Cmq = -2*eta*CLalpha*Vt*(lt/lb);
Cnr = Cmq;

% Hydrodynamic center for fins
```

```
zac = (b/4)+(D/2);  % From Etkin and Reid table C1 pg 355
yac = (b/4)+(D/2);

Xac1 = [-lt; 0 ; zac];
Xac2 = [-lt;-yac;0];
Xac3 = [-lt; 0 ; -zac];
Xac4 = [-lt;yac;0];
%%%%%%%%%%%%%%%%%%%%%%%%%%%%%%%%%%%%%%%%%%%%%%%%%%%%%%%%%%%%%%%


%%%%%%%%%% Spring and damping constants of tether %%%%%%%%%%
% Define the length of the pigtail
L = 50;
EA =  5000;
kbar = EA/L;
zeta = 1; % Assumed critically damped
omegan = sqrt(kbar/M(1,1)); % Second order system approx s^2 + (b/m)s + k/m
bbar = M(1,1)*2*zeta*omegan;
%%%%%%%%%%%%%%%%%%%%%%%%%%%%%%%%%%%%%%%%%%%%%%%%%%%%%%%%%%%%%%%


%%%%%%%%%% Define an initial state for simulation %%%%%%%%%%
U0 = 3;

x0 = 0;
y0 = 0;
z0 = 0;

phi0 = 0*pi/180;
theta0 = 0*pi/180;
psi0 = 0*pi/180;

V0 = 1*U0;
alpha0 = 0*(pi/180);
beta0 = 0*(pi/180);
RWindToBody0 = expm(hat([0;-alpha0;0]))*expm(hat([0;0;beta0]));
BodyVelocity0 = RWindToBody0*[V0;0;0];
u0 = BodyVelocity0(1);
v0 = BodyVelocity0(2);
w0 = BodyVelocity0(3);

p0 = 0;
q0 = 0;
r0 = 0;

sumtheta0 = 0;
sumphi0 = 0;

z20 = 0;
z40 = 0;

qbar0 = (1/2)*rho*U0^2;

% Initial deflection of pigtail
StaticDeflection = (0.0194*qbar0*Volb^(2/3)+CDbo*qbar0*Sb)/kbar;
```

```
%%%%%%%%%%%%%%%%%%%%%%%%%%%%%%%%%%%%%%%%%%%%%%%%%%%%%%%%%%%


%%%%%%%%%%%%%%%%%%%% Controller gains %%%%%%%%%%%%%%%%%%%%%%%%
% Pitch controller
Ti_pitch = 0.6;
Td_pitch = 1;
kp_pitch = 4;

Kpitch = zeros(2,16);
% Proportional control
Kpitch(1,5) = kp_pitch;
Kpitch(2,5) = kp_pitch;
% Integral control
Kpitch(1,13) = kp_pitch/Ti_pitch;
Kpitch(2,13) = kp_pitch/Ti_pitch;
% Derivative control
Kpitch(1,15) = kp_pitch*Td_pitch;
Kpitch(2,15) = kp_pitch*Td_pitch;

% Roll controller
Ti_roll = 0.5;
Td_roll = 0.3;
kp_roll = 2;

Kroll = zeros(2,16);
% Proportional control
Kroll(1,4) = -kp_roll;
Kroll(2,4) = kp_roll;
% Integral control
Kroll(1,14) = -kp_roll/Ti_roll;
Kroll(2,14) = kp_roll/Ti_roll;
% Derivative control
Kroll(1,16) = -kp_roll*Td_roll;
Kroll(2,16) = kp_roll*Td_roll;
%%%%%%%%%%%%%%%%%%%%%%%%%%%%%%%%%%%%%%%%%%%%%%%%%%%%%%%%%%%

% Define time span of interest
tfinal = 900;
Deltat = 0.1;
tspan = [0:Deltat:tfinal]';

%%%%%%%%%%%%%%%%%%%%%%%%%%%%%%%%%%%%%%%%%%%%%%%%%%%%%%%%%%%
% Generate random depressor motion %
RandomSignal = RandomSignalGenerator(tspan);
%%%%%%%%%%%%%%%%%%%%%%%%%%%%%%%%%%%%%%%%%%%%%%%%%%%%%%%%%%%


%%%%%%%%%%%%%%%%%%%%%%%%%%%%%%%%%%%%%%%%%%%%%%%%%%%%%%%%%%%
% Set initial conditions %
X0 = [x0;y0;z0;phi0;theta0;psi0;u0;v0;w0;p0;q0;r0;sumtheta0;sumphi0;z20;z40];
options = odeset('RelTol',1e-12);
[t,X] = ode15s('TowfishEOM',tspan,X0,options);
%%%%%%%%%%%%%%%%%%%%%%%%%%%%%%%%%%%%%%%%%%%%%%%%%%%%%%%%%%%
```

Equations of Motion File

```
function Xdot = TowfishEOM(t,X)

global rho lb Sb St U0 MII M Mcg Icg Volb CLalpha Cybeta Weight Buoyancy kbar bbar StaticDeflection
epsilon AR b L X0...
    Xac1 Xac2 Xac3 Xac4 Kpitch Kroll CDo CDbo CLalphab CMalphab Clp Cmq Cnr omega_Depressor
RandomSignal Deltat Xcg tspan

% Define states
x = X(1);
y = X(2);
z = X(3);
phi = X(4);
theta = X(5);
psi = X(6);
u = X(7);
v = X(8);
w = X(9);
p = X(10);
q = X(11);
r = X(12);
sumtheta = X(13);
sumphi = X(14);

z2 = X(15);
z4 = X(16);
thetadot = q*cos(phi)-r*sin(phi);
phidot = p+q*sin(phi)*tan(theta)+r*cos(phi)*tan(theta);
States = [X(1:14);thetadot;phidot];

% Controller
input = Kpitch*States + Kroll*States;
d2 = input(1);
d4 = input(2);

% Actuator rate equations
tau = 0.044;
z2dot = (1/tau)*(- z2 + d2);
z4dot = (1/tau)*(- z4 + d4);

% Define hydrodynamic angles
V = sqrt(u^2 + v^2 + w^2);
qbar = (1/2)*rho*V^2;
alpha = atan(w/u);

beta = asin(v/V);
mu = asin(sqrt((v^2 + w^2)/V^2));

% Water to body rotation matrix
RWindToBody = expm(hat([0;-alpha;0]))*expm(hat([0;0;beta]));

% Hydrodynamic force and moment on the body
CWb = -[0.3511*(mu^2)+0.0194; CLalphab*beta; CLalphab*alpha];
CBb = RWindToBody*CWb;
```

```
% Extra zero AOA drag due to skin friction
CWb2 = -[CDbo;0;0];
CBb2 = RWindToBody*CWb2;

BodyForce = CBb*qbar*Volb^(2/3) + CBb2*qbar*Sb; % See NACA report No. 432, Table 1
BodyMoment = [0;CMalphab*alpha*qbar*Volb;CMalphab*(-beta)*qbar*Volb]; % See NACA report No.
432, Table 1

% Hydrodynamic force and moment from control surfaces.
% +d2, +d4 gives +lift -pitch
% +d2, -d4 gives +roll
CW1 = -[((CLalpha*beta)^2)/(pi*epsilon*AR);CLalpha*(beta);0];
CW2 = -[((CLalpha*(alpha+z2))^2)/(pi*epsilon*AR);0;CLalpha*(alpha+z2)];
CW3 = -[((CLalpha*beta)^2)/(pi*epsilon*AR);CLalpha*(beta);0];
CW4 = -[((CLalpha*(alpha+z4))^2)/(pi*epsilon*AR);0;CLalpha*(alpha+z4)];

CB1 = RWindToBody*CW1;
CB2 = RWindToBody*CW2;
CB3 = RWindToBody*CW3;
CB4 = RWindToBody*CW4;

TailForce = (CB1 + CB2 + CB3 + CB4)*qbar*St*0.5;
TailMoment = (cross(Xac1,CB1) + cross(Xac2,CB2) + cross(Xac3,CB3) + cross(Xac4,CB4))*qbar*St*0.5;

% Body to Inertial rotation matrix
RBodyToInertial = expm(hat([0;0;psi]))*expm(hat([0;theta;0]))*expm(hat([phi;0;0]));

% Determine the relative position of the nose to the towfish
Xnose = [x;y;z] + RBodyToInertial*[(lb/2);0;0];

% Random depressor model
TimeIndex = floor(t/Deltat)+1;
Xdepressor =
((1.4/4)*[0;cos(omega_Depressor*tspan(TimeIndex));sin(omega_Depressor*tspan(TimeIndex))]+[0;Rando
mSignal(TimeIndex);RandomSignal(length(tspan)+1-TimeIndex)]);
Xdepressor = Xdepressor + [L + lb/2 + U0*t + StaticDeflection;0;0];
% Determine the relative velocity of the nose to the towfish
Unose = RBodyToInertial*cross([p;q;r],[(lb/2);0;0])+RBodyToInertial*[u;v;w];
Udepressor = [U0*(t+1)/(t+1);0,diff(Xdepressor(2))/Deltat;0,diff(Xdepressor(3))/Deltat];

DeltaX = Xdepressor - Xnose;
DeltaU = Udepressor - Unose;

% Towing force spring model
if norm(DeltaX) < L
   Ftowfishdepressor = [0;0;0];
else
   Ftowfishdepressor = [kbar*(norm(DeltaX)-L)+bbar*(dot(DeltaU,(DeltaX/norm(DeltaX))));0;0];
end

% Cable to inertial rotation matrix
gamma = atan(DeltaX(3)/DeltaX(1));
sigma = asin(DeltaX(2)/norm(DeltaX));
RCableToInertial = expm(hat([0;-gamma;0]))*expm(hat([0;0;sigma]));
```

```
TowingForce = RBodyToInertial'*RCableToInertial*Ftowfishdepressor;
TowingMoment = cross([(lb/2);0;0],TowingForce);

% Hydrodynamic damping moment
Lp = Clp*(qbar*St*b)*(b/(2*U0));
Mq = Cmq*(qbar*Sb*lb)*(lb/(2*U0));
Nr = Mq;

DampingMoment = [Lp*p;Mq*q;Nr*r];

% Weight and buoyant forces
WeightForce = (RBodyToInertial')*[0;0;Weight];
BuoyantForce = (RBodyToInertial')*[0;0;-Weight*1.03];

% CG offset moment
CGMoment = cross(Xcg,WeightForce);

% Hydrodynamic force and moment from body, control surfaces and towing
Force = TowingForce + BodyForce + TailForce + WeightForce + BuoyantForce;
Moment = TowingMoment + BodyMoment + TailMoment + DampingMoment + CGMoment;

% 12 Non-linear EOM and pitch and roll summation equations and actuator rate equations
Xdot = [RBodyToInertial*[u;v;w];...
      p+q*sin(phi)*tan(theta)+r*cos(phi)*tan(theta);...
      q*cos(phi)-r*sin(phi);...
      q*sin(phi)/cos(theta) + r*cos(phi)/cos(theta);...
      inv(MII)*[cross((M*[u;v;w] + (Mcg')*[p;q;r]),[p;q;r]) + Force;...
         Cross((Icg*[p;q;r] + Mcg*[u;v;w]),[p;q;r]) + Cross((M*[u;v;w] + (Mcg')*[p;q;r]),[u;v;w]) +
Moment];...
      theta;...
      phi;...
      z2dot;...
      z4dot];
```

Random Signal File

```
function Signal = RandomSignalGenerator(tspan)

% This file generates a random signal according to the JONSWAP wave spectrum

% Define universal parameters.
g = 9.80665;

% Define parameters for the JONSWAP wave spectrum and time series.
omega_1 = 0.01;
omega_2 = 3;
N = 100; % Number of frequencies represented in time series.
H = 1.4; % Significant wave height in meters (1.4 for moderate (code 4) seas).
TBar = 0.75*sqrt(70); % Modal period in seconds (0.75*sqrt(70) for moderate (code 4) seas).

% Plot the JONSWAP wave spectrum.
omega = [omega_1:(omega_2-omega_1)/100:omega_2]';
A = 172.75*(H^2)/(TBar^4);
B = 691/(TBar^4);
```

```
omega0 = (4*B/5)^0.25;
T0 = 2*pi/(omega0);
SB = (A./(omega.^5)).*exp(-B./(omega.^4)); % Bretschneider spectrum
gamma = le(omega,2*pi/T0)*0.07 + gt(omega,2*pi/T0)*0.09;
J = exp((-1./(2.*gamma.^2)).*((T0/(2*pi)).*omega-1).^2);
S = 0.658.*(3.3.^J).*SB; % JONSWAP Spectrum

% Compute a time series based on the wave spectrum above.  Select N random frequencies.
OmegaBounds = sort(omega_1 + (omega_2-omega_1)*rand(N+1,1));
DeltaOmega = diff(OmegaBounds);
omega = OmegaBounds(1:N) + (1/2)*DeltaOmega;
SB = (A./(omega.^5)).*exp(-B./(omega.^4)); % Bretschneider spectrum
gamma = le(omega,2*pi/T0)*0.07 + gt(omega,2*pi/T0)*0.09;
J = exp((-1./(2.*gamma.^2)).*((T0/(2*pi)).*omega-1).^2);
S = 0.658.*(3.3.^J).*SB; % JONSWAP Spectrum

% Generate time series as a sum of sinusoids with random phase shifts.
zeta0 = sqrt(2*S.*DeltaOmega); % Average wave amplitude at given center frequency, based on energy
density.
Signal = cos(tspan*omega'+2*pi*ones(size(tspan))*rand(1,N))*zeta0;
```

Skew-symmetric Matrix File

```
function xhat=hat(x)

% HAT This function takes an element in R3 and maps it to so(3)

xhat = zeros(3,3);
xhat(1,2) = -x(3);
xhat(2,1) = x(3);
xhat(1,3) = x(2);
xhat(3,1) = -x(2);
xhat(2,3) = -x(1);
xhat(3,2) = x(1);
```

References

1. Anderson, J. D., *Fundamentals of Aerodynamics*, 2nd ed., McGraw-Hill, New York, 1991.

2. Chapman, D.A., "Effects of Ship Motion on a Neutrally-Stable Towed Fish," *Ocean Engineering*, Vol. 9, No. 3, 1982, pp. 189-220.

3. Cominos, P., Munro, N., "PID controllers: recent tuning methods and design to specification," *IEE Proceedings-Control Theory and Applications*, Vol. 149, 2002, pp. 46-53.

4. Crane, J.W., "AEM Bathymetry Vehicle Design Tradeoff," Naval Coastal Systems Center, NCSC TN 1074-92, Panama City, Florida, January 1992.

5. Crane, J.W., Humphreys, D.E., "Modeling and Simulation of Underwater Vehicles," *SCS Summer Simulation Conference*, July, 1991.

6. Datta, A., Ho, M., Bhattacharyya, S.P., *Structure and Synthesis of PID Controllers*, Springer-Verlag London, Great Britain, 2000

7. Driscoll, F.R., Lueck, R.G., Nahon, M., "Development and Validation of a Lumped–Mass Dynamics Model of a Deep–Sea ROV System," *Applied Ocean Research*, Vol. 22, No. 3, 2000, pp.169-182.

8. Durham, W.C., *Aircraft Dynamics & Control*, 2002. [http://www.aoe.vt.edu/~durham/AOE5214/]

9. Etkin, B., *Dynamics of Flight—Stability and Control*, 2nd ed., John Wiley & Sons, New York, 1958

10. Fossen, T.I., *Guidance and control of Ocean Vehicles*, John Wiley & Sons Ltd., New York, 1995.

11. Fossen, T.I., *Marine Control Systems: Guidance, Navigation, and Control of Ships, Rigs and Underwater Vehicles*, Marine Cybernetics AS, Trondheim, Norway, 2002.

12. Franklin, G.F., Powell, J.D., Workman, M., *Digital Control of Dynamic Systems*, 3rd ed., Addison, Wesley Longman, Inc., California, 1998.

13. Freeman, H.B., "Force measurements on a 1/40-scale model of the U.S. Airship "Akron"," NACA Report No. 432, 1933

14. Freeman, H.B., "Pressure-distribution measurements on the hull and fins of a 1/40-scale model of the U.S. Airship "Akron"," NACA Report No. 443, 1934

15. Gargett, A.E., "Observing turbulence with a Modified Acoustic Doppler Current Profiler," *Journal of Atmospheric and Ocean Technology*, Vol. 11, No. 6, 1994, 1592-1610.

16. Henderson, J.F., Wright, R.C., "The Use of Active Control on Underwater Towed Bodies," *Computer Modeling in Ocean Engineering 91*, Proceedings of the Second International Conference on Computer Modeling in Ocean Engineering, Barcelona, 1991, pp. 397-405.

17. Hoerner, S.F., *Practical Information on Aerodynamic Drag and Hydrodynamic Resistance*, 1965.

18. Humphreys, D. E., Ruth, M. J., Sorrells, M. I., "The Impact of Shallow Water Missions on the Design of Towed Undersea Vehicles," Vehicle Control Technologies, Inc., Burke, VA.

19. Jiaming, W., Chwang, A. T., "A Hydrodynamic Model of a Two-part Underwater Towed System," *Ocean Engineering*, Vol. 27, No. 5 , 2000, pp. 455-472.

20. Leonard, N. E., "Stability of a Bottom-heavy Underwater Vehicle," Mechanical and Aerospace Engineering, Princeton University, Technecial Report 2048, Princeton, NJ, September, 1996.

21. Lewis, E. V., *Principles of Naval Architecture*, 2nd ed, Vol. III, The Society of Naval Architects and Marine Engineers, New Jersey, 1989

22. Lloyd, A.R.J.M., *Seakeeping: Ship Behaviour in Rough Weather*, Ellis Horwood, Chichester, 1989.

23. Nelson, R.C., *Flight Stability and Automatic Control*, 2nd ed., McGraw-Hill, New York, 1998.

24. Newman, J.N., *Marine Hydrodynamics*, The MIT Press, Cambridge, Massachusetts, 1977.

25. Ogata, K., *Modern Control Engineering*, 2nd ed., Prentice-Hall, New Jersey, 1990.

26. Perrault, D., Hackett, G., Nahon, M., "Simulation and Active Control of Towed Undersea Vehicles," *Oceans '97*, Proceedings of Oceans '97, Halifax, Canada, 1997, pp. 1277-1282.

27. Preston, J.M., "Stability of Towfish as Sonar Platforms and Benefits of the Two-part Tow," Defense Research Establishment Pacific, DREP Technical Memorandum 89-19, December, Victoria, British BC (CAN), 1989.

28. Preston, J. M., "Stability of Towfish used as Sonar Platforms," *Oceans '92*, Proceedings of Mastering The Oceans Through Technology, Newport, RI, 1992, pp.888-893.

29. Rodriguez, R.R., "Performance Evaluation of the Control Surface Actuators for the Towed Body for Mine Countermeasures Sensor Testing," Dahlgren Division Naval Surface Warfare Center, CSS/TR-97/20, Panama City, FL, September, 1997

30. Woolsey, C. A. and Gargett, A. E., "Passive and Active Attitude Stabilization for a Tow-fish," *IEEE Conference on Decision and Control*, Las Vegas, NV December, 2002, pp. 2099-2104.

31. Yamaguchi, S., Koterayama, W., Yokobiki, T., "Development of a Motion Controlled Method for a Towed Vehicle with a Long Cable," *Underwater Technology 2000*, Proceedings of the 2000 International Symposium on Underwater Technology, Tokyo,Japan, 2000, pp. 491-496.

32. Yamaguchi, S., Yokobiki, T; Koterayama, W, "Field Experiments on Motion Control Systems of the Towed Vehicle 'Flying Fish'," *Eighth International Offshore and Polar Engineering Conference*, Proceedings of the Eighth International Offshore and Polar Engineering Conference, Montreal, Canada, 1998, pp. 271-276.